DGAT1 + cysteine-oleosin expression in *Lolium perenne* leaves enhances photosynthetic efficiency, growth, and pasture energy density

---

A thesis

submitted in partial fulfilment

of the requirements for the Degree of

Doctor of Philosophy

at

Lincoln University

by

Zac Beechey-Gradwell

Lincoln University

2020

Abstract of a thesis submitted in partial fulfilment of the requirements for the Degree of Doctor of Philosophy

DGAT1 + cysteine-oleosin expression in *Lolium perenne* leaves enhances photosynthetic efficiency, growth, and pasture energy density

by

Zac Beechey-Gradwell

Two compelling strategies for enhancing food security are increasing photosynthesis and engineering higher levels of valuable nutrients such as lipids into plant tissues. Manipulation of many gene combinations has increased vegetative lipid content, but the effect of introducing a new energy-dense C sink on plant growth is typically negative. Winichayakul et al. (2013) reported long-term lipid accumulation in the leaves and roots of *Arabidopsis thaliana* by co-expressing diacylglycerol *O*-acyltransferase [DGAT1; the final enzyme in the triacylglycerol (TAG) biosynthesis pathway] and a novel lipid droplet-encapsulating protein (cysteine-oleosin) designed to confer greater stability to lipid droplets *in planta*. Remarkably, increased rates of photosynthesis and shoot growth also occurred in DGAT1 + cysteine-oleosin (collectively 'high metabolizable energy' or 'HME') Arabidopsis.

In this thesis, the effect of leaf HME expression on the growth and photosynthesis of the crop species *Lolium perenne* L. (perennial ryegrass) (PR) was studied. Leaf HME expression in PR increased leaf fatty acid content (FA) while simultaneously increasing growth. The primary objective of this thesis was to generate comprehensive evidence for this counterintuitive finding. The second objective was to investigate whole-plant, and especially leaf-level physiological and biochemical traits related to photosynthesis, under variable nitrogen (N) supply and both ambient and elevated atmospheric [CO_2], that could account for increased

HME PR growth. The final objective was to study the translation, from spaced pots indoors to field canopies, of the FA, energy, and growth enhancing traits associated with leaf HME expression in segregating PR populations, in order to quantify potential agronomic advantages of an HME cultivar.

Leaf HME expression caused a shift in leaf C storage in PR leaves; away from water-soluble carbohydrates (WSC) and towards FA. HME expression induced a high specific leaf area (leaf area per unit of mass), and in some genetic backgrounds also increased net photosynthetic rate per unit leaf area, contributing to a greater photosynthetic rate per unit leaf mass (A_{mass}) and per unit leaf nitrogen (PNUE). Under high N supply, total leaf area, relative growth rate, and total plant DW were enhanced for multiple independently-transformed HME lines/populations. The high HME PNUE was associated with enhanced mesophyll conductance to CO_2, greater N investment in electron transport and ATP synthesis, and higher estimated light absorptance per chlorophyll. The correspondence between high leaf FA and increased A_{mass}/PNUE/growth was found to depend upon a reduction in leaf WSC occurring. Further, HME expression made A_{mass} more responsive to elevated atmospheric [CO_2], suggesting that diverting a proportion of leaf WSC into FA may remove feedback inhibition of photosynthesis in some contexts.

Indoor and field experiments with HME PR populations grown in small canopies under simulated grazing showed that increasing leaf FA content by at least 0.8 %DW increased herbage gross energy (GE) concentration by up to 0.5 kJ gDW^{-1}. HME expression enhanced herbage DW accumulation (yield) in 'mini swards' arranged in spaced rows indoors but did not reliably enhance herbage production in dense swards indoors or field swards. Overall, this work supports the potential for using leaf lipids as alternative sinks for photosynthate to increase plant growth potential and for leaf lipid accumulation to enhance pasture energy density.

Keywords: biotechnology, carbon dioxide, fatty acids, feedback inhibition, field trial, gross energy, lipids, *Lolium perenne*, mesophyll conductance, metabolic engineering, metabolizable energy, nitrogen, pasture quality, perennial ryegrass, photosynthesis, source-sink, specific leaf area, triacylglycerol, transgenics, water-soluble carbohydrates.

Chapter 3 was published in *Journal of Experimental Botany* on 03 November 2019 with the title 'Storing carbon in leaf lipid sinks enhances perennial ryegrass carbon capture especially under high N and elevated CO_2' with the co-authors Luke Cooney, Somrutai Winichayakul, Mitchell Andrews, Shen Hea, Tracey Crowther, and Nick Roberts.

A combination of the data in chapter 2 and chapter 5 was published in *Frontiers in Plants Science* on 11 February 2021 with the title 'Changes in leaf-level nitrogen partitioning and mesophyll conductance deliver increased photosynthesis for *Lolium perenne* engineered to accumulate lipid carbon sinks' with the co-authors Luke Cooney (joint first author), Somrutai Winichayakul, Kim Richardson, Tracey Crowther, Phillip Anderson, Richard Scott, Greg Bryan, and Nick Roberts.

The data in chapter 4 was combined with data from the 2020 field trial and was submitted for publication in *Field Crops Research* on 14 May 2021 with the title 'Pasture grasses with higher energy density and growth potential under simulated grazing' with the co-authors Suhas Kadam, Gregory Bryan, Luke Cooney, Kelly Nelson, Kim Richardson, Ruth Cookson, Somrutai Winichayakul, Michele Reid, Philip Anderson, Tracey Crowther, Xiuying Zou, Dorothy Maher, Hong Xue, Richard Scott, Anne Allan, Alan Stewart, and Nick Roberts.

Preliminary data generated during this PhD was published in two *Journal of New Zealand Grasslands* articles titled 'High lipid perennial ryegrass growth under variable nitrogen, water and carbon dioxide supply' (published November 2018 with the co-authors Somrutai Winichayakul and Nick Roberts) and 'Progress towards delivering high metabolizable energy ryegrass' (accepted for publication February 2021).

Acknowledgements

I would first and foremost like to thank Dr. Luke Cooney for his huge contribution to the work in this thesis. Generating this body of work would have been impossible and far less enjoyable without Luke's contribution. Mostly I want to thank Luke for teaching me a great deal about the theory and measurement of photosynthesis, for the design and execution of the experiment in Chapter 2, photorespiration and CO_2 compensation point analysis in Chapter 3, field trial gas exchange work and statistical analysis in Chapter 4, and mesophyll conductance measurements in Chapter 5. I am very grateful to have had Luke as a mentor and collaborator throughout all parts of the research process.

I would like to acknowledge the exceptional contributions to the field of metabolic engineering made by my AgResearch supervisors Dr. Nick Roberts and Dr. Somrutai Winichayakul, which underly the physiology work in this thesis. I would also like to thank Nick and Somrutai both for providing exciting ideas and necessary encouragement over the years, and for showing the patience and generosity with lab resources which allowed me to investigate ideas freely. I have thoroughly enjoyed discovering some of the counterintuitive implications of their molecular manipulations.

I would like to thank my Lincoln University supervisor Associate Professor Mitchell Andrews for his excellent guidance in plant physiology and scientific writing. I would like to express my gratitude to Mitchell for being dependable and supportive, for helping with writing assignments at short notice, and for taking care of plants while I was hopping between islands. Finally, I would like to thank Mitchell for making me feel welcome in Lincoln and for getting me deadlifting properly.

I would like to thank everyone in the Plant Biotechnology group for providing generous help, advice, and the materials and equipment for experiments, and for being great company in the glasshouse and the lab. In particular I want to acknowledge Tracey Crowther and Philip Anderson for reliable and rapid FAMEs analysis, Hong Xue for WSC analysis and Ruth Cookson for Dot blot analysis. I want to thank Greg Bryan and Richard Scott for being great bosses, and Greg and Nick for having the master plan and for giving me a place within it. I would like to thank Kelly Nelson, Suhas Kadam, and the staff at the Greenley Memorial Research Centre for performing most of the field trial work, which gave this thesis relevance outside of the growth

chamber. I would like to thank Shen Hea for generous help with teaching and checking statistics and for useful R code. I would like to thank Catherine Kay for her excellent administrative services, which caused her (but spared me) much hassle sometimes. I would like to thank Cory Matthew for helpful comments and discussions during the planning and writing of Chapter 4, and for having made me aware of the high lipid project back in 2015. I would like to thank Roger Cresswell and the staff at the Lincoln analytical services laboratory for performing C/N analyses, and Felicity Jackson and the staff at the Massey Nutrition laboratory for perfoming pasture quality analyses.

The funding for my stipend and in-house experiments came from MBIE contract C10X1603 and SSIF fund PRJ0110170, while field trial costs were also covered by AgResearch industry partners; Dairy NZ, PGG Wrightson Seeds, Barenbrug Agriseeds, and Grasslanz Technology Ltd, for which I am grateful.

Finally I would like to thank my partner Jiajia Liu for keeping me happy and healthy over the last four years, for being great company during harvests and check-ups on experiments, for listening to me brainstorm, for unpaid labour, and for giving me a daily schedule to (usually) stick to. I would like to thank my parents Jonathan Gradwell and Nicky Beechey for encouragement throughout my education and for fostering my early interests in science, plants, food, and environment. I would like to thank all my friends, family, flatmates, co-workers and team-mates for providing many different types of welcome distractions from study over the years.

Table of Contents

List of Tables

List of figures

Table of acronyms

a[CO_2]; ambient atmospheric CO_2 concentration (400 p.p.m)

A_{area}; net photosynthetic rate per unit leaf area

A_{mass}; net photosynthetic rate per unit leaf mass

A_{sat}; net photosynthetic rate per unit leaf area under saturating irradiance

C_a; CO_2 concentration outside leaf

C_c; chloroplast CO_2 concentration

CE; rubisco carboxylation efficiency

C_i; intercellular CO_2 concentration

C_i*; intercellular CO_2 compensation point

C_i-C_c; CO_2 drawdown between intercellular airspace and chloroplast

Chl; chlorophyll

[Chl]; total chlorophyll per unit leaf area

CP; crude protein

Cyt *f*; cytochrome *f*

C16:0; palmitic acid

C16:1; palmitoleic acid

C18:0; stearic acid

C18:1; oleic acid

C18:2; linoleic acid

C18:3; linolenic acid

DAG; diacylglycerol

DGAT1; diacylglycerol *O*-acyltransferase 1

DOMD; dry organic matter digestibility

DW; dry weight

e[CO_2]; elevated atmospheric CO_2 concentration (760 p.p.m)

FA; fatty acid

FAME; fatty acid methyl-ester

F_m; maximum fluorescence

F_v; variable fluorescence

GC-MS; gas chromatography-mass spectometry

GE; gross energy

g_m; mesophyll conductance to CO_2

g_s; stomatal conductance to CO_2

HME; high metabolizable energy

HMW; high molecular weight

HL; high lipid

J; rate of electron transport

J_a; J derived via gas exchange under non-photorespiratory conditions

J_f; J derived via chlorophyll fluorescence under non-photorespiratory conditions

J_{max}; electron transport capacity

LA; leaf area per plant

LAI; leaf area per unit of ground area

LAR; total leaf area per unit of plant DW

LD; lipid droplet

LMF; leaf mass fraction

LMW; low molecular weight

ME; metabolizable energy

N; nitrogen

N_{area}; leaf nitrogen per unit area

NH_4^+; ammonium

N_e; leaf nitrogen invested in electron transport and ATP synthesis

N_{mass}; leaf nitrogen per unit mass

N_o; 'other' leaf nitrogen

NO_3^-; nitrate

N_p; leaf nitrogen invested in pigment-protein complexes

N_r; leaf nitrogen invested in rubisco

N_s; leaf nitrogen invested in soluble protein

$N_{s\text{-}r}$; leaf nitrogen invested in non-rubisco soluble protein

PAR; photosynthetically active radiation

PNUE; photosynthetic nitrogen use efficiency

$PNUE_{amb}$; photosynthetic nitrogen use efficiency under ambient irradiance

$PNUE_{sat}$; photosynthetic nitrogen use efficiency under saturating irradiance

PR; perennial ryegrass

PSI; photosystem I

PSII; photosystem II

R_d; day respiration

RGR; relative growth rate

RH; relative humidity

RMF; root mass fraction

SDS-PAGE; sodium dodecyl sulfate polyacrylamide gel electrophoresis

SLA; specific leaf area

TAG; triacylglycerol

T_0; isogenic first generation transgenic

T_2; third generation transgenic from a segregating population

VC; vector control

V_{cmax}; maximum rubisco carboxylation rate

V_o/V_c; ratio of rubisco oxygenation/carboxylation

WSC; water-soluble carbohydrate

WT; wild type control

Γ*; chloroplast CO_2 compensation point

Φ PSII; quantum efficiency of photosystem II

Chapter 1

Introduction

1.1 Challenges for agriculture in the 21st Century

Due to population growth and rising standards of living, demand for food and especially meat and milk products are projected to rise this century, which will place significant pressure to increase total agricultural production (Evans & Lawson, 2020). Simultaneously, many agricultural systems are expected to reduce their land and carbon footprint and to mitigate negative local externalities such as nitrogen losses. Further, agriculture must adjust to changes in climate that are expected to be mainly detrimental to plant growth (Rosenzweig et al., 2014). To achieve sustainable intensification will almost certainly require the 20th and early 21st century trends of increasing crop yields to continue (Balmford et al., 2018). For the most economically important grain crops however, opportunities to increase yield potential (the weight of harvested product per unit of ground area under optimum conditions) by increasing the efficiency of light capture and the harvest index have begun to plateau (Long et al., 2006). Therefore, much recent attention has shifted towards manipulating the fundamental processes underlying yield formation: photosynthesis and plant growth (Evans & Lawson, 2020; Zhu et al., 2020).

1.1.1 Requirements for plant growth

Yield potential is strongly associated with plant biomass accumulation (growth). Growth is primarily driven by the process of photosynthesis, during which light energy is used to convert atmospheric CO_2 and water into sugars and reducing equivalents. In addition to light, water and CO_2 substrate, photosynthesis requires the supply of nutrients, particularly nitrogen (N) from the soil. Sugars from photosynthesis are used to generate ATP, which together with NADH and NADPH, power growth and metabolic processes such as maintenance respiration, nutrient uptake and assimilation, and active transport (Poorter, 2002). The rate of plant growth is a function of total daily carbon assimilation from shoot photosynthesis, minus total daily carbon losses occurring throughout shoots and roots. The best descriptor of plant growth is relative growth rate (RGR), since increases in biomass are closely proportional to the biomass already present (Venus & Causton, 1979). However, when plants are grown in competition, RGR may be less suitable than total dry weight (DW) (Poorter et al., 1990).

1.1.2 *Lolium perenne*: economic importance and growth morphology

Grazed pastures occupy 70% of agricultural land worldwide and make a large contribution to global meat and milk supply (OECD, 2019). *Lolium perenne* L. (perennial ryegrass) (PR) is the primary plant species used in intensively managed pasture-based meat and milk production systems in temperate zones of Western Europe, Australia, and New Zealand (Chapman et al., 2017; McEvoy et al., 2011). The leafy component of PR 'tillers' (shoots) are the plant component that grazing animals consume. PR tillers consist of a basal meristem from which new leaves constantly develop, expand, then senesce. New leaves expand as a lamina attached to a sheath, and emerge from the encircling sheaths of older leaves, collectively called the 'pseudostem' (Parsons & Chapman, 2000). Once the rate of new leaf production is in equilibrium with the rate of senescence of older leaves, PR maintains three live leaves per tiller. Because PR leaf development, expansion and tillering occur near to the ground, PR 'swards' (canopies) can tolerate frequent defoliation. Defoliation removes most sward photosynthetic capacity, and the initial energy requirements for leaf area recovery come from remobilizing carbohydrate reserves in the remaining pseudostem (Fulkerson & Donaghy, 2001). Due to constant leaf turnover, regular defoliation is necessary to avoid leaf senescence and associated losses of sward nutritive value. Optimal management of PR swards involves adjusting the frequency and intensity of defoliation in order to maximize the long-term 'utilization' of pastures (i.e. the dynamic flow of digestible nutrients from plant photosynthesis to grazing animals) (Parsons & Chapman, 2000).

1.1.3 *Lolium perenne*: breeding for yield and nutritive value

Ruminant production is driven by the quantity and quality (nutritive value) of feed. PR nutritional quality traits receive less attention from PR breeders than traits related to DM yield, in part because of their relative difficulty of measurement and manipulation (Chapman et al., 2012). Breeding to improve PR DM yield aims to increase whole plant aerial biomass both annually and seasonally (Sampoux et al., 2011). Rates of genetic gain for PR DM yield have been estimated in the range of 0.2–0.6% per annum, with the majority of the improvement in yield concentrated in summer and autumn (Sampoux et al., 2011; Chapman et al., 2012). Due to the practical constraints of large scale phenotyping, much of the selection of PR in modern breeding programmes relies on visual assessment of PR plants grown in spaced plots or rows, and selection for aerial biomass occurs concurrently with other traits such as resistance to fungal rust (Faville et al., 2020; Gebremedhin et al., 2020). Genomic

selection in combination with high-throughput sensor-based phenotyping technologies are anticipated to increase the rates of genetic gain for PR DM yield (Faville et al., 2020; Gebremedhin et al., 2020).

PR is regarded as having superior nutritive value to most perennial pasture grasses due mainly to its high digestibility (Arojju et al., 2020; Capstaff & Miller, 2018). However, the performance of ruminants fed PR-based diets is significantly restricted by the overall nutritional composition of PR (Parsons et al., 2011). To illustrate, PR pasture-based dairy systems in NZ exhibit substantially lower per-animal production and higher emissions per kg of milk solids than feedlot dairy systems in Europe and the United States, where a high proportion of the diet is feed concentrate (Hagemann et al., 2011). There are strong economic and environmental incentives to enhance the PR nutritive value, in order to meet the production potential made possible by advances in animal genetics (Barrett et al., 2015; Ludemann et al., 2015). Previous successful targets for PR nutritive value improvement through breeding include increased digestibility (Sampoux et al., 2011; Wims et al., 2017) and increased leaf water-soluble carbohydrate (WSC) content (Edwards et al., 2007; Humphreys, 1989). Lipids contain over twice the energy density of carbohydrates, and as a dietary supplement can improve feed utilisation efficiency (Cosgrove et al., 2004; Schroeder et al., 2004). While increasing PR lipid content has historically ranked low among priorities for enhancing nutritional quality (Smith et al., 1997), renewed interest in enhancing forage lipid content through breeding has recently emerged (Morgan et al., 2020; Wilkinson et al., 2020).

1.2 Metabolic engineering to enhance plant lipid content

Oils are a class of lipids which are the most energy-dense metabolites found in plants and are a critically important commodity in food and fodder production. Global production of oilseed crops increased by 3.1% p.a. for the last decade, one of the highest growth rates for any agricultural commodity, with demand projected to continue rising (OECD, 2019). However, plant oil production is limited by the availability of suitable agricultural land and greater yields per hectare are required (FAO, 2019). Plant oils are typically extracted from seeds, with much of the plant's remaining biomass yielding levels too low for profitable extraction (Durrett et al., 2008). The main compound in plant oil, triacylglycerol (TAG), and its component fatty acids (FA) are synthesised from sugars derived from photosynthesis, a process which is highly demanding in terms of energy and reducing equivalents. This section gives an overview of FA

and TAG biosynthetic pathways and summarizes contemporary metabolic engineering strategies to enhance non-seed TAG content.

1.2.1 Leaf and seed lipids: natural roles

A typical leaf lipid profile reflects the structural roles of lipids in these organs. It consists predominately of polar lipids which make up plasma and organellular membranes. Neutral oils such as TAG are incapable of integrating into membranes, and instead form the hydrophobic core of short-lived lipid droplets (LDs); dynamic energy storage organelles with a phospholipid monolayer, embedded with proteins (Xu & Shanklin, 2016). Lipid storage is not a natural function of leaves, and so TAG exists in small quantities as a short-term intermediate for membrane turnover and remodelling (Chapman et al., 2013). Conversely, seeds specialize in energy storage and accumulate a significant proportion of their weight as TAG.

1.2.2 Fatty acid synthesis and triacylglycerol assembly

Fatty acid (FA) synthesis occurs in the plastid and involves a series of repeated additions of two carbon units to an elongating fatty acid chain. Briefly, glucose is converted into two three-carbon pyruvate molecules via glycolysis. Pyruvate is then converted into acetyl-CoA by the pyruvate dehydrogenase complex, releasing a CO_2 molecule in the process. Acetyl-CoA is converted to Malonyl-CoA by the acetyl-CoA carboxylase enzyme (ACCase), which is the committed step of FA synthesis. The fatty acid synthase complex transfers the Malonyl moiety to an acyl carrier protein and uses Malonyl-CoA as the primary substrate for FA chain elongation, which proceeds via repeated condensation reactions between acetyl-CoA and Malonyl-ACP (Ohlrogge & Jaworski, 1997). Each two carbon addition to an elongating FA chain utilizes 1 ATP and either 2 NADPH or 1 NADPH and 1 NADH as electron donors (Neuhaus & Emes, 2000).

When FA elongation is terminated, some FAs are exported from the plastid to the endoplasmic reticulum, where they are converted to acyl-coA molecules. Lipid biosynthesis proceeds via the ‘Kennedy pathway’, which involves sequential esterification reactions between glycerol-3-phosphate and the free acyl chains (with coA molecule recycling), or other chemical groups. The intermediate diacylglycerol (DAG) is used as a precursor for membrane lipid synthesis. Alternatively, DAG is used in the final and only committed step in the TAG biosynthesis pathway; addition of a third fatty acid. In the leaf, this step is predominantly catalysed by the

diacylglycerol *O*-acyltransferase 1 (DGAT1; EC2.3.1.20) enzyme, which co-limits the rate of TAG synthesis (Xu & Shanklin, 2016).

1.2.3 Metabolic engineering to enhance non-seed TAG

Metabolic engineering to increase TAG content in plant vegetative tissues is an ambitious strategy for meeting future plant oil demand (Durrett et al., 2008; Napier et al., 2014; Vanhercke et al., 2019). Many manipulations of TAG metabolism have been attempted, however early single-gene strategies failed to yield industrially-relevant increases in plant TAG (Vanhercke et al., 2014). For example, overexpression of the DGAT1 enzyme increased TAG assembly, but the resulting increase in plant lipid content was transient because the accumulated TAG was catabolized by TAG lipases, followed by FA recycling in the endoplasmic reticulum and beta-oxidation of FAs in the peroxisome (Winichayakul et al., 2008). To convey the property of TAG accumulation to a tissue requires that the long-term rate of rate of catabolism relative to synthesis is reduced (Allen, 2016). Therefore, the most successful engineering strategies have manipulated at least two of the following components of TAG metabolism: increasing fatty acid synthesis (push), increasing TAG assembly (pull), and reducing lipid turnover (protect) (Vanhercke et al., 2019; Vanhercke et al., 2014).

1.2.4 DGAT1 + cysteine-oleosin expression in *Arabidopsis thaliana*

An elegant two-gene strategy to elevate lipids in the leaves and roots of the model plant species *Arabidopsis thaliana* was reported by Winichayakul et al. (2013). The innovation allowing long-term TAG accumulation involved constitutive expression of a novel oleosin protein engineered to contain cysteine residues in its amphipathic arms (cysteine-oleosin). When co-expressed with Arabidopsis diacylglycerol *O*-acyltransferase (DGAT1; the final enzyme in the triacylglycerol (TAG) biosynthesis pathway), cysteine-oleosin conferred enhanced stability to lipid droplets (LDs) in vegetative tissues, allowing lipids to accumulate to approximately 7% of DW and increasing gross energy (GE) content by up to 0.8 kJ gDW^{-1}.

Oleosin proteins occur naturally in seeds and pollen and embed into the phospholipid outer layer of LDs, encapsulating and protecting them against lipase entry. Oleosins consist of a conserved hydrophobic central domain which extends into the hydrophobic core of LDs, and N and C-terminal amphipathic ‘arms’ which sit on the surface of LDs and are exposed to the cytoplasm (Tzen & Huang, 1992). Winichayakul et al. (2013) engineered between one and

seven cysteine residues along the amphipathic arms of oleosins isolated from *Sesame indicum*. Arabidopsis lines co-expressing DGAT1 and an oleosin with three cysteine residues introduced into each arm (termed 'high metabolizable energy' or 'HME' plants) accumulated high lipid levels and displayed increased C18:1 and C18:2 as a proportion of total FA. This configuration of cysteine residues resulted in the formation of inter-oleosin disulphide bonds between the arms of neighbouring oleosins on the surface of LDs, which had the effect of 'crosslinking' them (Winichayakul et al., 2013). LDs encapsulated by crosslinked cysteine-oleosin proteins showed a high level of resistance to cysteine-protease degradation, and partial resistance to serine-proteases compared to a native oleosin protein *in vitro* (Winichayakul et al., 2013). The authors proposed that cysteine-oleosin conferred greater stability to LDs *in planta* by slowing the entry of TAG lipases into LDs. This allowed TAG to accumulate in the leaves and roots, and the diversion of FAs into stable LDs generated a continuous demand for *de novo* FA synthesis (Winichayakul et al., 2013).

A remarkable finding reported by Winichayakul et al. (2013) was that HME expression gave Arabidopsis an increase in CO_2 assimilation rate per unit leaf area, and an increase in shoot biomass relative to WT. This was not observed in plants expressing DGAT1 and an un-modified oleosin. A positive correlation between FA/TAG accumulation and CO_2 assimilation rate was found among independent HME lines. It was speculated that a 'CO_2 recycling' phenomenon associated with increased *de novo* FA synthesis in green seeds (Schwender et al., 2004) could account for the increase in CO_2 assimilation rate in HME Arabidopsis leaves (Winichayakul et al., 2013), but CO_2 recycling was not demonstrated experimentally. Since the publication of Winichayakul et al. (2013), no reported manipulations of TAG metabolism have led to increased plant growth.

1.2.5 DGAT1 + cysteine-oleosin expression in *Lolium perenne* leaves

A promising commercial application of the HME technology is in enhancing the leaf energy density and nutritive value of the economically important pasture species *Lolium perenne* (PR). Traditional plant breeding methods offer restricted potential for increasing the lipid content of PR due to limited natural variation in PR herbage lipids (Hegarty et al., 2013; Morgan et al., 2020). Further, the observed variation in PR lipid levels has a large management and environmental component (Dewhurst et al., 2003), which has the potential to mask the comparatively smaller genetic component (Hegarty et al., 2013). Given that root TAG

accumulation is of no agronomic benefit in PR, the HME technology has been expressed under light-regulated promoter sequences. Preliminary analysis of multiple HME lines showed that like HME Arabidopsis, HME PR has elevated leaf FA and TAG, greater proportions of C18:1 and C18:2, and possibly faster growth. HME lines contained 23–100% more leaf FA (4.3–7.0 %DW) than wild type (WT) and vector control (VC) lines (with ~3.5 %DW), while leaf TAG accumulated to 2.5 %DW in the highest expressing HME line, compared to only 0.18 %DW in the WT (Pers. Comm., Dr Somrutai Winichayakul). Both leaf FA and TAG content correlated positively with the expression of cysteine-oleosin. All of these changes were sustained over a typical PR regrowth interval (3–4 weeks) under repeated mechanical defoliation. Preliminary observations revealed a possible leaf expansion and/or regrowth advantage in the HME lines with ~5–6 %DW leaf FA content relative to WT and VC, while HME lines with a leaf FA content greater than ~6.5 %DW appeared to incur a growth penalty (Pers. Comm., Dr Somrutai Winichayakul). However, these observations were not demonstrated in formal growth (RGR) experiments.

1.3 Research objectives

The efficacy of the HME technology to enhance PR leaf lipids could deliver the economic and environmental benefits of higher pasture energy density whilst maintaining low input pastoral farming practices. However, the suitability of HME PR for adoption into pastoral agriculture is unknown because it is unclear how HME expression influences the physiology of PR under diverse growing conditions. There has been limited basic research on the effects of engineering higher lipids on carbon assimilation physiology. There are very few reports on high lipid plant performance under realistic growing conditions, and none for high lipid pasture species. The primary research objective of this thesis was to test the hypothesis that leaf HME expression could increase *Lolium perenne* growth. The second research objective was to investigate whole-plant, and especially leaf-level physiological, morphological, and biochemical traits related to photosynthesis, that could account for increased growth under variable N supply, and both ambient and elevated atmospheric [CO_2]. The final research objective was to study the translation from spaced pots indoors to field canopies, of the FA, GE and growth enhancing traits in HME segregating PR populations, in order to quantify potential agronomic advantages of an HME PR cultivar.

Chapter 2

DGAT1 + cysteine-oleosin expression corresponds with increased leaf fatty acids, photosynthesis, specific leaf area and growth in *Lolium perenne*

2.1 Introduction

Metabolic engineering to increase vegetative oil is seen as a promising strategy to increase plant oil production (Napier et al., 2014). While this strategy has received growing attention for increasing plant oils in species used for biofuel and fodder, little attention has been paid to engineering elevated plant oils in pastoral species for improved forage quality. The main compound in plant oil, triacylglycerol (TAG), and its component fatty acids (FA), represent the primary targets for bioengineering strategies. Early attempts to increase vegetative TAG and FA focused on single gene transformations, resulting in small increases in both TAG and FA (Vanhercke et al., 2014). Greater increases have resulted from multi-gene transformations, the most successful of these producing 30–33% TAG (as a %DW) in the leaves of *Nicotiana tabacum* (Chu et al., 2020; Vanhercke et al., 2017). However, most of these gene combinations have also coincided with a growth penalty (Vanhercke et al., 2019). The only exception is the combination of diacylglycerol *O*-acyltransferase (DGAT1) and cysteine-oleosin expression (collectively 'high metabolizable energy' or 'HME') reported by Winichayakul et al. (2013), which resulted in increased FA content and coincided with an increase in both shoot biomass and CO_2 assimilation per unit leaf area (1.2.4).

Lolium perenne L. (perennial ryegrass) (PR) is for several reasons an excellent candidate for HME transformation. It is of considerable economic importance, representing the major pastoral species in many parts of Europe, Australia, and New Zealand, due to its ease of establishment, tolerance of frequent grazing and high digestibility (Chapman et al., 2017). Initial examination has shown that HME PR exhibits increased leaf FA and gross energy (as a percentage of DW) compared to untransformed control PR (Winichayakul et al., 2020). However, the growth and photosynthesis benefit observed in HME Arabidopsis (Winichayakul et al., 2013) has yet to be convincingly demonstrated in PR. Examination of multiple HME PR lines varying in transgene expression is needed to test the theory that HME can increase photosynthesis and growth in PR. In this chapter, five HME-transformed PR lines derived from three genetic backgrounds were examined through the measurement of leaf fatty acids,

water-soluble carbohydrates, relative growth rate, specific leaf area (SLA) and photosynthesis. An additional objective of examining multiple HME lines was to test whether the level of HME expression corresponded with traits related to photosynthesis and growth, and to identify a high-expressing HME line suitable for detailed investigation of photosynthesis-related traits at both the whole-plant level (Chapter 3), and at the level of leaf physiology and biochemistry (Chapter 5).

2.2 Materials and methods

2.2.1 Plant Transformation

The coding sequences for a cysteine-oleosin and diacylglycerol *O*-acyltransferase (DGAT1; EC2.3.1.20; S205A mutation) were optimised for expression in rice and placed in a back-to-back orientation under the control of the rice CAB and rubisco small subunit promoters, respectively. For Agrobacterium-mediated transformation, the expression cassette was cloned into the pCAMBIA1300 binary vector while for particle bombardment the cassette was cloned into a pUC-based vector. Transformed lines were generated from *Lolium perenne* callus induced from immature inflorescences and transformed by *Agrobacterium*-mediated transformation or particle bombardment. Plants generated from *Agrobacterium*-mediated transformation were generated as per Bajaj et al. (2006) while plants from microprojectile bombardment (gene gun) used the method described by Altpeter et al. (2000).

2.2.2 SDS-PAGE analysis of DGAT1 and cysteine-oleosin

Protein samples were prepared by collecting four fresh leaf blades (approximately 2 cm long) in a 2-ml screw cap micro tube containing 150 µl of sterile H_2O, 200 µl of 2x protein loading buffer [1:2 diluted 4x lithium dodecyl sulphate (LDS) sample buffer (Life Technologies, Carlsbad, CA, USA)], 8 M urea, 5% [v/v] β-mercaptoethanol, 0.2 M dithiothreitol and 40 µl of NUPAGE™ sample reducing agent (NP0009, ThermoFisher Scientific, Waltham, MA, USA). The mixtures were homogenised using the Bead Ruptor 24 model (Omni International, Kennesaw, GA, USA). The samples were heated at 70°C for 10 min, centrifuged at 20,000 g for 30 sec and collected for the soluble protein suspension. Equal quantities of proteins were determined and separated by SDS-PAGE (Mini-PROTEAN® TGX stain-free™ precast gels; Bio-Rad, Hercules, CA, USA) and blotted onto Bio-Rad polyvinylidene difluoride (PVDF) membrane for the DGAT1 immunoblotting. Equivalent amounts of proteins were separated on gradient 4–12% Bis-Tris gel (NUPAGE; Life Technologies) and blotted onto nitrocellulose membrane for the cysteine-

oleosin immunoblotting. Immunoblotting was performed as described previously in (Winichayakul et al., 2013). Chemiluminescent activity was developed using WesternBright ECL spray (Advansta, Menlo Park, CA, USA) and visualised by ChemiDoc™ imaging system (Bio-Rad Laboratories Inc.). Volume intensity of protein bands was quantified using Image Lab™ software for PC version 5.2.1 (Bio-Rad Laboratories Inc.).

2.2.3 Plant material and growing conditons

Replicate plants consisted of isogenic clones. The T_0 control genotypes (WT1-3) were untransformed and were selected for amenability to transformation and regeneration. The T_0 HME genotypes were derived from independent WT transformation events which resulted in successful incorporation of the HME construct into their genome. Five T_0 HME PR lines (labelled HME1-5) were selected from three genetic backgrounds. The HME1 and HME2 lines were generated from an 'Alto' cultivar control genotype labelled WT1. The HME3-5 lines were generated from two 'Impact' cultivar individuals labelled WT2 and WT3. Clonal replicates were generated from mature, vegetative plants by splitting them into ramets consisting of 5 tillers and cutting to 10 cm of combined root and shoot length. A total of 40 x 5-tiller ramets were produced for each line, 10 of which were immediately harvested to confirm comparable starting weights (Supplementary table A1.1). The remaining 30 ramets per line were transplanted into 1.3 L washed sand. Plants were grown in a controlled temperature room with ~600 µmol photons m^{-2} s^{-1} red/blue light provided by 600W NanaPro LED lights (LEDgrowlights, Hamilton, NZ), 20 °C/15 °C day/night temperature and a 12 h photoperiod. While the ramets established a root system, pots were flushed thrice weekly with 100 ml of basal nutrient media described in Andrews et al. (1989) containing N as 2 mM KNO_3. Preliminary work indicated that supplying sub-optimal NO_3^- limited establishment phase growth enough to avoid 'pot-limited' conditions (Poorter et al., 2012a) early in the subsequent regrowth phase, while also avoiding severe 'transplanting shock'.

2.2.4 Relative growth rate

Three weeks after propagation, shoot material was harvested 5 cm above the sand, and used to rank plants from smallest to largest. The five smallest and five largest plants per line were discarded and 10 of the remaining 20 plants per line were randomly selected and harvested (post-establishment harvest). The remaining ten plants per line were grown for another three weeks, with 4 mM NH_4NO_3 applied to pots as described above and harvested (final harvest).

Relative growth rate (RGR) was calculated as in Hoffmann & Poorter (2002); RGR = (ln W_2 – ln W_1)/(t_2 – t_1) where W_1 = post-establishment dry weight, W_2 = final harvest dry weight, t_1 = day 22 and t_2 = day 43. RGR calculation eliminated possible confounding differences in absolute DW data arising from clonal propagation.

2.2.5 Photosynthetic gas exchange

One week prior to the final harvest, three tillers were selected per plant, and on the youngest fully expanded leaves, net photosynthesis per unit leaf area (A_{area}) and stomatal conductance (g_s) was analysed using a Li-COR 6800 infrared gas exchange system (Li-COR Biosciences Ltd, Nebraska, USA). Leaves were 'adjusted' under the following chamber conditions: 600 µmol photons m^{-2} s^{-1} red/blue light, at 400 ppm CO_2, 70% relative humidity and 20 °C for 15 mins prior to data-logging. The three leaves were then abscised, photographed, dried, and weighed. Leaf area was calculated using GIMP 2.8.22 (GNU Image Manipulation Program, http://www.gimp.org) and specific leaf area (SLA) was calculated as leaf area divided by DW. Net photosynthesis per unit leaf DW (A_{mass}) was calculated as A_{area} x SLA and total projected leaf area was calculated as SLA x total leaf DW.

2.2.6 Fatty acid analysis

Leaf material was collected on the final day of the experiment and immediately frozen in liquid nitrogen, then freeze-dried and ground via a bead mill. From a 10 mg subsample, fatty acids (FA) were extracted in hot methanolic HCl, modified after Browse et al. (1986). FA were quantified by GC-MS (QP 2010 SE, Shimadzu Corp., Kyoto, Japan) against an internal standard of 10 mg C15:0, and total FA was calculated as the sum of palmitic acid (16:0), palmitoleic acid (16:1), stearic acid (18:0), oleic acid (18:1), linoleic acid (18:2) and linolenic acid (18:3).

2.2.7 Water-soluble carbohydrate quantification

Total water-soluble carbohydrates (WSC) were analysed using the anthrone method. Leaves were sampled at midday and immediately frozen in liquid nitrogen. Using 25 mg freeze-dried, ground leaf material, low molecular weight carbohydrates (LMW) were twice extracted in 1 ml, 4:1 EtOH: H_2O at 65 °C for 30 mins, centrifuged, and the supernatant was collected and combined after each extraction. High molecular weight carbohydrates (HMW) were then twice extracted in 1 ml H_2O at 65 °C for 30 mins, centrifuged, and the supernatant was collected and combined after each extraction. The carbohydrate extracts were mixed with anthrone reagent (Sigma-Aldrich, St Louis, MO, USA) for 25 mins at 65 °C, then A_{620} was

determined using a Versamax tuneable plate reader (Molecular Devices Corporation, Sunnyvale, CA, USA) and compared to LMW and HMW standards, prepared using sucrose and insulin, respectively.

2.2.8 Statistical analysis

All statistical analyses as well as normality and variance tests were performed using R version 3.3.3 (R Foundation, Vienna, Austria). Two-way factorial ANOVAs were used to evaluate the relationship between each of the following dependent variables: FA, WSC, gas exchange parameters, biomass, RGR, SLA and independent factors: genetic background (3 levels) and line (8 levels i.e. 3 WT and 5 HME). Benjamini-Hochberg (BH) tests were used for post-hoc analysis. Kruskal-Wallis tests were used to evaluate the effect of HME expression on the non-normal variables; projected total leaf area and A_{mass}, and their *p*-values were adjusted using a Bonferroni correction. The relationship between the relative increase in fatty acids between HME lines, and relative changes in DGAT1 and cysteine-oleosin expression, leaf WSCs, SLA, and RGR were identified by fitting linear, polynomial (2^{nd} or 3^{rd} order), logarithmic and exponential models to each and the best fit was identified by comparing the models using ANOVAs.

2.3 Results

2.3.1 Leaf biochemistry

Five T_0 HME lines were examined, four generated via *Agrobacterium*-mediated transformation (HME1-4), one via gene gun (HME5), and the presence of transgenic proteins was confirmed via SDS-page analysis (Figure 2.1). All HME lines displayed a significant increase in the percentage DW of leaf fatty acids (FA), ranging from 18–75% of the respective non-transformed wild-type (WT) control level (Figure 2.1). For the HME lines, total leaf FA constituted 4.7–5.1% of leaf DW, whereas WT lines ranged from 2.9–4% of leaf DW (Table 2.1). The relative increase in total FA for each HME line, compared to respective WT control, strongly correlated with DGAT1 expression (r^2=0.82; p=0.03), with the HME5 line exhibiting both the highest DGAT1 protein content and FA increase relative to WT (Figure 2.1). No significant correlation was found between cysteine-oleosin protein content and FA (r^2=0.67; p<0.05).

Leaf low molecular weight water-soluble carbohydrates (LMW) and high molecular weight water-soluble carbohydrates (HMW) were significantly lower in HME3-5, compared to the respective WT controls (Table 2.1), resulting in a reduction in total leaf water-soluble carbohydrates (WSC) of 57–69% (Table 2.1). In contrast, there was no statistical difference in LMW, HMW or total WSC between HME1, HME2 and the WT1 control (Table 2.1). The relative difference in total leaf WSC for each HME line, compared to the respective WT control, correlated negatively with the relative increase in total leaf FA for each HME line (r^2=0.95; p=0.04; Figure 2.2) i.e. those HME lines with the largest increase in leaf FA also displayed the largest reduction in leaf WSC. Both LMW and HMW carbohydrates were significantly lower for WT1, than for both WT2 and WT3 (Table 2.1).

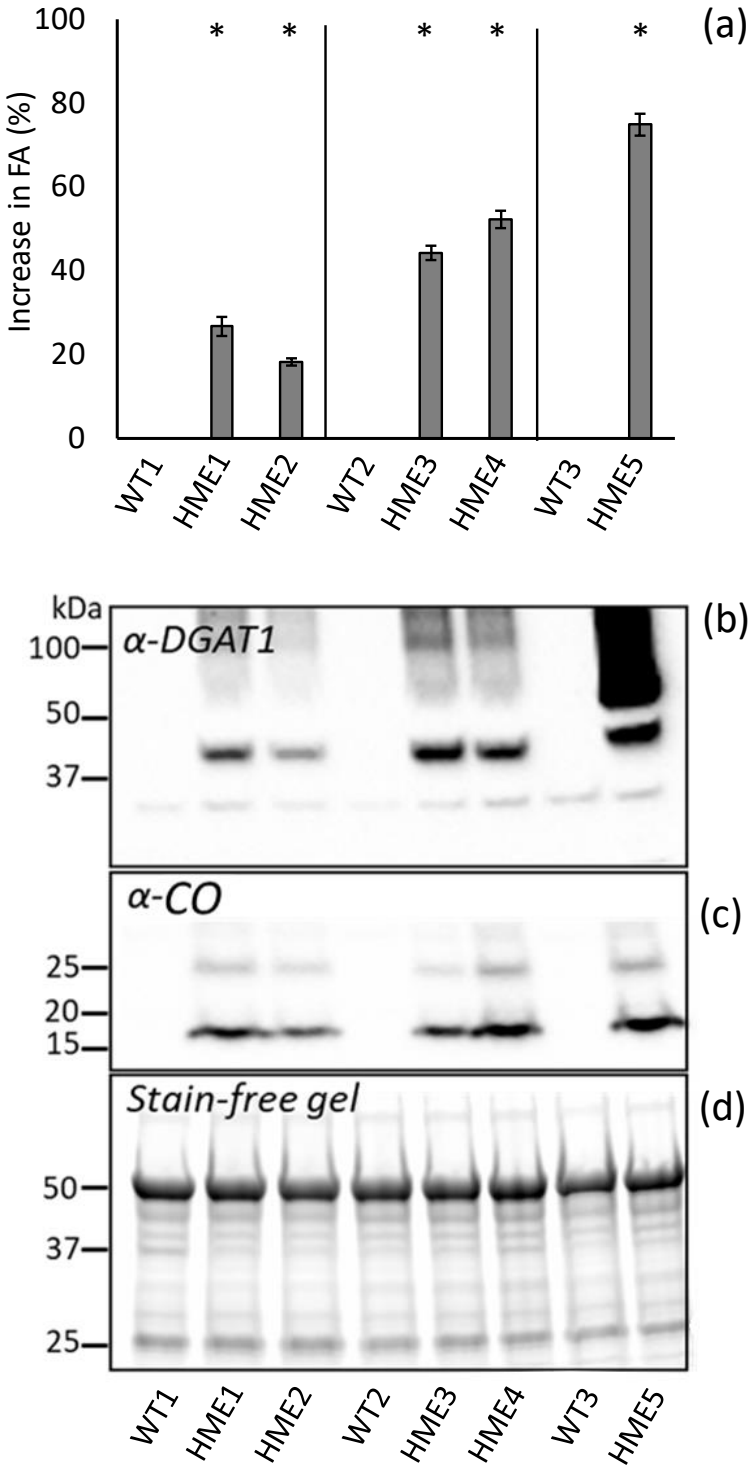

Figure 2.1. Percent difference in mean leaf fatty acids for five independently transformed clonal HME *Lolium perenne* genotypes (HME1-5) and three non-transformed control genotypes (WT1-3) (a), alongside recombinant protein contents for DGAT1 (b), cysteine-oleosin (c), and a stain-free gel showing equal protein loading for each cell (d). Matching genetic backgrounds are grouped together. * = p<0.01.

Table 2.1. Total leaf fatty acids (FA), low molecular weight (LMW), high molecular weight (HMW), and total leaf water-soluble carbohydrates (WSC) for five independently transformed clonal HME *Lolium perenne* genotypes (HME1-5) and three non-transformed control genotypes (WT1-3) regrown under 4 mM NH_4NO_3.

	Total leaf FA (mg gDW^{-1})	**LMW WSC (mg gDW^{-1})**	**HMW WSC (mg gDW^{-1})**	**Total leaf WSC (mg gDW^{-1})**
WT1	40.4 ± 1.0	67.1 ± 5.2	4.4 ± 1.1	71.5 ± 6.0
HME1	51.2 ± 0.9 ***	72.3 ± 6.0	4.1 ± 1.3	76.4 ± 7.1
HME2	47.8 ± 0.3 ***	78.7 ± 5.6	2.4 ± 0.4	81.1 ± 5.8
WT2	36.4 ± 1.0	97.5 ± 6.6	44.9 ± 7.0	142.4 ± 12.6
HME3	52.5 ± 0.6 ***	54.8 ± 3.4 ***	2.7 ± 0.3 ***	57.4 ± 3.6 ***
HME4	55.4 ± 0.8 ***	58.8 ± 3.3 ***	3.4 ± 0.4 ***	62.1 ± 3.7 ***
WT3	29.2 ± 1.0	165.8 ± 6.0	74.1 ± 5.1	239.9 ± 8.6
HME5	51.1 ± 0.8 ***	65.7 ± 6.5 ***	8.0 ± 1.3 ***	73.7 ± 7.3 ***

Matching genetic backgrounds are grouped together. Data represent means ± S.E. (n=10). Asterisks indicate statistically significant differences within different genetic backgrounds, obtained from two-way ANOVA, with p-values adjusted according to the BH method. *** = p<0.001.

2.3.2 Growth and photosynthesis

Of the five T_0 HME lines examined here, two (HME1 and HME2) showed no significant difference in net photosynthesis per unit leaf area (A_{area}) or biomass, compared to WT1 (Table 2.2; Table 2.3). In contrast, HME3-5 were between 59–82% larger than their respective WT controls at final harvest, displaying a significant increase in shoot, root, and total plant DW (Table 2.2). Differences in establishment growth (i.e. the growth in the three weeks following propagation) explained some of the total plant DW difference for these lines (Supplementary table A1.1), however, the relative growth rate (RGR) between the post-establishment harvest and final harvest was also significantly higher for HME3-5, compared to the respective WT controls (Table 2.2). The increase in RGR for each line, compared to the respective WT controls, appeared to correlate positively with the percent increase in leaf fatty acids (Figure 2.2), and this correlation was nearly significant at the 5% level (r^2=0.93; *p*=0.065). The percent increase in leaf FA did correlate positively with an increase in specific leaf area (SLA) (Figure 2.2; r^2=0.99; *p*=0.01) and SLA was significantly higher for HME3 and HME5 compared to the respective WT controls (Table 2.3). HME4 SLA did not significantly differ from WT2 (Table 2.3). Regardless, HME3-5 all displayed a significant increase in A_{mass} and in projected total leaf area (leaf DW x SLA), compared to the respective WT controls (Table 2.2). HME3-5 displayed a significant increase in A_{area} compared to respective WT controls (Table 2.3). HME3 and HME4 also displayed a significant increase in g_s compared to WT2, however, no statistical difference in g_s was detected for HME5 compared to WT3 (Table 2.3).

Table 2.2. Shoot, root, and total plant DW, relative growth rate (RGR), and total projected leaf area (LA) for five independently transformed clonal HME *Lolium perenne* genotypes (HME1-5) and three non-transformed control genotypes (WT1-3) regrown under 4 mM NH_4NO_3.

	Shoot DW (g)	**Root DW (g)**	**Total DW (g)**	**RGR ($g\ g^{-1}\ day^{-1}$)**	**Total LA (cm^2)**
WT1	2.8 ± 0.1	0.9 ± 0.06	3.7 ± 0.1	0.088 ± 0.003	444 ± 19
HME1	2.7 ± 0.1	0.7 * ± 0.03	3.4 ± 0.1	0.094 ± 0.002	451 ± 15
HME2	2.7 ± 0.1	0.9 ± 0.07	3.6 ± 0.2	0.090 ± 0.003	454 ± 11
WT2	1.4 ± 0.1	0.4 ± 0.03	1.9 ± 0.1	0.077 ± 0.002	206 ± 15
HME3	2.4 ± 0.1 **	0.9 ± 0.05 **	3.3 ± 0.1 ***	0.086 ± 0.002	359 ± 9 ***
HME4	2.5 ± 0.1 **	0.9 ± 0.06 **	3.4 ± 0.1 ***	0.091 ± 0.003 **	415 ± 19 ***
WT3	2.1 ± 0.1	0.5 ± 0.04	2.5 ± 0.2	0.070 ± 0.002	197 ± 17
HME5	3.2 ± 0.2 **	0.8 ± 0.06 **	4 ± 0.3 ***	0.079 ± 0.003 *	433 ± 31 ***

Matching genetic backgrounds are grouped together. Data represent means ± S.E. (n=10). Asterisks indicate statistically significant differences within different genetic backgrounds, obtained from two-way ANOVA, with p-values adjusted according to the BH method. * = p<0.05, ** = p<0.01, *** = p<0.001.

Table 2.3. Specific leaf area (SLA), photosynthetic rate per unit leaf area (A_{area}) and stomatal conductance (g_s) measured at 600 µmol photons m^{-2} s^{-1}, and photosynthesis per unit leaf mass (A_{mass}) for five independently transformed clonal HME *Lolium perenne* genotypes (HME1-5) and three non-transformed control genotypes (WT1-3) regrown under 4 mM NH_4NO_3.

	SLA (cm^2 gDW^{-1})	**A_{area}** (µmol m^{-2} s^{-1})	**g_s** (mol m^{-2} s^{-1})	**A_{mass}** (µmol gDW^{-1} s^{-1})
WT1	274 ± 8	17.4 ± 0.7	0.27 ± 0.01	0.475 ± 0.021
HME1	283 ± 9	16.6 ± 0.9	0.26 ± 0.02	0.468 ± 0.028
HME2	284 ± 8	17.6 ± 1.0	0.28 ± 0.02	0.499 ± 0.029
WT2	260 ± 15	11.6 ± 0.5	0.15 ± 0.01	0.301 ± 0.020
HME3	290 ± 5 *	18.5 ± 0.3 ***	0.34 ± 0.01 ***	0.536 ± 0.011 ***
HME4	287 ± 8	17.3 ± 0.3 ***	0.30 ± 0.01 ***	0.497 ± 0.013 ***
WT3	213 ± 8	12.0 ± 0.5	0.20 ± 0.01	0.256 ± 0.017
HME5	343 ± 9 ***	14.4 ± 0.7 *	0.20 ± 0.01	0.493 ± 0.027 ***

Matching genetic backgrounds are grouped together. Data represent means ± S.E. (n=10). Asterisks indicate statistically significant differences within different genetic backgrounds, obtained from two-way ANOVA, with p-values adjusted according to the BH method. * = p<0.05, ** = p<0.01, *** = p<0.001.

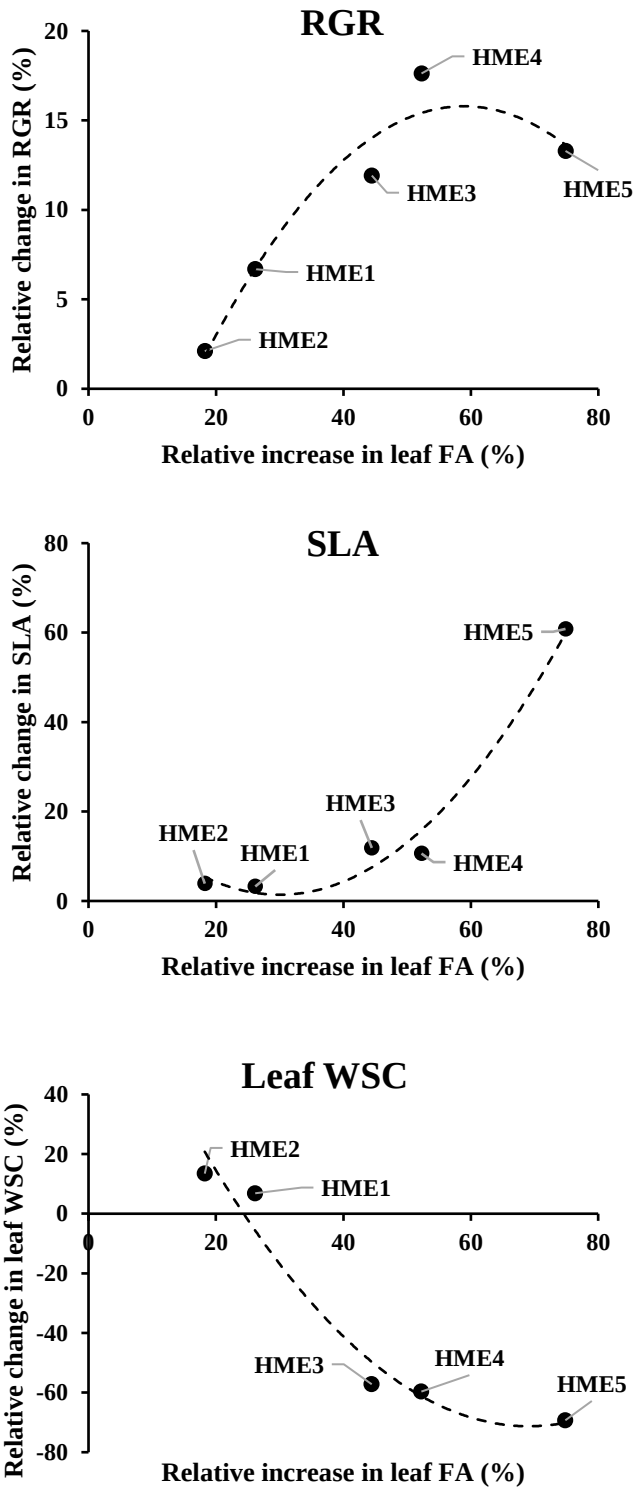

Figure 2.2 Relationship between relative increase in leaf FA concentration versus relative changes in whole-plant relative growth rate (RGR), specific leaf area (SLA), and leaf water-soluble carbohydrate (WSC) for five independently transformed clonal HME *Lolium perenne* genotypes (HME1-5) compared to corresponding non-transformed controls. Plants were regrown under 4 mM NH_4NO_3. The curved dotted lines indicate a significant non-linear relationship at $p<0.1$.

2.4 Discussion

Co-expression of DGAT1 + cysteine-oleosin (HME) in the leaves of *Lolium perenne* (PR) increased fatty acid (FA) content (Figure 2.1), which coincided with several other biochemical, physiological, and morphological changes in leaves. Leaf FA correlated positively with DGAT1 protein content (Figure 2.1) and for those lines with the largest increase in FA, there was a significant reduction in leaf water-soluble carbohydrate (WSC) content, in both the LMW and HMW fractions (Table 2.1), and a significant increase in A_{area} and especially A_{mass} (Table 2.3). For HME5, the line with the largest relative increase in leaf FA, there was a strongly significant increase in specific leaf area (SLA) (Table 2.3). A repeat SLA measurement was performed for the lines WT2 and HME4, and here, HME4 SLA was significantly higher than for WT2 (Supplementary table A1.2). First generation (T_0) transgenics were used in this experiment, which required clonal propagation to generate replicates. Since changes in plant DW are proportional to the biomass present at the beginning of a period (Causton & Venus, 1981), a relative growth rate (RGR) measurement was used to account for possible differences in plant size at the beginning of the growth measurement phase (i.e. the regrowth). Collectively, these data showed that for multiple clonal HME lines, the elevation of FA in leaves, at the expense of leaf WSC, coincided with traits that increased net carbon assimilation and subsequently increased RGR. The finding that HME expression can enhance PR shoot growth is consistent with earlier observations in Arabidopsis (Winichayakul et al., 2013). The inclusion of a root DW and whole plant RGR measurement ruled out the possibility that the HME growth advantage could be explained by an increase in partitioning of DW from roots to shoots.

2.4.1 Enhanced growth rate in HME *Lolium perenne* depends upon reduced leaf carbohydrate

The mechanisms by which HME expression increases growth and photosynthesis remain speculative and were not a major focus of this chapter. While all five HME lines displayed an increase in leaf FA, only the lines with a significant reduction in leaf WSC (HME3-5) displayed an increase in A_{area} and A_{mass}. Similarly, the high SLA trait was only present in HME3-5 (Table 2.3; Supplementary table A1.2); the lines with the largest relative increase in FA and largest relative reduction in WSC. We also found an increase in shoot, root, and total plant DW and RGR (Table 2.2) for those lines with a significant reduction in WSC. Those HME lines with small increases in FA and no change in leaf WSC displayed no change in SLA, A_{area}, A_{mass}, total plant DW or RGR. Regulation of photosynthetic capacity is determined by, among other things, the

availability of carbon (source strength), relative to the demand for carbon (sink strength) and leaf carbohydrate content plays a key role in signalling carbon availability (Paul & Foyer, 2001). The correlative data here are consistent with the hypothesis that a shift in carbon allocation from sugars to lipids may be responsible for inducing the changes which increase carbon assimilation and growth in HME PR.

2.4.2 Enhanced growth rate in HME *Lolium perenne* may be cultivar-dependent

Only three of the five HME lines examined displayed an increase in photosynthesis and growth compared to the respective WT controls, and the reason for this inconsistency was not clear. Perhaps carbon allocation into lipids was too low in HME1 and HME2, and greater HME expression is required. Alternatively, the morphological and physiological responses to HME expression may differ depending on the genotype or cultivar used for transformation. HME3-5; the lines that displayed increased photosynthesis and growth, were derived from transformation genotypes from the cultivar 'Grasslands Impact'. In contrast, HME1 and HME2 were derived from a transformation genotype from the cultivar 'Alto', a newer cultivar with 'Grasslands Impact' and 'NZ Agriseeds Bronsyn' in its pedigree (Zhong, 2017). Why the effect of HME differed amongst these transformation genotypes is a matter of speculation, however, a number of those traits affected by HME transformation in the 'Impact' transformation genotypes (an increase in growth, photosynthesis and a decrease in leaf sugar) were already present in the 'Alto' transformation genotype. It may be that physiological plasticity is greater in the 'Impact' background, and there is little capacity to increase photosynthesis or growth in certain genetic backgrounds, such as 'Alto', via addition of a new carbon sink. An assessment of high expressing HME events in 'Alto' and other genetic backgrounds is required to test these ideas (Chapter 4; Chapter 5).

2.4.3 Growth strategy tradeoffs

Plant growth strategies often represent a trade-off between carbon acquisition and stress resilience (Wright et al., 2004). For example, acclamatory responses to drought stress include down-regulation of photosynthesis, and reduced SLA and stomatal conductance (g_s) (Chaves et al., 2003); traits which mitigate water loss but impair CO_2 assimilation. Here, we observed a significant increase in g_s for HME3 and HME4 compared to WT2 (Table 2.3). Additionally, given that HME5 exhibited an increased SLA (Table 2.3), total transpiration was likely higher for this line as well. Given these observations, there is a need to assess HME PR in the field,

and under water limited conditions. Regardless, HME1 and HME2 show that modest increases in FA accumulation can be achieved without secondary effects on growth and photosynthesis.

Chapter 3

DGAT1 + cysteine-oleosin expression enhances *Lolium perenne* carbon capture especially under high N and elevated CO_2

3.1 Introduction

Greater yields from major crops are required to ensure food security in the face of growing global demand for food and energy. Two compelling strategies for enhancing food security are increasing photosynthesis (Long et al., 2006), and engineering higher levels of valuable nutrients such as lipids into plant tissues (Vanhercke et al., 2019). Genetic manipulation of CO_2 capture and light energy use efficiency could feasibly enhance photosynthesis, growth, and yield (Wu et al., 2019). However, translating improved photosynthesis into greater yields will depend upon the capacity for plants to effectively utilize or store additional photosynthates through sink development (Paul & Foyer, 2001; White et al., 2015). Plant-derived oils are an economically valuable, energy-dense carbon sink in plants, containing approximately 38 kJg^{-1}. Using metabolic engineering, a number of groups have reported large and sustained increases in lipids in leaves and other non-seed organs, some of which are being tested in the field as oil production platforms (Hofvander et al., 2016; Zale et al., 2016). However, most studies also report plant growth penalties associated with oil accumulation (Vanhercke et al., 2019).

Long-term storage of lipids in the leaves and roots of *Arabidopsis thaliana*, mainly in the form of TAG, was achieved when the diacylglycerol *O*-acyltransferase (DGAT1) enzyme was co-expressed with cysteine-oleosin (1.2.4; Winichayakul et al., 2013). This novel lipid droplet-encapsulating protein slowed the degradation of lipid droplets in vegetative tissues, and *in vitro* in the presence of cysteine-protease (Winichayakul et al., 2013). An increase in photosynthesis and shoot biomass were also observed in HME Arabidopsis which was initially speculated to be the result of a CO_2 recycling phenomenon associated with higher *de novo* fatty acid (FA) synthesis (Schwender et al., 2004; Winichayakul et al., 2013). Similarly, for multiple first generation *Lolium perenne* (PR) HME lines, the elevation of FA in leaves, at the expense of leaf WSC, coincided with traits that increased carbon assimilation and subsequently increased relative growth rate (RGR) (2.3.2). Manipulation of many genes and gene combinations have been used to increase non-seed lipid content. However, the HME technology remains the only reported case that increases plant biomass.

It is now pertinent to ask how HME expression in PR leaves will influence the physiology of C assimilation under diverse growing conditions. Plant available nitrogen (N) is a major driver of crop growth and occurs in the soil primarily in two forms; nitrate (NO_3^-) and ammonium (NH_4^+), each of which has distinct effects on photosynthesis (Guo et al., 2007) and plant growth (Andrews et al., 2013). Elevated atmospheric CO_2 levels (e[CO_2]) can increase photosynthesis in the short term, but if photosynthate utilization is inadequate, a source-sink imbalance can arise, leading to end-product (carbohydrate) accumulation and subsequent downregulation of photosynthetic capacity (Ainsworth & Rogers, 2007; Ainsworth et al., 2004). It has also been disputed whether N form influences the way that plants respond to e[CO_2] (Andrews et al., 2013; Bloom, 2015).

From multiple HME lines with a range of transgene expression levels (Chapter 2), a high expressing HME transformant was selected for detailed investigation of the physiology associated with the inherently faster growth of *Lolium perenne* plants expressing HME. Growth, biomass allocation, leaf structure, gas exchange and water-soluble carbohydrates were analysed for plants grown under 1–10 mM NO_3^- and NH_4^+ supply at ambient and elevated atmospheric CO_2. The response of HME photosynthetic parameters to e[CO_2] led to speculation that by behaving as uniquely stable leaf carbon sinks, cysteine-oleosin-encapsulated lipid droplets may reduce feedback inhibition of photosynthesis and drive greater C capture. HME technology is compared with other lipid accumulation strategies and the general implications of introducing lipid sinks into non-seed organs on plant energy homeostasis and growth are discussed.

3.2 Materials and methods

3.2.1 Plant material and experimental layout

The untransformed wild type control genotype labelled 'WT' used in this chapter was derived from the *Lolium perenne* (PR) cultivar 'Grasslands Impact'. WT is the same transformation genotype labelled 'WT3' in Chapter 2. Replicate plants consisted of isogenic vegetative clonal ramets of WT, or independent WT-transformed T_0 HME genotypes. The HME genotype used in the main experiment in this chapter labelled 'HL' is the same genotype labelled 'HME5' in Chapter 2. HL was selected out of the five T_0 HME PR lines examined in Chapter 2 on the basis of having the largest relative increase in leaf FA (Table 2.1) and A_{mass} (Table 2.3), and the

largest relative reduction in leaf WSC (Table 2.1) compared to WT. In the main experiment described in this chapter, a detailed comparison of WT and HL was made across two growth chambers, in a regrowth trial at ambient and elevated atmospheric [CO_2] under different levels of NO_3^- and NH_4^+ supply.

3.2.2 Establishment phase

WT and HL clones were made from mature plants by splitting them into ramets consisting of 3–4 tillers and cutting to 10 cm of combined root and shoot length. Approximately 200 clonal ramets of each genotype were generated and placed in individual cylindrical plastic pots containing washed sand (1.6 L). The ramets were given 23 days to establish a root system (as in 2.2.3) in a Conviron BDW 120 plant growth room at ambient CO_2 (Thermo-Fisher, Auckland, NZ). Metal halide bulbs (400 W Venture Ltd., Mount Maunganui, NZ) and soft tone, white incandescent bulbs (100 W, Philips, Auckland, NZ) provided ~500 ± 50 μmol photosynthetically active radiation (PAR) m^{-2} s^{-1} as white light, under a 12 h photoperiod, with light levels ramping at dawn/dusk for 60 mins. The day/night temperature and humidity were 20/15 °C and 60/68% RH, respectively. A top-down airflow pattern, with a controlled flow of outdoor air, maintained ambient atmospheric CO_2 levels (~400 ppm CO_2). At the end of the establishment phase, plants were defoliated and the DW of leaf clippings from 5 cm above the pot media surface were determined after oven-drying at 80°C overnight. Of the 200 clones of each genotype generated, 140 were selected for use in the experimental regrowth phase. Selection was based on the leaf DW at the end of the establishment phase, which averaged 0.118 ± 0.036 g for the WT genotype and 0.113 g ± 0.020 for the HL genotype (Mean ± SD, *n*=140). A subset of defoliated plants (*n*=5) was destructively sampled at this time, oven dried and weighed for 'sheath' (0–5 cm from the pot surface) and root DW, enabling the later calculation of relative growth rate (RGR).

3.2.3 Experimental regrowth phase

Following defoliation of the established plants, half of the material was moved into a second Conviron BDW 120 plant growth room, with identical settings to those described above, except that the CO_2 level was maintained at 760 ppm with G214 food grade CO_2 (BOC, Auckland, NZ). The two cabinets were previously tested for uniformity (Andrews et al., 2019). The CO_2 levels in both growth rooms were measured continuously using PP Systems WMA-4 Gas Analysers (John Morris Scientific, Auckland, NZ). Pots were randomly allocated to different

N treatments (*n*=5) then flushed with 150 ml of basal nutrient media containing either 1, 2, 3, 4, 5, 7.5 or 10 mM of N as either NO_3^- or NH_4^+ every two days for the regrowth phase. The pH of the nutrient media solutions was in the range of 5.4–5.6. Potassium concentrations were balanced in all cases with the highest potassium treatment (10 mM) using K_2SO_4, but sulphate was not balanced.

3.2.4 Gas exchange and flourescence measurements

In the third week of the regrowth phase, plants treated with a high N supply (5–7.5 mM) were sampled for measurements of net photosynthesis under saturating irradiance (A_{sat}), specific leaf area (SLA), photosynthesis response to intercellular CO_2 (A-C_i) and the ratio of rubisco oxygenation/carboxylation (V_o/V_c). A_{sat} and A-C_i analysis were determined using a using a Li-COR 6400XT (Li-COR Biosciences, Nebraska, USA) with a 6 cm^2 leaf chamber. Three youngest fully expanded leaves per replicate pot were given 15–20 mins to adjust to the following chamber conditions; CO_2 was supplied at the growth room CO_2 level, light was supplied at 1500 µmol photons m^{-2} s^{-1}, leaf temperature was 23 °C, flow rate was 300 µmol s^{-1} and sample humidity was maintained at 65–75% RH. After 15–20 mins, net photosynthesis was logged. The CO_2 supply was then subsequently decreased stepwise to 50 ppm, then taken back up to 1300 ppm, with 2–3 mins adjustment time per measurement. A-C_i data were modelled using the Sharkey et al. (2007) Excel tool to give estimates of the maximum velocity of rubisco carboxylation (V_{cmax}), the rate of electron transport, and mesophyll conductance to CO_2 (g_m). To improve the A-C_i model outputs, we substituted our accurate estimate of the intercellular CO_2 compensation point in the absence of dark respiration in the light (C_i*) (Supplementary table B2.2) into the model. After gas exchange analysis, the leaves were photographed for leaf area determination, then oven dried and weighed for specific leaf area (SLA). V_o/V_c and the proportion of photosynthesis inhibited by ambient oxygen was determined with a 6400-40 leaf chamber fluorometer attachment. Leaves were given 15–20 mins to adjust to the following chamber conditions; CO_2 was supplied at the growth room CO_2 level, light was supplied at 550 µmol photons m^{-2} s^{-1}, leaf temperature was 21 °C, flow rate was 300 µmol s^{-1} and sample humidity was maintained near 65% RH. V_o/V_c was calculated as per Bellasio et al. (2014) and the proportion of net photosynthesis inhibited by ambient oxygen was calculated as; 100 x (1-[A_{20}/A_2]) where A_{20} = net photosynthesis at ambient O_2 and A_2 = net photosynthesis at 2% oxygen.

3.2.5 Harvest

Plants were destructively harvested after 29–30 days regrowth and divided into 'leaf' (5 cm above the pot surface), 'sheath' (0–5 cm from the pot surface) and roots. Leaf subsamples were taken from plants treated with 3, 5, 7.5 and 10 mM N, snap frozen in liquid N, stored at -80 °C, then freeze-dried, ground to a powder, and analysed. The remaining leaf material was oven dried at 65 °C for 4–6 days then weighed. Roots were cleaned and oven dried at 65 °C for 4–6 days before weighing. The fraction of biomass allocated to leaves (LMF) was calculated by dividing leaf DW by total plant DW. RGR was calculated from differences in paired plant DW, determined after defoliation (Supplementary figure B2.1), as described in 2.2.4. A non-biased plant pairing method (Poorter, 1989b) was used, based on end of establishment leaf DW.

3.2.6 Fatty acid and water-soluble carbohydrate analyses

The freeze-dried and ground leaves were analysed for fatty acids (FA) and water-soluble carbohydrates (WSC) as described in 2.2.6 and 2.2.7, respectively. Leaf subsamples were taken towards the end of the photoperiod (between 14.00 and 22.00 h) in order to maximize differences in genotype leaf WSC levels during the natural diurnal cycle.

3.2.7 Statistical analysis

A complete randomised study design was used to investigate the relationship between genotype, CO_2, N form and N concentration on various growth, morphology and gas exchange parameters, leaf FA and leaf WSC. Two or three-way ANOVA was used to compare the gas exchange, leaf structure and fluorescence data (collected at a single N concentration). For growth parameters, N concentration was treated as a continuous variable. For leaf FA and leaf WSC, N concentration was treated as a factor. A forward stepwise procedure was used for selecting variables. Variables and interaction terms with a *p*-value of <0.05 were retained in the final models. Due to residual heteroskedasticity, total plant DW data were log-transformed before modelling. Treatment means were compared and post hoc multiple comparison *p*-values were adjusted using the Benjamini-Hochberg (BH) method. Means and S.E. values are presented in the tables and figures, while *p*-values in the tables and text were obtained from the final statistical models. All statistical analyses were performed in R (Version 3.4.3, R foundation).

3.3 Results

3.3.1 Leaf C storage

The high expressing HME genotype (HL) had a substantially higher (67–96%) leaf FA concentration than the WT under two CO_2 levels and 3–10 mM N supply (Genotype effect $p<0.001$) (Figure 3.1). For both WT and HL, total leaf FA concentration decreased slightly at e[CO_2] and increased with increasing N supply up until 5–10 mM, before stabilizing (Figure 3.1). HL leaf WSC concentration was substantially lower than in the WT under both a[CO_2] and e[CO_2] (Genotype effect $p<0.001$) (Figure 3.1), especially in the high molecular weight fraction (HMW, primarily fructans) which was 3–5 fold lower for HL than WT leaves at 7.5–10 mM N supply (Figure 3.1). Leaf WSC was higher at e[CO_2] (Figure 3.1), and tended to decrease with increasing NO_3^- supply (N form x N concentration interaction $p<0.01$). Since FAs contain more energy and C than carbohydrates, the total C stored as leaf FA and WSC was calculated for each genotype. The overall differences in WT and HL leaf C storage were such that the total concentration of C stored as leaf FA and WSC combined was substantially less in HL than in the WT (Figure 3.1).

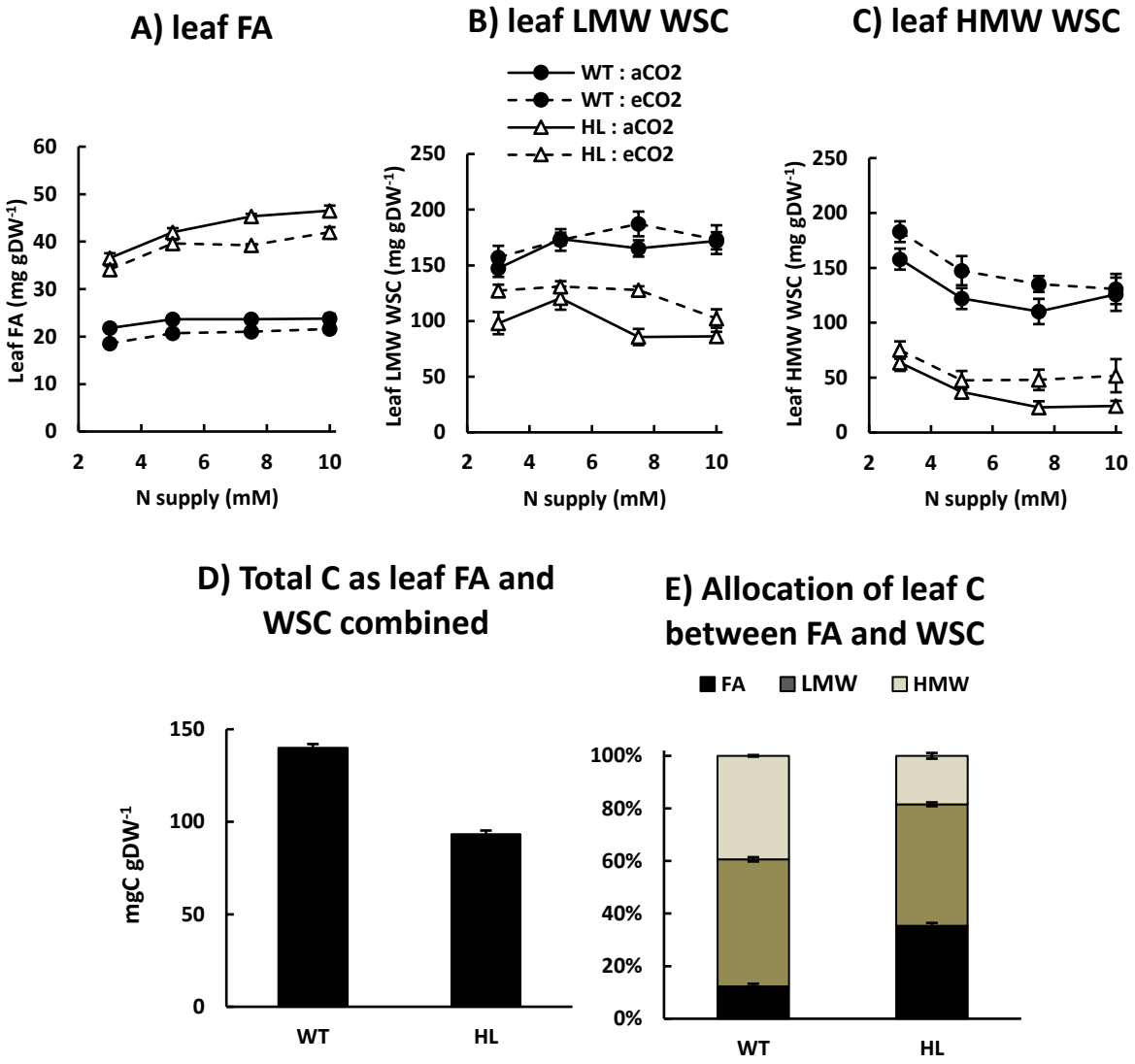

Figure 3.1. Leaf C storage of a clonal HME *Lolium perenne* transformant (HL; open triangles) and a wild type control (WT; closed circles) genotype. A) leaf fatty acids (FA), B) LMW (low molecular weight) leaf water-soluble carbohydrates (WSC), C) HMW (high molecular weight) leaf WSC, D) total C allocated to leaf FA and WSC combined, E) the proportions of leaf C as FA and WSC relative to one another (where 100% = total leaf C allocated to these potential storage pools). Plants were regrown for 28–29 days after defoliation at 1–10 mM N supply at either ambient (400 ppm) or elevated CO_2 (760 ppm). In A, B and C data points represent means for plants regrown under NO_3^- and NH_4^+ (*n*=10) ± S.E. In D and E bars represent an average over all N and CO_2 treatments (*n*=80) ± S.E. aCO_2 = ambient CO_2, eCO_2 = elevated CO_2.

3.3.2 Growth

After 28–29 days regrowth under the different [CO_2] and N treatments, total plant dry biomass (DW) increased by 7 to 23-fold. For both WT and HL, DW was greater under e[CO_2] than a[CO_2] and increased with N supply up until 4–10 mM (N concentration effect $p<0.001$), then stabilized or decreased thereafter (Quadratic N concentration effect $p<0.001$). The DW of (defoliated) plants at the end of the establishment phase was 18% greater for WT than for HL plants ($p<0.01$; student's t-test) (Supplementary figure B2.1). By the final harvest however, HL DW was greater than WT at high N supply, and similar at low N supply (Genotype x N concentration interaction $p<0.05$) (Figure 3.2). The relative growth rate (RGR) between post-establishment defoliation and the final harvest was also greater for HL than WT, and at most levels of N supply (Genotype effect $p<0.001$) (Figure 3.2). DW was slightly greater under high NO_3^- supply compared to high NH_4^+ supply (N form x concentration interaction $p<0.05$), but the increase in DW that occurred at e[CO_2] relative to a[CO_2] was similar with NO_3^- and NH_4^+ (i.e. no CO_2 x N form interaction occurred).

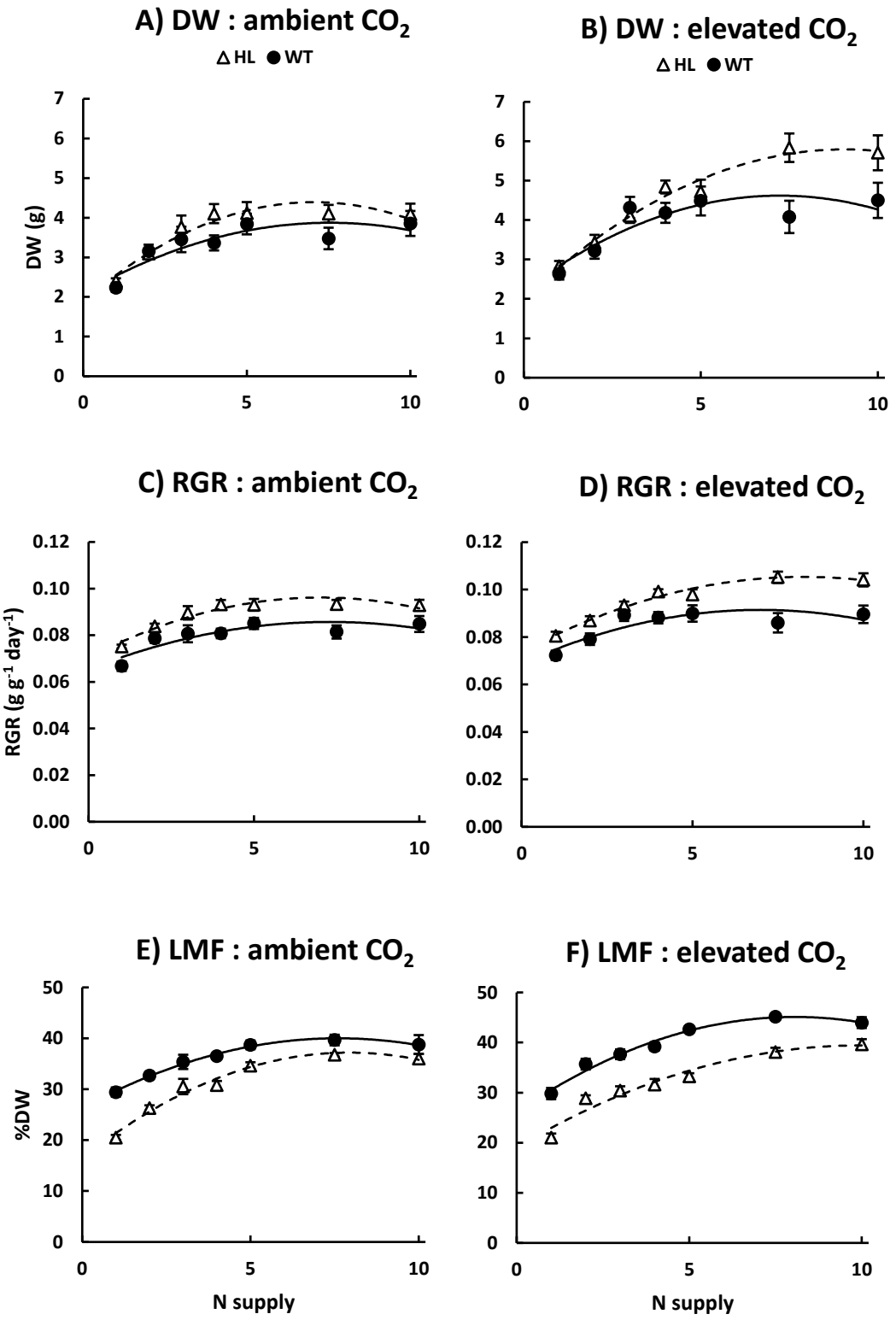

Figure 3.2. Growth parameters of a clonal HME *Lolium perenne* transformant (HL; open triangles) and a wild type control (WT; closed circles) genotype. A) and B) total plant DW, C) and D) relative growth rate (RGR), E) and F) the proportion of total plant DW allocated to leaves (LMF). Plants were regrown for 28–29 days after defoliation at 1–10 mM N supply at either ambient (400 ppm) or elevated CO_2 (760 ppm). Data points represent means for plants regrown under NO_3^- and NH_4^+ (*n*=10) ± S.E.

3.3.3 Morphology

The fraction of biomass allocated to leaves (LMF) increased with increasing N supply up until 5–7.5 mM, then stabilized thereafter (Quadratic N concentration effect $p<0.001$) (Figure 3.2). LMF was substantially lower for HL at low N supply, but this difference became progressively smaller as N supply increased, such that at 7.5 mM N supply, HL had only a slightly lower LMF than WT (10% when averaged across [CO_2] levels and N forms) (Quadratic N concentration x Genotype interaction $p<0.001$) (Figure 3.2). HL had a correspondingly larger fraction of biomass allocated to roots than WT and a similar fraction of biomass allocated to sheath. At 7.5 mM N supply, HL had a substantially higher SLA than WT (52% when averaged across [CO_2] levels and N forms) (Genotype effect $p<0.001$) (Table 3.1). For both WT and HL, SLA was lower at e[CO_2] than a[CO_2] and higher under NO_3^- than NH_4^+ supply (Table 3.1). HL had a higher projected total leaf area to total plant DW ratio than WT (35% when averaged across [CO_2] levels and N forms).

Table 3.1. Specific leaf area (SLA), light saturated photosynthetic rate per unit leaf area (A_{sat}), stomatal conductance (g_s), photosynthesis per unit leaf mass (A_{mass}) and ratio of leaf intercellular CO_2 to ambient CO_2 concentration (C_i/C_a) of a clonal HME *Lolium perenne* transformant (HL) and a wild type control (WT) genotype. Plants were regrown at 7.5 mM N supply at either ambient (400 ppm) or elevated CO_2 (760 ppm).

CO_2	N form	Genotype	SLA ($cm^2\ gDW^{-1}$)	A_{sat} ($\mu mol\ CO_2\ m^{-2}\ s^{-1}$)	g_s ($CO_2\ m^{-2}\ s^{-1}$)	A_{mass} ($\mu mol\ CO_2\ gDW^{-1}\ s^{-1}$)	C_i/C_a
Ambient	NO_3^-	WT	211 ± 9 C	19.1 ± 0.9 D	0.32 ± 0.03 B	0.41 ± 0.03 D	0.71 ± 0.01 AB
		HL	290 ± 8 A	23.3 ± 0.2 C	0.40 ± 0.01 A	0.68 ± 0.02 B	0.71 ± 0.01 AB
	NH_4^+	WT	155 ± 3 DE	15.6 ± 0.6 E	0.22 ± 0.01 D	0.24 ± 0.01 E	0.67 ± 0.01 BC
		HL	244 ± 9 B	24.8 ± 1.2 C	0.36 ± 0.02 AB	0.60 ± 0.02 C	0.66 ± 0.01 C
Elevated	NO_3^-	WT	174 ± 11 D	25.3 ± 0.9 C	0.23 ± 0.02 D	0.44 ± 0.04 D	0.72 ± 0.02 A
		HL	277 ± 9 A	30.8 ± 0.6 B	0.30 ± 0.02 BC	0.85 ± 0.01 A	0.73 ± 0.02 A
	NH_4^+	WT	150 ± 7 E	18.8 ± 0.9 D	0.13 ± 0.01 E	0.29 ± 0.03 E	0.67 ± 0.02 BC
		HL	231 ± 3 BC	34.6 ± 1.1 A	0.25 ± 0.02 CD	0.80 ± 0.03 A	0.66 ± 0.02 C
	ANOVA	G	***	***	***	***	-
		N	***	-	***	***	***
		CO_2	**	***	***	***	-
		G x N	-	***	-	**	-
		G x CO_2	-	**	-	***	-
		N x CO_2	-	-	-	-	-
		G x N x CO_2	-	*	-	-	-

Data points represent the means of plants regrown under NO_3^- or NH_4^+ (n=5) ± S.E. G = genotype effect, N = N form effect, CO_2 = CO_2 effect significant in a three-way ANOVA. * = p<0.05, ** = p<0.01, *** = p<0.001. Different letters indicate statistically significant differences in predicted means obtained from three-way ANOVA, with p-values adjusted according to the BH method.

3.3.4 Gas exchange

HL displayed a higher A_{sat} than WT at a[CO_2] (Genotype effect p<0.001) (Table 3.1). Similar results were also obtained when A_{area} was measured at growth room irradiance. For both WT and HL, A_{sat} increased and stomatal conductance (g_s) decreased at e[CO_2] (CO_2 effect, p<0.001), however the increase in A_{sat} at e[CO_2] compared to a[CO_2] was greater for HL than for WT (Genotype x CO_2 interaction, p<0.01) (Table 3.1). Relative to NO_3^- supply, NH_4^+ increased HL A_{sat} (by 9%) and decreased WT A_{sat} (by 29%) (Genotype x N form interaction p<0.001). Within [CO_2] treatments, light saturated g_s and A_{area} correlated well (r^2=0.79 under a[CO_2] and 0.74 under e[CO_2], respectively; Figure 3.3) and the ratio of leaf intercellular CO_2 to ambient CO_2 concentration (C_i/C_a) did not differ between WT and HL, regardless of [CO_2] level or N form (Table 3.1). A-C_i analysis, determined for plants supplied with NO_3^- only, showed that HL had a substantially higher A_{sat} at low (rubisco-limited) C_i (68–83% at 69–72 ppm C_i) compared to WT. This difference became smaller at high (RuBP regeneration-limited) C_i (10–12% at 1023–1099 ppm C_i) (Figure 3.4). The modelled maximum velocity of rubisco carboxylation (V_{cmax}) decreased at e[CO_2] (CO_2 effect, p<0.01), especially for the WT (Figure 3.4). HL had a greater Φ PSII than WT (Genotype effect, p<0.001) and a lower V_o/V_c and % inhibition of A_{area} at 20% O_2 than the WT (Genotype effect, p<0.001) (Table 3.2). V_o/V_c and the inhibition of A_{area} at 20% O_2 decreased at e[CO_2] (CO_2 effect, p<0.001) and V_o/V_c also decreased with NH_4^+ compared to NO_3^- supply (N form effect, p<0.05) (Table 3.2).

Table 3.2. Quantum efficiency of PSII (Φ PSII), ratio of rubisco oxygenation/carboxylation (V_o/V_c), and the proportion of photosynthesis inhibited by ambient oxygen of a clonal HME *Lolium perenne* transformant (HL) and a wild type control (WT) genotype. Plants were regrown at 5 mM N supply at either ambient (400 ppm) or elevated CO_2 (760 ppm).

CO_2	N form	Genotype	Φ PSII	Vo/Vc	% inhibition of A_{area} at 20 % O_2
Ambient	NO_3^-	WT	0.42 ± 0.02	0.35 ± 0.02	34 ± 1
		HL	0.54 ± 0.01	0.29 ± 0.01	29 ± 1
	NH_4^+	WT	0.40 ± 0.02	0.41 ± 0.02	37 ± 2
		HL	0.54 ± 0.01	0.31 ± 0.03	30 ± 2
Elevated	NO_3^-	WT	0.40 ± 0.01	0.18 ± 0.01	15 ± 2
		HL	0.55 ± 0.01	0.13 ± 0.01	8 ± 2
	NH_4^+	WT	ND	ND	ND
		HL	ND	ND	ND
	ANOVA	G	***	***	***
		N	-	*	-
		CO_2	-	***	***
		G x N	-	-	-
		G x CO_2	-	-	-

Data points represent the means of plants regrown under NO_3^- or NH_4^+ (n=5) ± S.E. A_{area} = net photosynthesis determined at 550 photons m^{-2} s^{-1}. G = genotype effect, N = N form effect, CO_2 = CO_2 effect significant in a three-way ANOVA. * = p<0.05, ** = p<0.01, *** = p<0.001. ND = Not determined.

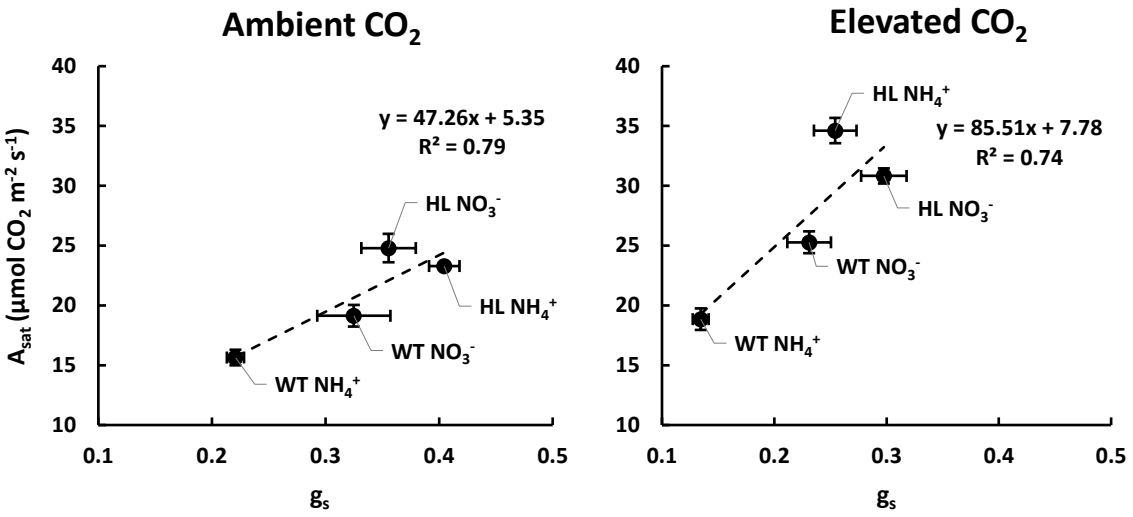

Figure 3.3 Relationship between light saturated photosynthetic rate per unit leaf area (A_{sat}) and stomatal conductance (g_s) of a clonal HME *Lolium perenne* transformant (HL) and a wild type control (WT) genotype. Plants were regrown for 28–29 days after defoliation at 7.5 mM N supply at either ambient (400 ppm) and elevated CO_2 (760 ppm). Data points represent the means of plants regrown under NO_3^- or NH_4^+ (*n*=5) ± S.E

Figure 3.4. Response of net photosynthesis per unit leaf area (A) to intercellular CO_2 concentration (C_i) of a clonal HME *Lolium perenne* transformant (HL; open triangles) and a wild type control (WT; closed circles) genotype. Modelled maximum velocity of rubisco carboxylation (V_{cmax}), rate of electron transport (J_{1500}), and mesophyll conductance to CO_2 (g_m) using Sharkey et al. (2007).

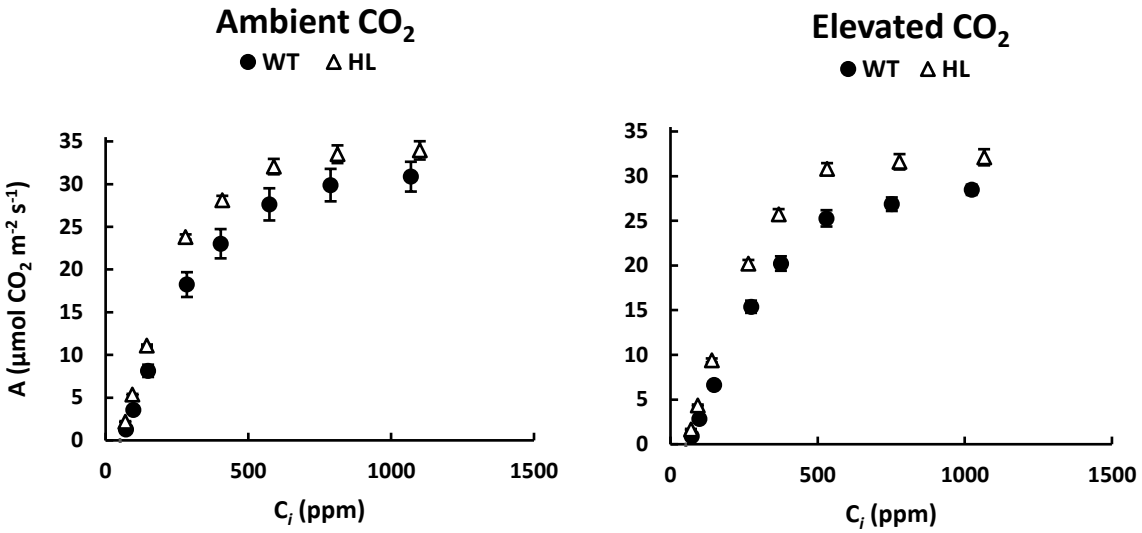

CO_2	Genotype	V_{cmax} (µmol m^{-2} s^{-1})	J_{1500} (µmol m^{-2} s^{-1})	g_m (µmol m^{-2} s^{-1} pa^{-1})	V_{cmax}/J	Model fit
Ambient	WT	161.78 ± 9.77 A	178.08 ± 8.92 A	1.39 ± 0.17 A	0.91 ± 0.03 A	0.41 ± 0.10
	HL	112.86 ± 7.46 BC	171.73 ± 6.07 A	4.29 ± 0.51 B	0.65 ± 0.02 C	0.51 ± 0.13
Elevated	WT	122.48 ± 4.74 B	160.76 ± 3.26 A	1.30 ± 0.09 A	0.76 ± 0.02 B	1.56 ± 0.24
	HL	97.46 ± 5.24 C	165.66 ± 4.71 A	5.17 ± 1.18 B	0.59 ± 0.02 C	2.39 ± 0.68
ANOVA	G	***	-	***	***	
	CO_2	**	-	-	**	
	G x CO_2	-	-	-	-	

Plants were regrown at 5 mM NO_3^- supply under ambient CO_2 (400 ppm) and at 7.5 mM NO_3^- supply under elevated CO_2 (760 ppm). Values represent means (n=5) ± S.E. G = genotype effect, CO_2 = CO_2 effect significant in a two-way ANOVA. * = p<0.05, ** = p<0.01, *** = p<0.001. Different letters indicate statistically significant differences in predicted means obtained from two-way ANOVA, with p-values adjusted according to the BH method.

3.4 Discussion

3.4.1 HME expression confers a lipid carbon sink in leaves and a growth advantage

In the selected *Lolium perenne* (PR) T_0 line 'HL' with high leaf diacylglycerol *O*-acyltransferase and cysteine-oleosin (HME) expression, an increase in leaf FA concentration of 67–96% coincided with a decrease in total leaf WSC concentration of 68–170% compared to a WT control across the N and [CO_2] treatments (Figure 3.1). For both WT and HL, total plant DW was greater under e[CO_2] than a[CO_2] and increased with N supply up until 4–10 mM then stabilized or decreased thereafter. These growth responses to N availability and e[CO_2] are similar to those reported previously for other crop plants (Andrews et al., 2019). Total plant DW at harvest was 7–24% greater for HL than WT at medium to high N supply (4–10 mM), and similar for the two lines at low N supply (Figure 3.2). The RGR between post-establishment defoliation and the final harvest was also greater for HL than WT at most levels of N supply (Figure 3.2).

3.4.2 Reasons for the growth advantage with HME expression in leaves: increased SLA and A_{area}

RGR was greater for HL than WT at most N levels under a[CO_2] and e[CO_2], indicating that net photosynthesis per plant was greater for HL than WT under most treatments. However, LMF was lower for HL than WT under most treatments (Figure 3.2). Also, leaf DW was lower for HL than WT under all but the highest levels of N supply (7.5–10 mM). Therefore, greater photosynthesis per HL plant was not explained by greater allocation of DW to leaves, which was on the other hand, a factor linked to increased growth with increased N supply for both HL and WT. An increase in both SLA and A_{area} could account for the increase in the HL RGR, consistent with data from a multi-line T_0 HME growth experiment (2.3.2). SLA, multiplied by the proportion of DW allocated to leaves (LMF) determines the total leaf area per unit of plant DW, which strongly dictates light interception and growth rate (Poorter, 1989a). HL had a slightly lower LMF than WT at 7.5 mM N supply, but a much higher SLA (Table 3.1), and therefore a higher projected total leaf area to total plant DW ratio than WT. A medium to high N supply (4–10 mM) maximised the RGR difference between the HL and WT (Figure 3.2). Two morphological features could have contributed to this altered growth response to N in HME PR. Firstly, HL allocated substantially less biomass to leaves at low N supply, but HL LMF increased more steeply as N supply increased. Secondly, and more speculatively, since a high SLA generally increases photosynthetic N use efficiency (Poorter, 1989a), the C gain per

incremental increase in leaf N may be higher for an HME leaf, although confirming this will require further testing (Chapter 5).

Although approximately half of the HL SLA advantage could be directly accounted for by the lower combined FA and WSC concentration in the HL leaves, it was still highly significant when SLA was calculated on a FA and WSC-free (i.e. structural) basis. Across five HME *Lolium perenne* lines, SLA was positively correlated with leaf FA concentration (Figure 2.2), indicating a possible causal relationship between leaf lipid accumulation and the increase in SLA. The mechanisms governing SLA plasticity have not been studied in detail, but SLA generally increases under conditions of low C availability/low carbohydrate accumulation, such as low light (Poorter et al., 2009), or specifically, when the sink: source ratio increases in PR due to frequent defoliation (Lee et al., 2010; Van Loo, 1993). In both of these cases, increased SLA is associated with an allocation adjustment towards an increased LMF, although a regulatory link between leaf carbohydrate levels and SLA or LMF (or shoot to root ratio) has not been established (Andrews et al., 2005; Poorter et al., 2009). Here, the increase in HL SLA was associated with low leaf carbohydrates, but unexpectedly also coincided with a decreased LMF. The trade-off between FA and WSC accumulation in HL leaves suggests that cysteine-oleosin-encapsulated lipid droplets behave as an additional energy-consuming C sink in leaves, with sufficient strength to induce a large shift in the instantaneous leaf energy balance, and perhaps even penalize leaf growth under some conditions. However, the biomass of the HL sheath and root system was greater than for the WT, implying that there was no long-term penalty to the export of C from leaves to sink organs. Further work will be needed to explore DW and C partitioning and diurnal variation in WSC, FA and gross energy within and between different HME PR organs.

The increase in HL photosynthesis at 7.5 mM N supply was coupled to an increase in stomatal conductance (g_s) (Figure 3.3). Across diverse growth conditions, g_s coordinates closely with the CO_2 requirement of the mesophyll such that the C_i/C_a ratio remains constant (Wong et al., 1979). In this experiment, C_i/C_a did not differ between WT and HL, implying that the HL mesophyll was a stronger sink for CO_2. A-C_i analysis showed that an increase in HL A at low C_i occurred which was independent of g_s (Figure 3.4). Common explanations for a steeper A-C_i curve at low (rubisco-limited) C_i include increased rubisco carboxylation efficiency and/or content per leaf area, or increased mesophyll conductance to CO_2 (g_m). In an initial modelling

exercise using the Sharkey et al. (2007) A-C_i analysis function, the apparent maximum velocity of rubisco carboxylation (V_{cmax}) and electron transport rate (J_{1500}) were lower for HL than WT (Figure 3.4), however when improved estimates of g_m and R_d (Table 5.2; Supplementary table D4.2) were later fixed in the A-C_i model, HL had a higher V_{cmax} and J_{1500} than WT (Supplementary table B2.1). We also investigated the CO_2/O_2 ratio in the chloroplast in order to assess possible changes in rubisco carboxylation efficiency associated with a possible 'CO_2 recycling' phenomenon occurring in HME leaves (Winichayakul et al., 2013). Compared to a WT control, HL displayed a decrease in two measures of photorespiration (Table 3.2), which coincided with increased photosynthetic sensitivity to e[CO_2] (Table 3.1) and a higher intercellular CO_2 compensation point (Supplementary table B2.2). In contrast, decreased photosynthetic sensitivity to e[CO_2] and a lower intercellular CO_2 compensation point were observed in Arabidopsis plants engineered to have lower photorespiration and a greater CO_2/O_2 ratio in the chloroplast (Kebeish et al., 2007). Thus, our gas exchange data did not support the hypothesis that CO_2 recycling makes an important contribution to the increase in HME photosynthesis (Winichayakul et al., 2013).

We did not quantify rubisco or g_m in this chapter, but we contend that the large increase in HL SLA makes an increased rubisco content per unit leaf area less likely than an increase in g_m to explain the steeper initial A-C_i response in HL leaves. HL plants regrown at 5 mM NO_3^-, for example, had a 56% greater SLA than WT, so an approximate doubling in leaf rubisco concentration would have been required to deliver the 35−40% increase in HL A at a C_i of ~150 ppm. Greater g_m is an important mechanism by which leaves with an inherently high SLA achieve greater photosynthetic efficiency than low SLA leaves (Onoda et al., 2017). Initial modelling of the A-C_i curves using Sharkey et al. (2007) gave a high estimate of g_m for HL (Figure 3.4), but such 'curve fitting' estimations of g_m are highly unreliable (Pons et al., 2009), and so further work will be needed here (Chapter 5). Finally, since Φ PSII contributes to photosynthetic efficiency and is modulated by various stresses, we sought to show that the differences in Φ PSII and photosynthesis between WT and HL (Table 3.2) were unrelated to photoinhibition 'stress' in the WT, by measuring these parameters alongside the maximum quantum efficiency of photosystem II (F_v/F_m). The increase in HL photosynthesis and Φ PSII coincided with an exceedingly small (~1%) increase in F_v/F_m compared to the WT (Supplementary table B2.2). This suggested that photoinhibition 'stress' in the WT could not explain the increase in HME photosynthesis.

3.4.3 Leaf HME expression made A_{mass} more responsive to e[CO_2] at high N supply

Expression of HME in PR leaves enhanced the stimulation of light saturated photosynthesis at e[CO_2] at 7.5 mM N supply (Table 3.1), consistent with results from a preliminary experiment under near-identical growth chamber settings (Supplementary table B2.3). Parameterization of the A-C_i curves at a[CO_2] and e[CO_2] suggested that HME expression also reduced the severity of photosynthetic downregulation at e[CO_2] (Figure 3.4). Interestingly, the changes in mass-based photosynthetic rate (A_{area} x SLA = A_{mass}) at e[CO_2] were modulated by changes not only in A_{area} but also SLA. Under NO_3^- supply, HL SLA did not significantly decrease at e[CO_2], while WT SLA did significantly decrease at e[CO_2] (Table 3.1). A_{mass} correlates better with growth than A_{area} in spaced pots (Poorter, 1989a) and typically changes less than A_{area} with changes in atmospheric [CO_2] due to compensatory changes in SLA (Poorter et al., 2009; Temme et al., 2017).

When the sink: source ratio decreases, carbohydrates generally accumulate in the leaves (Paul & Foyer, 2001). This was well-illustrated in this experiment; increasing the CO_2 supply (increasing source activity) or decreasing NO_3^- supply (decreasing sink development) caused leaf WSC concentration to increase (Figure 3.1). Due to the limited capacity of PR to produce new sinks, leaf carbohydrates can build up rapidly upon exposure to e[CO_2], leading to potentially severe downregulation of photosynthetic capacity (Fischer et al., 1997). In free air CO_2 enrichment trials, however, PR sustained large increases in photosynthesis at e[CO_2] when practices that increased the canopy sink: source ratio were employed, such as regular defoliation and N fertilizer application (Ainsworth et al., 2003; Guo et al., 2006). In this experiment, HL leaf WSC concentration increased at e[CO_2], but not beyond the levels in WT leaves regrown at a[CO_2]. We speculate that the diversion of carbohydrate into a lipid C sink could mitigate signals to downregulate photosynthesis in a PR leaf at e[CO_2], and thus leaf HME expression could allow a greater magnitude of photosynthetic stimulation at e[CO_2].

Unexpectedly, we found that NH_4^+ supply (compared to NO_3^-) increased A_{sat} for HL whereas the reverse effect occurred for the WT control (Table 3.1). We observed minor growth toxicity symptoms in the WT at high NH_4^+ supply (7.5–10 mM) suggesting that this may have been a consequence of different capacities for NH_4^+ assimilation and detoxification (possibly due to a larger root system for HL). Otherwise, the form of N had general effects on processes relating to photosynthesis and growth which were independent of genotype or [CO_2] level. Plants

supplied with NH_4^+ had a lower SLA, A_{mass}, g_s and C_i/C_a than plants supplied with NO_3^- (Table 3.1). The maximum DW achieved was also lower under NH_4^+ supply than NO_3^-. While not significant, we observed a slightly greater magnitude of DW stimulation at e[CO_2] under NO_3^- supply (32% and 44% for WT and HL, respectively) compared to NH_4^+ supply (17% and 24% for WT and HL, respectively). Therefore, our PR regrowth data provide little evidence to support the claim that stimulation of growth by e[CO_2] is inhibited under NO_3^- supply in C_3 plants (Bloom, 2015). This finding agrees with recent results for wheat published by Andrews et al. (2019).

3.4.4 Could storing lipids in leaves improve yield?

It has been speculated previously that introducing a new C sink in the form of TAG in leaves might influence photosynthesis (Fan et al., 2019; Vanhercke et al., 2017; Vanhercke et al., 2019; Xu & Shanklin, 2016), but few measurements related to photosynthesis or C assimilation have been reported for high TAG plants. Transgenic rice expressing the glycerol-3-phosphate dehydrogenase enzyme with high plastid lipids exhibited enhanced CO_2 assimilation (Singh et al., 2016). Upregulation of photosynthetic genes occurred in high TAG/low starch tobacco overexpressing WR1, DGAT1 and OLE1 (Vanhercke et al., 2017), but broadly the opposite changes in gene expression occurred in tobacco leaves expressing WR1 alone, which coincided with decreased photosynthetic capacity (Grimberg et al., 2015). Changes in several photosynthetic parameters were absent in Arabidopsis mutants with various disruptions in starch synthesis and lipid metabolism, even though these mutations generated a wide variation in leaf soluble sugar levels (Fan et al., 2019; Yu et al., 2018).

So why do many successful efforts to increase leaf TAG not increase photosynthesis and/or growth? Given the substantial energetic costs of FA synthesis (1.2.2), should not maintaining even *the same* biomass as untransformed plants require that high TAG plants undergo changes delivering greater C assimilation? In many cases, manipulations of lipid metabolism result in growth penalties due to pleiotropic effects, or when TAG accumulates to extremely high levels, because competition for C inhibits normal development (Vanhercke et al., 2019). Indeed, HME PR lines with a leaf FA concentration above ~6.5 %DW incur a growth penalty relative to controls (1.2.5). Here it should be emphasised that the economic value of higher non-seed TAG could easily compensate for possible biomass penalties (Vanhercke et al., 2019). As well as the importance of optimizing lipid levels, we contend that expression pattern

is critical here. Green tissue-specific FA/TAG accumulation will enhance the probability of a positive growth effect by minimizing excessive competition for C by heterotrophic tissues (Winichayakul et al., 2013). We further speculate that lipid protection may be important, and in this regard, the mechanism by which we propose cysteine-oleosin prevents lipid droplet breakdown may be relatively unique. We reported that cysteine-oleosin conferred enhanced stability to lipid droplets in vegetative tissues, and *in vitro* in the presence of cysteine-protease, whereas protection was not achieved with a native oleosin (Winichayakul et al., 2013). If futile cycles of TAG biosynthesis and catabolism followed by either FA recycling in the endoplasmic reticulum or beta-oxidation impose a significant energetic penalty, then avoiding growth penalties may not be possible without TAG protection. Inhibiting lipid catabolic pathways (by for example silencing the activity of the TAG lipases) might be effective for this purpose (Kelly et al., 2013; Vanhercke et al., 2017) if normal processes are not disrupted. In plants with high concentrations of unprotected TAG and high rates of FA turnover, the fate of CO_2 released during the pyruvate to acetyl-coA conversion may be important (Vanhercke et al., 2017) and confining CO_2 release to chloroplasts via green tissue-specific FA synthesis/TAG accumulation seems sensible (Schwender et al., 2004).

To maintain energy homeostasis and survive, it is critically important that plants can sense their carbohydrate status and respond by adjusting their physiological state appropriately (Lee et al., 2010; Smith & Stitt, 2007). For example, rates of starch synthesis and degradation are tightly regulated during the day to ensure a sufficient supply of C during the night, when CO_2 fixation is unavailable (Smith & Stitt, 2007). Plants with impaired starch synthesis have higher FA synthesis and turnover at night, suggesting that FA become important respiratory substrates for normal growth in starchless mutants (Fan et al., 2019; Yu et al., 2018). Given their distinct natural functions in cells, lipid accumulation and remobilization may not be subject to the same fine-tuned regulation as carbohydrates, and inevitable losses of energy and C may occur when lipids function as an energy store (Yu et al., 2018). However, being the site of photosynthesis, well-illuminated leaves have an abundant local supply of energy and reductant. Our results show that under favourable growing conditions, the manipulation of lipid biosynthesis and storage can drive greater C assimilation. Further work will be needed to identify the optimal levels and expression patterns of FA/TAG accumulation, and how various strategies to package and protect accumulated TAG influence plant energy homeostasis and growth under other conditions.

Chapter 4

Lolium perenne pastures with higher energy density and growth potential under simulated grazing

4.1 Introduction

A fundamental productivity constraint for pastoral agriculture is the inefficient utilization of plant energy and protein by grazing ruminants. Perennial ryegrass (*Lolium perenne* L.) (PR) is a widely used plant species in pastoral agriculture, due to its ease of establishment, high digestibility, and balanced seasonal dry matter production (Chapman et al., 2017). However, a large proportion of the energy in PR occurs in fibre fractions which are inaccessible to rumen microbial degradation. Further, the low fermentable carbohydrate: protein ratio in PR causes high levels of rumen proteolysis, resulting in inefficient protein utilisation and N losses to the environment (Capstaff & Miller, 2018; Kingston-Smith & Theodorou, 2000). Although there is a strong impetus to improve PR nutritional quality and optimize ruminant performance, nutritional quality traits including metabolizable energy (ME) receive less attention from PR breeders than traits related to yield, in part because of their relative difficulty of measurement and manipulation (Arojju et al., 2020; Chapman et al., 2017). Recently, new tools such as genomic selection and gene technologies have been developed, which offer compelling prospects for enhancing PR nutritional quality (Arojju et al., 2020; Barrett et al., 2015).

Lipids are an energy-dense class of compounds, containing approximately 38 kJ g^{-1}, while carbohydrates and protein contain approximately 17 kJ g^{-1}. However, due to their natural roles in leaves as structural constituents of cell membranes, lipids, and their component fatty acids (FA) occur in low levels in PR pastures (averaging 2.3 %DW ± 0.8) (Glasser et al., 2013). Variation in PR herbage FA content exists between cultivars (Elgersma et al., 2003b; Palladino et al., 2009) and genotypes (Hegarty et al., 2013; Morgan et al., 2020) and progress has been made in identifying the genetic loci involved (Hegarty et al., 2013). However, this genetic variation is limited in scope, with the maximum reported herbage FA levels in modern cultivars rarely exceeding ~5 %DW. Further, the observed variation in pasture FA levels has a large management and environmental component (Dewhurst et al., 2003), which has the potential to mask the comparatively smaller genetic component (Glasser et al., 2013; Hegarty et al., 2013). While increasing lipid content has historically ranked low among priorities for

enhancing PR nutritional quality (Smith et al., 1997), renewed interest in enhancing forage lipids through breeding has recently emerged (Morgan et al., 2020; Wilkinson et al., 2020).

The development of a gene technology to increase plant lipid concentrations ('high metabolizable energy' or HME technology) represents a promising step towards delivering PR pastures with higher lipid concentrations, and possibly greater ME. Co-expression of diacylglycerol *O*-acyltransferase (DGAT1) and a lipid droplet-stabilizing protein called cysteine-oleosin (collectively 'HME') in PR leaves enhanced leaf FA by up to 75%, while also increasing relative growth rate (RGR) compared to non-transformed controls (2.3.2). Nutritional and *in vitro* rumen fermentation profile analysis showed that despite having lower leaf sugars than control PR, lab-grown T_0 HME PR with up to 6.5% leaf FA also had 6–7% higher GE (Winichayakul et al., 2020). Compared to control PR, total gas and methane as a proportion of total gas emitted was lower during HME PR rumen fermentation, while the proportion of valuable unsaturated FAs (including *trans*-vaccenic acid and conjugated linoleic acid) retained in the products of biohydrogenation was greater (Winichayakul et al., 2020). Thus far, analysis of HME PR has been confined to indoor spaced pot trials, and it is unclear if these findings translate into realistic growing conditions.

As a consequence of feedback effects occurring during growth in a canopy and interactions with the prevailing environment, plant performance in indoor spaced pot trials does not reliably correlate with performance in field canopies (Poorter et al., 2016). Sustaining trait improvement in perennial pastures is challenging when G x E interactions are poorly understood (Parsons et al., 2011). While some spaced pot PR characteristics, such as leaf extension rate correlate with yield in canopies, other characteristics such as tiller production are neutralized by size/density compensation effects in dense swards (Barre et al., 2015). Although manipulation of many gene combinations can deliver large increases in vegetative lipid contents (Vanhercke et al., 2019), there are few reports on high lipid plant performance under realistic growing conditions, and none for high lipid pasture species. Most manipulations of lipid metabolism are associated with plant growth penalties, even under favourable growing conditions (Mitchell et al., 2020; Vanhercke et al., 2019). Therefore, it is unclear whether they increase harvestable GE per unit ground area, a feature which would be economically beneficial for perennial forage crops like PR.

The objective of this chapter was to examine the translation of the previously described FA, GE and yield (herbage DW) enhancing traits associated with the HME expression in PR (Chapter 2; Chapter 3; Winichayakul et al., 2020), from indoor spaced pots through to field swards. T_2 PR populations segregating for the HME transgenes were grown in canopy-like conditions under regular mechanical defoliation. Under controlled indoor conditions, spacing between plants was varied in order to manipulate above-ground competition for light, before growing plants for a season in the field in miniswards with 0.18 m^2 internal ground area. This workflow allowed transgene x light competition effects to be studied before introducing stress from stochastic field conditions. The data presented are a significant advancement upon spaced pot work with T_0 HME PR lines because plants were grown in canopies with populations for comparison. Our thorough analysis of HME trait translation from lab to field supports the overall potential for HME technology to enhance pasture energy density and yield potential.

4.2 Materials and methods

4.2.1 Plant material

T_2 populations segregating for the HME transgenes were used to compare HME and control PR. In all cases, 'HME+' refers to plants that tested positive for the expression of the oleosin protein in leaves – see 'transgene status identification' section (4.2.7). 'Null control' refers to the corresponding non-transgenic plants from that population (i.e. those that tested negative for the oleosin protein). All of the HME+ progeny was hemizygous for the HME transgenes, and since the seed was collected from the transgenic parents, both the HME+ and null progeny were free of fungal endophyte.

The T_2 population used for the indoor component of this work was produced by crossing the gene gun-derived green tissue-expressing T_0 HME event 'ODR4501' (T_0 event HME2) with a genotype from the cultivar 'Bronsyn', with T_1 seed collected from the transgenic parent. Subsequently, one of the T_1 HME+ progeny was crossed with a single plant from the cultivar 'Alto', and T_2 seed was collected from the HME+ parent. This population was studied first in spaced pots, then later under simulated grazing over a longer time period. Identical growth room settings were used, which facilitated comparisons between different growth arrangements. Two different T_2 populations were used in the field trial. Material was produced by crossing the gene gun-derived green tissue-expressing T_0 HME event 'ODR6205' (T_0 event HME1) with a 'Bronsyn' genotype (T_1) then one of the T_1 HME+ progeny was crossed

with one of two 'Alto' plants (M and O) (T_2). The two HME populations used in the field trial are referred to as family M (HME1-M) and family O (HME1-O).

4.2.2 Indoor growth conditions

The indoor work was conducted in controlled temperature rooms set to 20/15 °C day/night temperature. Plants were grown ~1m below a series of 600W NanaPro LED lights (LEDgrowlights, Hamilton, NZ) under a 12 h photoperiod. Photosynthetically active radiation (PAR) at plant height was recorded at 500 ± 100 µmol m^{-2} s^{-1}. The effect of the uneven light distribution was minimized by rearranging the pots in space every 1–2 days. Relative humidity and atmospheric CO_2 level were not controlled. An attempt was made to eliminate plant nutrient and water limitations by regularly flushing the pots with a complete basal nutrient solution (Andrews et al., 1989) containing N as 4 mM NH_4NO_3. The volume of nutrient solution applied to the pots was regularly adjusted to meet plant demand. For example, young seedlings in trays received 20 ml of solution every second day, while mature swards grown in 4 L pots received up to 500 ml every day at the end of a regrowth cycle.

4.2.3 Indoor spaced pot experiment

Seeds from the HME2 T_2 population described above were germinated on moist washed sand. Seedlings (54) that germinated uniformly were transplanted into 4 L pots containing washed sand (18 x 18 cm width, 20 cm depth), with one plant per pot. Every 2–3 days for 40 days, tiller number was counted. For the primary tiller, leaf lamina length, width, and area, sheath height, leaf elongation rate and duration were measured as described in Sartie et al. (2009), until the 6^{th} leaf on the primary tiller had completed expansion. All shoot material was harvested 5cm above the potting media surface 40 days after germination. After defoliation, the plants were regrown for an additional 23 days and then shoot and root DW was determined destructively.

4.2.4 Indoor sward experiment

Seeds from the same HME2 T_2 population used in the spaced pot experiment were germinated on moist washed sand. There were 48 null and 48 HME2+ seedlings, which were transplanted into 4L pots (dimensions as above) containing washed sand (*n*=12, four plants per pot). Black plastic sheeting was attached to the sides of these pots to exclude light up to the defoliation height of ~5cm. These 'miniswards' were grown under regular mechanical defoliation to simulate grazing. Null and HME2+ miniswards were kept in an alternating arrangement, and interplant shading inevitably occurred. A total of 11 defoliation events took place. Harvest 1

occurred 40 days after germination. The regrowth interval for harvests 2–11 was between 14 and 21 days. For harvests 2–6 the miniswards were arranged in 'spaced rows', with 12 cm gaps between rows. For harvests 7–9, the miniswards were packed together into a 'dense sward' to maximize competition for space and light (Supplementary figure C3.1). DM yield per pot was determined after oven drying the harvested material for 4–5 days at 65 °C, and the average herbage growth rate was calculated by dividing herbage DW by the number of days between defoliation.

4.2.5 Field site and conditions

The field experiment was conducted from May to October 2019 at the Greenley Memorial Research Centre, near Novelty, MO, USA (40.0216° N, 92.1903° W). Climatic data (average and maximum daily temperatures, solar radiation, and precipitation) and irrigation information for this period are summarized in Table 4.1. The soil type was Putnam (fine, smectitic, mesic Vertic Albaqualf) silt loam. The experimental plot was removed from *Zea mays/Glycine max* (corn/soybean) rotation and used for a PR growth trial from May to October 2017. It remained fallow from October 2017 to May 2019, with any volunteer plants removed by herbicide application or mechanical tillage. A minimum of 58 m from the borders of the plot were kept fallow. The plot was fertilized with 34 kg N ha^{-1} as Urea (SuperU, Kock Agronomic Services, Wichita, USA) on May 25. For the rest of the trial, 34 kg N ha^{-1} fertilizer applications were made within a day of each harvest.

Table 4.1 Summary of climatic data from the field trial site, June-October 2019, and comparison of daily photosynthetically active radiation (PAR) integrals and photothermal ratio between the field trial and growth chamber.

	Dates	Average daily temperature (°C)	Average maximum daily temperature (°C)	Average total daily solar radiation (MJ m^{-2})	Total precipitation (mm)	Daily PAR integral (mol PAR m^{-2} day^{-1})	Photothermal ratio (mol PAR m^{-2} $°C^{-1}$)
Harvest 1	25th June – 23rd July	25.2	30.9	21.81	63	45.1	1.79
Harvest 2	24th July – 18th August	23.0	28.4	20.98	42	43.4	1.89
Harvest 3	19th August – 16th September	21.3	26.4	15.83	67	32.8	1.54
Harvest 4	17th September – 8th October	19.4	25.3	12.90	170	26.7	1.38
Growth chamber		17.5	-	-	-	21.6	1.23

Field daily PAR integrals and photothermal ratios were estimated assuming that PAR = 0.45 x solar radiation (Monteith, 1972). A growth chamber PAR level of 500 µmol photons m^{-2} s^{-1} was assumed. Supplemental irrigation was provided on 16 July (41 mm), 6 August (28 mm), and 16 September (30 mm).

4.2.6 Field sward experiments

Seeds from the HME1 T_2 families M and O described above were germinated on moist sand in seedling trays under LED lights on March 18, 2019. The seedling trays were moved to a glasshouse and regularly received half-strength Hoagland's nutrient solution (containing 7.5 mM total N) for approximately 2 months. In total, 45 null and 45 HME positive (HME+) seedlings from each of the families M and O were trimmed and transplanted into field swards on 12 May 2019. Individual swards consisted of 5 rows of 5 plants each, with 10 cm spaces between plants within a row, and 20 cm spaces between rows. Only the centre 9 plants were analysed, while the outer 15 were treated as border plants and were not analysed. Each family was treated as an independent experiment. The field trial layout, and the dimensions of a replicate sward are presented in Supplementary figure C3.2. There were 10 swards per experiment (*n*=5, nine experimental plants per sward), arranged in a random sequence in a row east to west. The plants were defoliated 38 days after transplanting into the field. Since the plants were newly established and acclimating to field conditions during this time, these data were excluded from the analysis. After this, the swards were harvested 4 times to a defoliation height of ~5cm. The regrowth interval between harvests was 22–29 days. Yield per sward and average herbage growth rate were calculated as above.

4.2.7 Transgene status identification

Because T_2 segregating populations were used, the transgene status of seedlings was unknown at the time of sowing. Transgene status was determined by leaf immunoblot for the recombinant oleosin protein. Leaf laminae (3 x 1 cm lengths) were cut and placed in 96 well plates containing steel beads with 114 µl sterile MQ H_2O. The plates were sealed with an aluminium sheet (4titude Thermal Bond seals, 4ti-0591), then the leaves were macerated in a TissueLyser (Qiagen) for 30 s, and 120 µl of 2X Laemmli Buffer (Sigma S3401-10VL) was added to each well. The plates were vortexed briefly and heated at 70 °C for 10 mins. After briefly centrifuging the plates, 2 µl of the supernatant was pipetted onto a nitrocellulose membrane, which was subsequently air-dried for 30 mins. Immunoblotting proceeded following Winichayakul et al. (2013) with minor modifications, and the resultant chemiluminescence was visualised using Advanta Western Bright ECL spray (K-12049-D50) and the Bio-Rad ChemiDoc^{TM} XRS^{+} imaging system. In the indoor spaced pot experiment, transgene status identification occurred just before the first harvest (meaning that all the measurements up until 40 days post-germination were performed 'blind'). In the indoor and the field sward

experiments, genotype identification occurred just prior to transplanting into swards. In almost all cases, the presence of the oleosin protein in leaves corresponded with high leaf/herbage FA and high C18:1/C18:3 ratios characteristic of HME plants (Winichayakul et al., 2013) (Supplementary figure C3.3).

4.2.8 Chemical analysis

Chemical analyses were performed on oven-dried herbage material ground to a particle size less than 1 mm. In some cases, herbage from replicate swards or plants within a sward were pooled before analysis. FAs were extracted and analysed by FAMEs GC-MS (2.2.6; Browse et al., 1986) and GE was determined using bomb calorimetry. Neutral detergent fibre (NDF), crude protein (CP), water-soluble carbohydrate (WSC) and dry organic matter digestibility (DOMD) were determined as described in Winichayakul et al. (2020).

4.2.9 Gas exchange, specific leaf area and LAI

For the indoor spaced pot experiment, gas exchange measurements were made with a Li-COR 6400XT near saturating irradiance (1500 photons m^{-2} s^{-1}) as described in 3.2.4. Sward gas exchange measurements were made with a Li-COR 6800 (Li-COR Biosciences Ltd, Nebraska, USA) near the ambient irradiance of 500 photons m^{-2} s^{-1} indoors and 1000 photons m^{-2} s^{-1} in the field. Measurements were made on abscised leaves in order to facilitate uniform leaf orientation and light acclimation for all replicates. Tiller selections were made pre-dawn, then the base of the youngest fully-expanded leaf was re-cut while submerged under water and stored in the dark. For 30 mins prior to measurement, leaves were illuminated with LED lights, then 5 mins prior to measurement were acclimated in the chamber at 20 °C, 70% RH, 400 ppm CO_2 and a flow rate of 400 µmol s^{-1}. Measurements were completed within 4 h of abscission. We independently tested the effect of abscission on PR and found no significant decline in A or g_s for up to 4 h, for abscised leaves compared to those attached to the plant (Supplementary table C3.1). Specific leaf area (SLA) was determined on a 3 cm section of the youngest fully-expanded leaves as described in 3.2.4. Leaf area index (LAI) was calculated by multiplying the average sward SLA by the herbage DW per unit ground area. For field swards, a ground area of 0.18 m^2 per sward was used, assuming that experimental and border plants shared the ground area between them equally. In the growth chamber work, ground area was calculated from the measured total area of the bench used for the experiment (including the ~12 cm of leaf growth into the border regions).

4.2.10 Statistical analysis

All statistical analyses were performed in R (Version 3.6.2, R foundation). *p*-values < 0.05 were considered significant. All data collected from swards at multiple time-points were analysed using a linear mixed model (REML) with transgene status and sward position as fixed factors and harvest number as the repeated measure. The 'lmerTest' R package was used to estimate *p*-values with Satterthwaite's method, followed by pairwise treatment comparisons which were obtained with *p*-values adjusted according to the Benjamini-Hochberg (BH) procedure. All data collected from plants at one timepoint were analysed by Student's t test, Wilcoxon rank sum test, and one or two-way ANOVA without repeated measures. Leaf extension data were analysed using a linear mixed model from the 'lme4' R package. Leaf number was nested within plant number, and the time parameter (days) was rescaled for modelling and was calculated from the observation day minus the day of the first non-zero observation for each leaf. A quadratic term, and interactions between transgene status, leaf number and day were fitted to allow for different leaf growth curve responses. Field trial A_{area} and g_s data from family O were log transformed to achieve normality.

4.3 Results

4.3.1 Indoor spaced pot experiment – Shoot morphology

HME2+ progeny had 5.16 ± 0.09 %DW leaf FA content while null progeny had 3.91 ± 0.06 %DW leaf FA content (p<0.001; mean ± SE, n=26–28). The number of tillers per plant did not significantly differ between HME2+ and null progeny during the first 40 days of growth from seed ('primary growth') (Figure 4.1). Leaf (lamina) extension rates and final leaf length increased for each successive leaf on the primary tiller. Leaf extension rate and the final length of leaf 6 was significantly greater for the HME2+ progeny compared to the null progeny (p<0.001) (Figure 4.1). Final leaf width, however, was consistently 5–9% lower for the leaves of HME2+ progeny (Figure 4.1). Therefore, only for HME2+ leaf 6 was the final leaf area significantly greater (by 12%) than for null leaf 6 (Figure 4.1). HME2+ sheath height was also 10–11% greater for leaves 4–6 (Figure 4.1). There was no significant difference in leaf extension duration between HME2+ and null progeny.

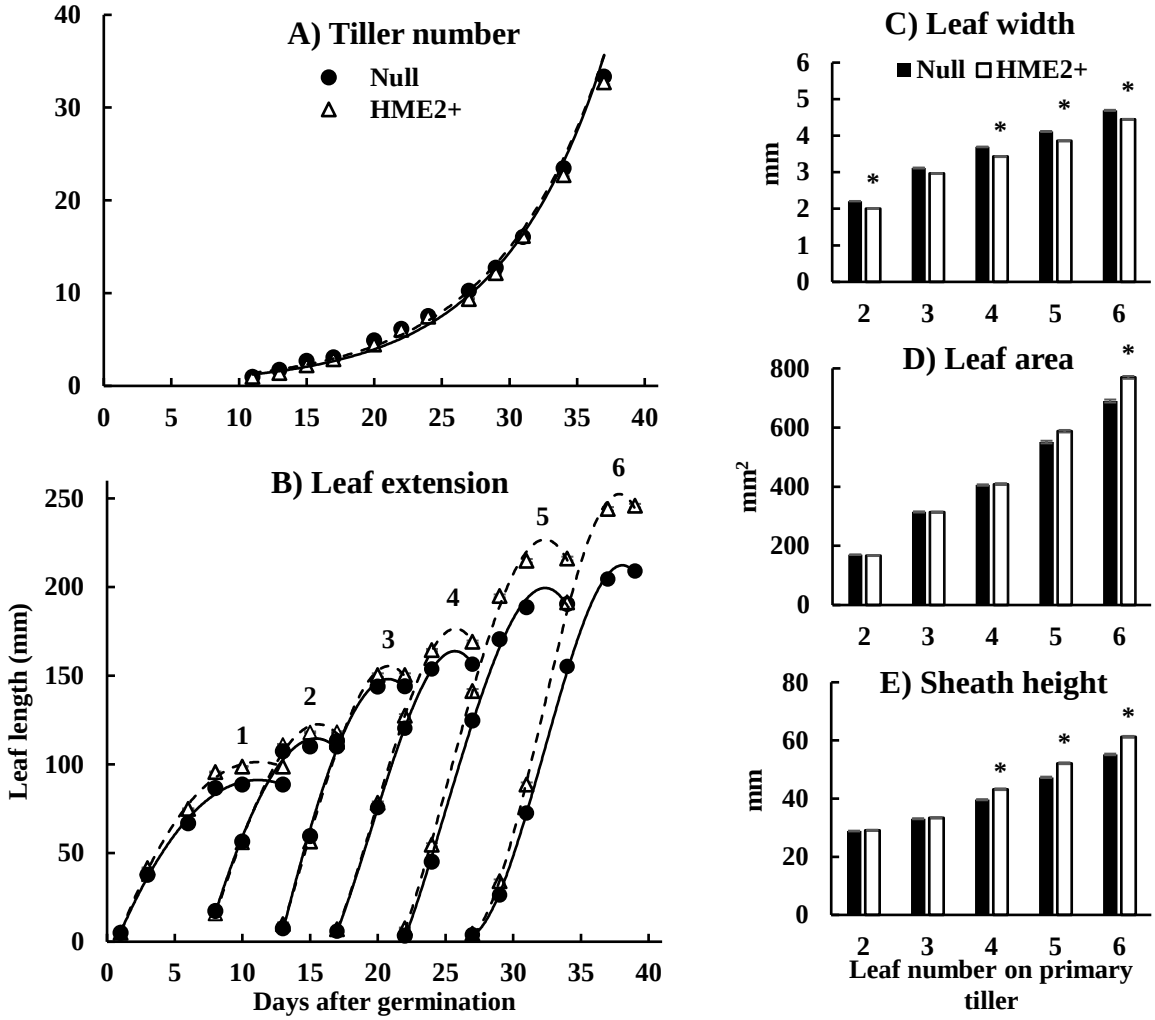

Figure 4.1 Shoot morphology parameters during the first 40 days growth from seed of an HME+ and null segregating T_2 *Lolium perenne* population (HME2) grown in spaced pots indoors. Data points represent means ± S.E. (*n*=26–28). Note the error bars are small. The * symbol above the bars in C-E indicates a significant difference at $p<0.05$.

4.3.2 Indoor spaced pot experiment – Leaf level photosynthesis and growth

Primary growth leaf DW and light saturated photosynthetic rate per unit area (A_{sat}) did not significantly differ for HME2+ and null progeny. However, HME2+ progeny exhibited a 16% increase in specific leaf area (SLA) and there was an associated 18% increase in the photosynthetic rate per unit leaf mass (A_{mass} = SLA x A_{sat}) (Table 4.2). Compared to the primary growth, A_{sat} was lower, and SLA was higher during regrowth after defoliation, and both A_{sat} and SLA were similar for null and HME2+ leaves during regrowth (Table 4.2). After 21 days of regrowth, HME2+ progeny had higher leaf DW (9%) than the null progeny, while sheath DW did not differ. HME2+ progeny also had a higher root DW (35%) and total plant DW (13%) than the null progeny (Table 4.2).

Table 4.2. Biomass (A) and leaf-level photosynthetic traits (B) of an HME+ and null segregating T_2 *Lolium perenne* population (HME2) grown in spaced pots indoors.

A)		**Leaf DW (g)**	**Sheath DW (g)**	**Root DW (g)**	**Total DW (g)**	**RMF (%DW)**
Primary growth	**Null**	0.83 ± 0.02	-	-	-	-
	HME2+	0.87 ± 0.03	-	-	-	-
	***p*-value**	*0.37*	-	-	-	-
Regrowth	**Null**	6.88 ± 0.14	4.31 ± 0.15	3.31 ± 0.16	14.50 ± 0.37	22.6 ± 0.6
	HME2+	7.51 ± 0.14	4.33 ± 0.12	4.49 ± 0.25	16.33 ± 0.42	27.0 ± 0.9
	***p*-value**	*0.002*	*0.91*	*<0.001*	*0.002*	*<0.001*

B)		**A_{sat} ($\mu molCO_2\ m^{-2}\ s^{-1}$)**	**SLA ($cm^2\ gDW^{-1}$)**	**A_{mass} ($\mu molCO_2\ gDW^{-1}\ s^{-1}$)**	**g_s ($CO_2\ m^{-2}\ s^{-1}$)**	**Total LA (cm^2)**
Primary growth	**Null**	25.6 ± 0.9	194 ± 6	0.50 ± 0.02	0.59 ± 0.04	165 ± 7
	HME2+	26.2 ± 0.5	226 ± 6	0.59 ± 0.02	0.59 ± 0.02	201 ± 8
	***p*-value**	*0.62*	*0.002*	*0.013*	*0.98*	*0.009*
Regrowth	**Null**	20.9 ± 0.5	266 ± 6	0.55 ± 0.01	0.42 ± 0.02	1867 ± 52
	HME2+	21.7 ± 0.4	260 ± 5	0.56 ± 0.01	0.48 ± 0.02	1967 ± 34
	***p*-value**	*0.29*	*0.47*	*0.72*	*0.069*	*0.173*

RMF = root mass fraction, A_{sat} = net photosynthesis near saturating light, g_s = stomatal conductance, A_{mass} = photosynthesis per unit leaf mass, SLA = specific leaf area, LA = leaf area. Plants were grown from seed for 40 days ('Primary growth'), defoliated, then destructively harvested after 21 days regrowth. *p*-values were obtained using Student's t test or Wilcoxon rank sum test. Values represent means ± S.E. In A) *n*=26–28 and in B) *n*=20.

4.3.3 Indoor sward experiment – FA, GE, and herbage growth rates over time

Over 8 consecutive defoliation events, herbage harvested from HME2+ miniswards exhibited a 34% higher average herbage FA concentration than null controls (range 23–40%, +0.8–1.5 %DW) (Figure 4.2), and a 2% higher average herbage gross energy (GE) concentration (range 1.3–2.9%, +0.2–0.5 kJ gDW^{-1}) (Figure 4.2). For harvests 4–6, when the pots were arranged in spaced rows with a 17 day regrowth interval, HME2+ miniswards displayed a 6–10% faster herbage growth rate per pot than null miniswards (Figure 4.2). For harvests 7–9, when the pots were packed into a dense sward, herbage growth decreased and the HME2+ miniswards had a similar herbage growth rate to the null miniswards. GE per pot (GE concentration x herbage DW) was 5–12% higher for HME+ miniswards for harvests 3–7 (Figure 4.2). Tiller number and size was lower in a dense sward compared to a spaced row. Tiller number was similar for the null and HME2+ miniswards in both pot arrangements, but the reduction in tiller size in a dense sward compared to a spaced row was greater for HME2+ miniswards than null miniswards (Table 4.3).

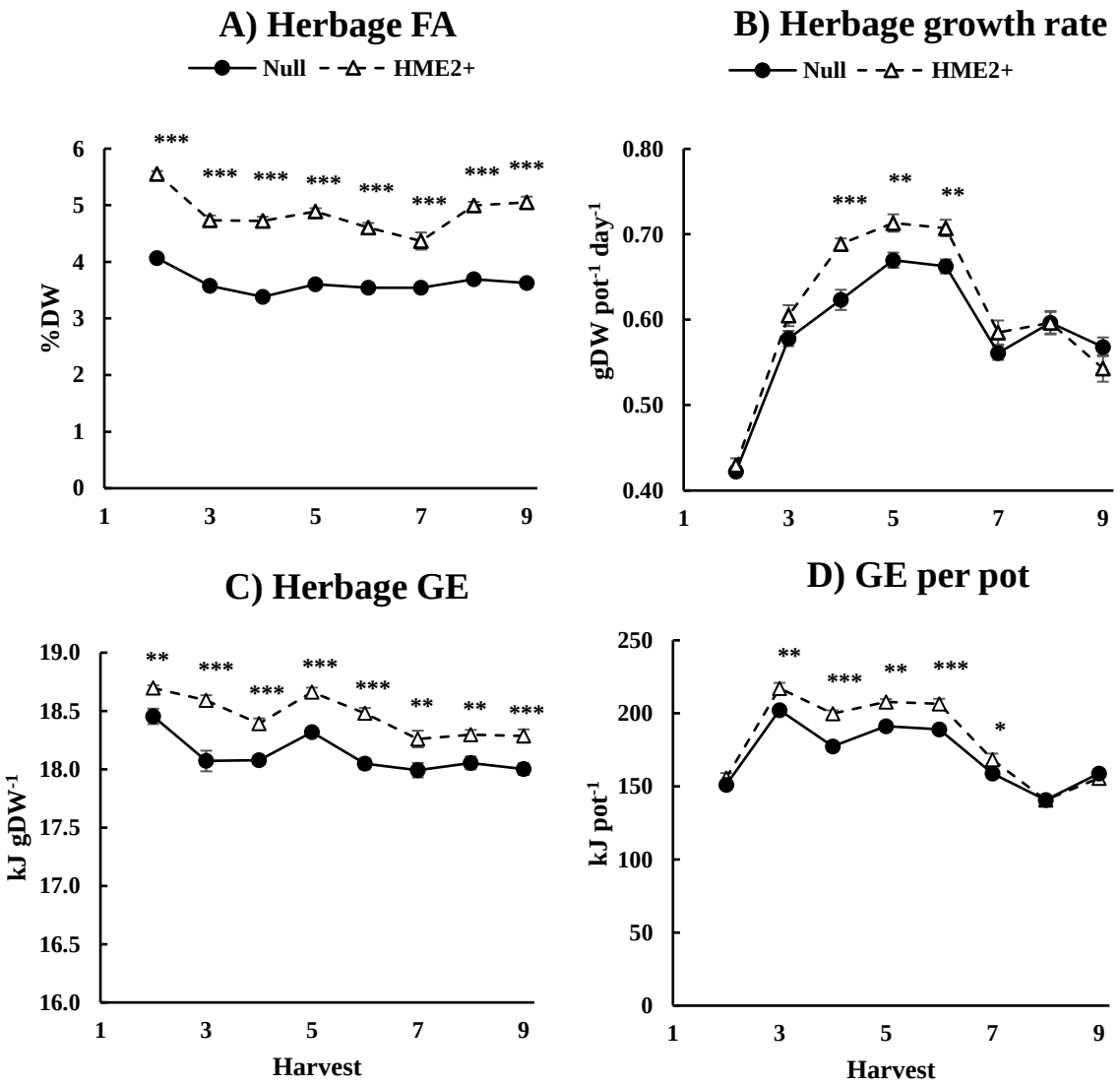

Figure 4.2. Herbage fatty acids (FA), growth rate, and gross energy (GE) in an HME+ and null segregating T_2 *Lolium perenne* population (HME2), grown in indoor miniswards under regular defoliation. Pots were spaced apart from one another for harvests 2–6 and packed tightly together for harvests 7–9. Data points represent means ± S.E. * = p<0.05, ** = p<0.01, *** = p<0.001 indicate differences between HME+ and null segregating progeny, obtained using the BH method. In B) n=12, and in A, C and D) n=6.

Table 4.3. Harvest 11 sward structure parameters for an HME+ and null segregating T_2 *Lolium perenne* population (HME2), grown in indoor miniswards under regular defoliation.

Spacing	Genotype	TN	TW (mg)	L:NL ratio	SLA ($cm^2\ gDW^{-1}$)	R
Dense sward	**Null**	491 ± 14 A	49.9 ± 1.3 B	0.90 ± 0.03 B	315 ± 7 B	34.6 ± 1.4 C
	HME2+	475 ± 9 A	45.2 ± 1.9 B	1.00 ± 0.04 AB	362 ± 10 A	43.9 ± 1.8 A
Spaced row	**Null**	506 ± 13 A	50.8 ± 2.5 B	1.04 ± 0.05 AB	297 ± 12 B	35.7 ± 2.7 BC
	HME2+	511 ± 10 A	58.7 ± 2.1 A	1.11 ± 0.04 A	302 ± 3 B	41.8 ± 1.4 AB
ANOVA						
Spacing		*	**	**	***	ns
Transgene		ns	ns	ns	**	***
Spacing x Transgene		ns	**	ns	*	ns

For the 10th and 11th defoliation/regrowth cycles the higher-yielding miniswards were reassigned to a spaced row, while the lower-yielding miniswards were kept in the tightly packed pot arrangement (*n*=6). For harvest 11, rather than cutting to ~5cm, tillers were harvested at the base destructively for size, structure, and density analysis. Total tiller number per pot was counted, then a subsample of 10 tillers was taken from each pot, separated into leaf and non-leaf material, and weighed. Tiller dissection data and SLA were used to estimate the tiller shape parameter R (Matthew et al., 1995). TN = tiller number, TW = tiller weight, L:NL = leaf to non-leaf ratio, SLA = specific leaf area, R = tiller shape index. Different letters indicate significant differences at $p<0.05$ between treatments, obtained using the BH method, after performing a two-way ANOVA. Values represent means ± S.E. (*n*=6).

4.3.4 Field sward experiment – FA, GE, and herbage growth rates over time

For the final three harvests of the field season, herbage from both HME1+ families (M and O) contained 15–30% higher FA content than the null control swards (Figure 4.3). For both families at harvest 4, when HME1+ herbage FA content was 29–30% (+0.9–1 %DW) higher than for the null control swards, HME1+ herbage GE was also 1.5–2.9% (+0.3–0.5 kJ gDW^{-1}) higher (Figure 4.3). At harvest 3, when HME1+ herbage FA content was only 20–24% (+0.6 %DW) higher than for the null controls, HME1+ and null herbage GE were similar (Figure 4.3). Herbage growth rates differed significantly between harvests, but did not differ for HME1+ and null swards during harvests 1–3 (Figure 4.3). During harvest 4, HME1-M+ swards displayed a 27% faster herbage growth rate than the corresponding null swards (p=0.04), however, no growth difference between HME1-O+ and null swards was detected (Figure 4.3).

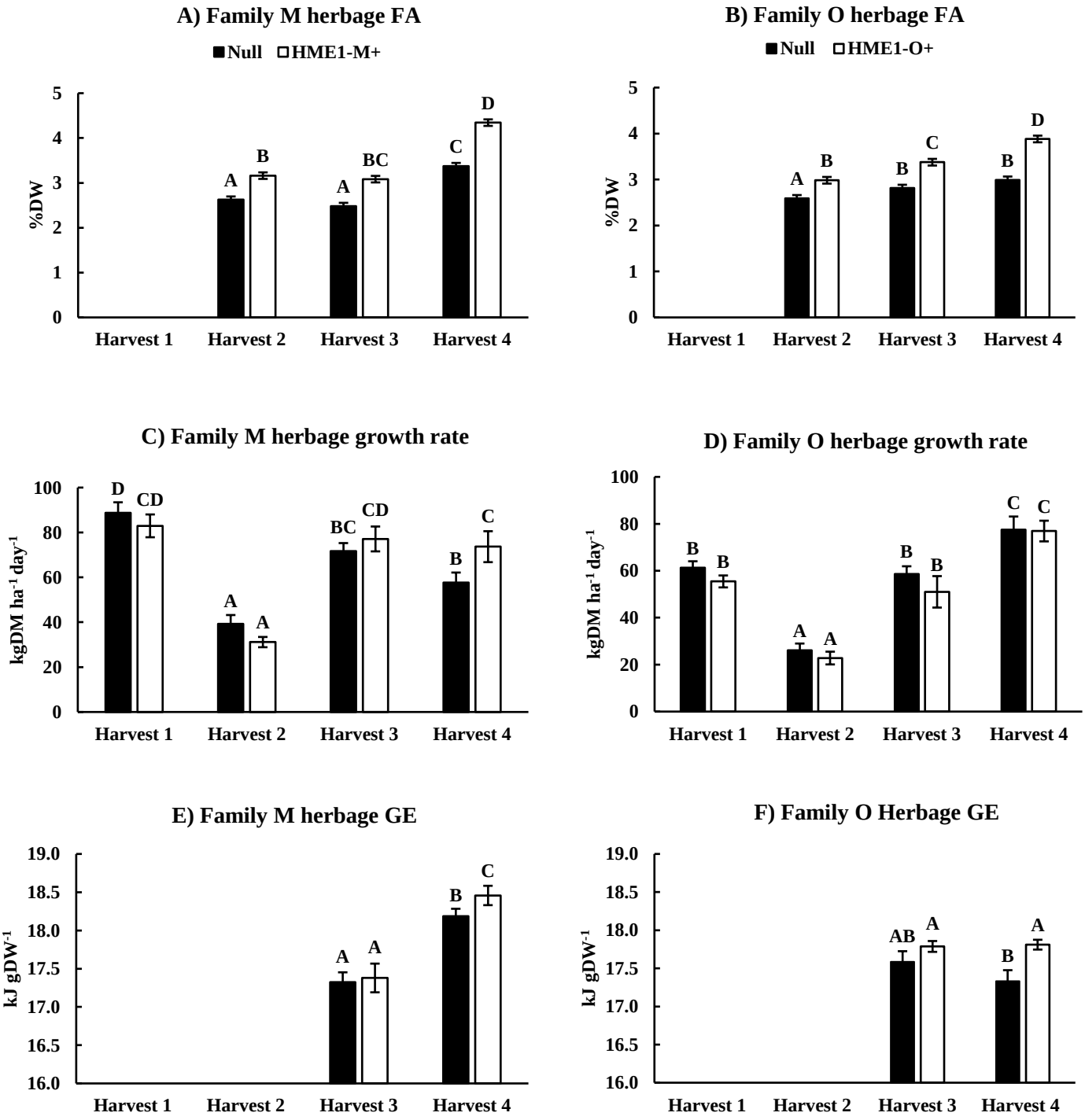

Figure 4.3. Herbage fatty acids (FA), growth rate, and gross energy (GE) in two HME+ and null segregating T_2 *Lolium perenne* families (HME1-M and HME1-O) grown in field miniswards under regular defoliation. Bars represent means ± S.E. (*n*=5). Different letters indicate significant differences at $p<0.05$ between treatments, obtained using the BH method.

4.3.5 Field sward experiment – Herbage FA profile

At the final harvest of the field season, C18:1 and C18:2 as a percentage of total FA were both higher for HME1+ compared to null control herbage (Table 4.4). C18:0 did not differ, while C16:0, C16:1 and C18:3 as a percentage of total FA were lower for HME1+ compared to null control herbage (Table 4.4). Similar FA profile trends were obtained from HME2+ and null control swards grown indoors (Supplementary table C3.2).

Table 4.4. Harvest 4 fatty acid (FA) profiles for HME1+ and null segregating T_2 *Lolium perenne* populations (HME1-M, HME1-O) grown in field miniswards.

Family	Transgene status	C16:0 (%FA)	C16:1 (%FA)	C18:0 (%FA)	C18:1 (%FA)	C18:2 (%FA)	C18:3 (%FA)	Total FA (%DW)
HME1-M	Null	15.5 ± 0.1	2.4 ± 0.1	1.6 ± 0.1	2.1 ± 0.2	11.8 ± 0.3	65.3 ± 0.6	3.4 ± 0.1
	HME1-M+	14.4 ± 0.3	2.0 ± 0.1	1.3 ± 0.2	5.7 ± 0.8	19.2 ± 1.6	56.2 ± 2.2	4.4 ± 0.2
	p-value	*<0.001*	*0.002*	*0.032*	*<0.001*	*<0.001*	*<0.001*	*<0.001*
HME1-O	Null	16.2 ± 0.2	2.1 ± 0.0	1.4 ± 0.0	1.9 ± 0.1	13.9 ± 0.3	63.6 ± 0.5	3.0 ± 0.1
	HME1-O+	14.7 ± 0.1	1.9 ± 0.1	1.5 ± 0.0	6.1 ± 0.1	22.2 ± 0.3	52.0 ± 0.2	3.9 ± 0.1
	p-value	*<0.001*	*0.097*	*0.184*	*<0.001*	*<0.001*	*<0.001*	*<0.001*

Values for each FA class represent the mean percentage of total FA ± S.E. (*n*=5). *p*-values were obtained using Student's t test.

4.3.6 Comparison of field and indoor swards – Leaf level photosynthesis and LAI

Photosynthesis (A_{area}) and stomatal conductance (g_s) measured near ambient irradiance, specific leaf area (SLA), and leaf area index (LAI) values were lower in PR field swards compared to indoor miniswards, regardless of transgene status. A_{area}, g_s and SLA did not differ for HME1+ and null control plants grown in field swards, while LAI was significantly higher for HME1-M+ swards (Table 4.5). Indoors, A_{area} and g_s did not significantly differ between HME2+ and null control swards (Table 4.5). SLA and LAI did not differ for HME2+ and null control swards for harvests 2–8 (Table 4.5), but SLA was significantly higher for HME2+ leaves from dense swards for harvest 9–11 (Table 4.5; Table 4.3).

Table 4.5. Leaf-level photosynthetic traits and leaf area index (LAI) for HME+ and null segregating T_2 *Lolium perenne* populations (HME1-M, HME1-O and HME2) grown in the field (A) and in indoor miniswards (B).

		Transgene status	A_{area} ($\mu molCO_2\ m^{-2}\ s^{-1}$)	g_s ($CO_2\ m^{-2}\ s^{-1}$)	SLA ($cm^2\ gDW^{-1}$)	LAI ($m^2\ m^{-2}$)
A) Field experiment (HME1)	**HME1-M (harvest 3-4)**	Null	16.4 ± 1.3	0.20 ± 0.02	267 ± 7	3.4 ± 0.3
		HME1-M+	13.4 ± 1.3	0.21 ± 0.05	287 ± 7	4.7 ± 0.5
		p-value	*0.221*	*0.280*	*0.055*	*0.034*
	HME1-O (harvest 3-4)	Null	12.6 ± 1.3	0.14 ± 0.04	284 ± 9	4.8 ± 0.4
		HME1-O+	15.1 ± 1.3	0.19 ± 0.04	259 ± 8	4.5 ± 0.3
		p-value	*0.299*	*0.469*	*0.072*	*0.572*
B) Indoor experiment (HME2)	**Spaced row (harvest 6)**	Null	18.1 ± 0.7	0.45 ± 0.01	349 ± 11	8.6 ± 0.3
		HME2+	17.1 ± 0.4	0.40 ± 0.02	354 ± 13	8.0 ± 0.4
		p-value	*0.181*	*0.118*	*0.767*	*0.183*
	Dense sward (harvest 8-9)	Null	17.8 ± 0.5	0.53 ± 0.03	330 ± 12	10.2 ± 0.4
		HME2+	17.9 ± 0.5	0.47 ± 0.03	384 ± 12	11.3 ± 0.3
		p-value	*0.788*	*0.123*	*0.004*	*0.036*

Net photosynthesis (A_{area}) and stomatal conductance (g_s) were determined at 1000 photons $m^{-2}\ s^{-1}$ in the field before harvest 3 (*n*=20), while specific leaf area (SLA) was determined before harvest 4 (*n*=10–15). A_{area} and g_s were determined indoors at 500 photons $m^{-2}\ s^{-1}$ before harvests 6 and 8, while SLA and was determined before every harvest, but only data from harvests 6 and 9 are presented (*n*=12). Values represent means ± S.E. *p*-values for the field experiment were obtained using the BH method, after performing a two-way ANOVA. *p*-values for the indoor experiment were obtained using Student's t test.

4.4 Discussion

T_2 populations derived from gene-gun transformed HME PR lines segregated approximately 1:1 HME+:null. In small canopies under regular defoliation, the HME+ progeny from these populations exhibited 23–40% higher herbage FA content indoors and 15–30% higher herbage FA content in the field, compared to null controls. In all instances where FA content differences between HME+ and null herbage exceeded 0.8 %DW, HME+ swards also exhibited +0.2–0.5 kJ gDW^{-1} higher herbage GE. In spaced pots indoors, HME+ progeny produced 9% more leaf biomass, and 13% more total plant DW than the controls. The use of PR populations segregating for the HME transgenes ruled out the possibility that the HME growth advantage could be explained by somaclonal variation between T_0 transgenics, which can arise during tissue culture procedures (Badenhorst et al., 2016). The HME biomass advantage translated into greater herbage production in miniswards arranged in spaced rows but did not reliably translate into greater herbage production in dense swards indoors or field swards, except for the final harvest of the field season for the HME1-M+ progeny. This highlights the complex transition from the lab to the field when testing novel pleiotropic traits. Despite significant changes in PR growth form between the lab and the field, HME technology enhanced the FA and GE content of PR leaves under realistic growing conditions.

4.4.1 Methods used

We used an industry-standard 5 x 5 plant field minisward design (Pers. comm, Dr Alan Stewart) with ~0.18 m^2 internal ground area to assess herbage FA, GE, and growth per unit ground area. Border plants were used and replicate miniswards were well-spaced, allowing treatment effects to be fully attributed to transgene expression. In the indoor experiments, transgenic and null miniswards were grown in close proximity (Supplementary figure C3.1); however, the authors feel that any possible competitive interactions between HME+ and null plants did not significantly impact the results.

4.4.2 HME PR nutritional composition in canopy-like conditions

The 23–40% higher herbage FA content (+0.8–1.5 %DW) observed in indoor-grown HME2+ miniswards translated into +0.2–0.5 kJ gDW^{-1} higher herbage GE over 8 consecutive harvests compared to null controls (Figure 4.2). Similarly, HME1+ field-grown swards exhibiting 29–30% higher end-of-season herbage FA content (+0.9–1.0 %DW) also had +0.3–0.5 kJ gDW^{-1} higher GE (Figure 4.3). These herbage FA and GE levels were achieved with the HME

transgenes expressed in the hemizygous condition, which probably limits the degree of HME FA accumulation (Winichayakul et al., 2013). For field harvest 3, herbage FA differences between HME+ and null progeny were ~0.6 %DW, and GE did not significantly differ. The smallest measured FA difference between HME1+ and null herbage occurred at field harvest 2, which coincided with low herbage growth rates (Figure 4.3) and sustained high temperatures (Table 4.1). Larger increases in FA, (+2.2–2.5 %DW) and correspondingly GE (+1.0–1.2 kJ gDW^{-1}) were reported for lab-grown T_0 HME PR compared to control PR (Winichayakul et al., 2020). Assuming an energy density of 38 kJ gDW^{-1} for FA, substituting 1% of DW for FA should enhance the GE of plant material with a baseline GE of 17–18 kJ gDW^{-1} (Monteith, 1972), by ~0.2 kJ gDW^{-1}. The actual increase in GE for HME+ compared to null PR herbage in these experiments (average 0.3 kJ gDW^{-1}) was ~50% greater than predicted by this simple substitution (and the measured differences in leaf FA content determined by FAMEs GC-MS), supporting earlier speculation that other compositional changes may occur in HME PR (Winichayakul et al., 2020). Interestingly, FA content for both HME2+ and null herbage determined by FAMEs was lower, and only approximately proportional to the amount of crude fat measured from ether extracts (r^2=0.36).

Trade-offs between lipids and other plant components could arise from indirect dilution effects or direct physiological effects. Other workers have reported positive correlations between FA and CP (Glasser et al., 2013), and negative correlations between FA and both WSC (Cosgrove et al., 2009; Palladino et al., 2009) and NDF (Morgan et al., 2020) between PR varieties. In our data, such changes were not consistently apparent in oven-dried HME2+ herbage. No FA-WSC trade-off was detected (Supplementary figure C3.4), although these samples lost a large and variable proportion of WSC during drying and storage. CP was lower and DOMD was higher in HME2+ herbage for harvests 4–7 (Supplementary figure C3.4); the same harvests for which HME2+ miniswards exhibited a 6–10% faster herbage growth rate, and an 8–12% higher C:N ratio (Supplementary figure C3.4). Since the miniswards were grown in restricted rooting volumes (i.e. above 'pot limits') (Poorter et al., 2012a), the HME2+ miniswards may have approached N-deficient status earlier during each regrowth, which could influence overall nutritional composition (King et al., 2012). Further field studies are needed to better understand HME compositional changes, because of the potential advantages and drawbacks of accumulating each plant component. For example, enhancing the WSC: CP ratio may reduce N excretion, but may increase CH_4 production by ruminants

(Ellis et al., 2011; Ellis et al., 2012), while high lipids may reduce CH_4 production (Grainger & Beauchemin, 2011; Winichayakul et al., 2020). Although DOMD-based estimates of forage ME are commonplace e.g. (Arojju et al., 2020; Badenhorst et al., 2018; Wims et al., 2017), these methods may not be suitable for high-lipid forages, since they do not explicitly account for differences in the energy density of digestible plant components (Weiss, 1998). Translation of the high GE trait into high ME will depend on whether lipids accumulate primarily at the expense of digestible or indigestible plant fractions, with a reduction in the latter expected to deliver larger increases in ME (Faville et al., 2010). Digestible energy from fat is used efficiently in ruminant production because it does not contribute to methane or urine production (Weiss, 1998).

4.4.3 HME PR growth in canopy-like conditions

Indoors in spaced rows, HME2+ miniswards consistently yielded 6–10% more 'herbage DW' (shoot material harvested from 5cm above the potting media) under mechanical defoliation than the null controls (Figure 4.2). Tiller density per pot did not differ between HME2+ and controls; however, faster leaf extension (Figure 4.1) enhanced the size and 'leafiness' of the HME2+ tillers which contributed to the observed increase in HME2+ productivity. The HME2+ leaf growth advantage which occurred under moderate light competition (harvest 4–6, LAI ~ 6.8–9.1) was neutralized during later regrowth cycles in a dense canopy (harvests 7–9, LAI ~ 10.8–11.7) (Figure 4.2). Interestingly, HME2+ leaf FA content was higher and tiller size was lower under strong light competition compared to moderate light competition, while the degree of light competition had no effect on leaf FA content or tiller size for the null controls (Supplementary table C3.2; Table 4.3). The energetic costs of synthesizing additional lipids under shade may mean that HME PR performance is highly light-sensitive (Pers. Comm., Dr Somrutai Winichayakul).

Field sward LAI values were lower (3.4–4.8), while estimated daily PAR integrals (total daily solar radiation x 0.45) (Monteith, 1972) were generally higher than indoors (Table 4.1). Therefore, light availability was less likely to limit assimilation in the field, and the general absence of a HME1+ growth rate advantage in the field may be attributed to other environmental factors such as high temperatures (Table 4.1). The segregating populations studied in the field and indoors were derived from independent HME transformation events, so a transformation event/genetic background effect cannot not be ruled out either.

Regardless, the genetic backgrounds of the HME1 and HME2 segregating populations were similar, as was the relative increase in leaf FA content for the HME+ compared to the corresponding null progeny. The data suggest that PR can support ~30% higher leaf FA with little impact on sward growth rate under normal water and fertilizer input. Further field studies could examine relationships between elevated lipids, herbage productivity and interplant competition (LAI) by measuring herbage yield in HME populations with a range of lipid levels under different defoliation frequencies.

4.4.4 Limits to plasticity in leaf C assimilation traits?

Unlike several T_0 HME genotypes regrown in spaced pots (2.3.2), the T_2 HME+ progeny studied here did not exhibit a significant increase in photosynthetic rate per unit leaf area (A_{area}) compared to their null siblings. However, an 18% increase in A_{mass} associated with a high SLA (p=0.002) was recorded in HME2+ progeny grown in spaced pots (Table 4.2). The absence of an HME A_{area} advantage here might relate to the comparatively low 'expression levels' in the T_2 compared to the parental T_0 HME+ material (gene dosage effect) (Supplementary Figure C3.3). Alternatively, the HME A_{area} advantage might have been diminished by the introduction of new germplasm (2.4.2), or more speculatively, because young perennials already maximize short-term C assimilation (Parsons et al., 2013). The HME2+ SLA advantage seen in spaced pots (Table 4.2) was not initially detected in indoor miniswards under defoliation; however it re-appeared in densely-packed HME2+ swards during the final three harvests of the indoor experiment (Table 4.3; Table 4.5), which contributed to a higher HME2+ tiller leaf area: volume ratio (Matthew et al., 1995) (Table 4.3). There were no distinct differences between HME1+ and null SLA in the field (Table 4.5). The reasons for these inconsistent HME SLA effects are a matter of speculation. We previously showed that the relative increase in leaf FA content correlated positively with SLA and negatively with leaf WSC for multiple T_0 HME lines regrown in spaced pots (Figure 2.2). A transiently higher SLA was also recently reported in high lipid/low sugar transgenic tobacco (Mitchell et al., 2020). In the present work, there was also a positive association between PR SLA and the degree of interplant competition (Table 4.2; Table 4.3), consistent with literature reports on the influence of competition on SLA (Poorter et al., 2016). Perhaps the positive relationship between leaf FA content and SLA can be confounded by external factors that reduce C availability such as shading, although this requires further testing.

4.4.5 Future challenges for commericalizing an HME cultivar

From an agronomic perspective, annual variation between small field studies is large (Poorter et al., 2016), hence, the results obtained here require multi-year validation at multiple sites in temperate latitudes. To simplify the process of generating an HME cultivar, only 'single copy' T_0 events will be introduced into elite PR breeding accessions. Therefore, it needs to be established whether single-copy HME transformation events bred into the homozygous condition can enhance PR herbage FA beyond ~1.0 %DW and GE beyond +0.3–0.5 kJ gDW^{-1}. The associated impacts of additional lipids on sward growth and nutritional composition will then need to be tested. Animal feeding trials are needed to accurately quantify ME and to validate preliminary *in vitro* rumen fermentation findings associated with HME expression, such as reduced methane emissions and rumen biohydrogenation (Winichayakul et al., 2020).

The HME PR physiology provides an interesting contrast to that of the 'high sugar grasses'; PR varieties selected to accumulate fructans in the leaf lamina (Edwards et al., 2007; Humphreys, 1989). It was speculated that accumulating carbohydrate in leaves might deflect carbon from plant growth, and detailed growth analyses by Turner et al. (2001) supported this speculation. Our data show that creating internal competition for photosynthate in leaves can increase PR growth, if moderate amounts of leaf FA, rather than WSC, accumulate. This is counterintuitive given that even small increases in lipid synthesis likely impose an energetic cost. However, leaf carbohydrates are not an inert sink for photosynthate; their accumulation signals to downregulate photosynthesis as part of energy homeostasis (Paul & Foyer, 2001). In contrast, photosynthesis may be effectively 'blind' to leaf lipid accumulation (Paul and Eastmond, 2020), especially when leaf lipids are encapsulated (3.4.4). We previously showed that the intrinsically high growth rate of HME PR was contingent upon enhanced leaf FA accumulation leading to partial depletion of leaf carbohydrate stores (2.4.1). A logical extension of this finding is that environmental factors that also deplete leaf sugars (for example low light or high temperatures) may diminish the intrinsic growth advantage of HME plants. Regardless, the results in this chapter support the potential for HME technology to enhance pasture energy density and yield potential under realistic growing conditions. Further research on encapsulated leaf lipids as 'alternative sinks for photosynthate' (Evans & Lawson, 2020) may benefit the field of photosynthesis research.

Chapter 5

Mechanisms by which leaf DGAT1 + cysteine-oleosin expression enhances photosynthetic nitrogen use efficiency in *Lolium perenne*

5.1 Introduction

Nitrogen (N) is the mineral element required in the greatest quantity by plants and plays a critical role in attaining the high yields required of modern agriculture (Andrews et al., 2013). N is a constituent of many vital cellular components, but in crop leaves, up to 80% of total N is invested in the machinery of photosynthesis (Evans & Seemann, 1989). Given the large N requirement of photosynthesis, leaf CO_2 assimilation per unit area (A_{area}) often correlates with leaf N content per unit area (N_{area}). However, there also exists substantial variation in photosynthetic rate for leaves with a similar N_{area} (Evans, 1989). The CO_2 assimilation rate per unit leaf nitrogen (A_{area}/N_{area} = PNUE) is an important metric of photosynthetic efficiency which is influenced by a range of leaf chemical and physical traits (Poorter & Evans, 1998). PNUE contributes to between-cultivar (intraspecific) variation in whole-plant N-use efficiency for major grain crops (Chen et al., 2014; Ju et al., 2015; Pang et al., 2015), although there is little detailed knowledge about the underlying physiological mechanisms (Mu et al., 2016).

Ecological research has highlighted the importance of interspecific differences in PNUE associated with variation in specific leaf area (SLA): the leaf area per unit of mass. Interspecific variation in SLA has no consistent effect on A_{area}, despite a higher SLA often leading to dilution of leaf N on an area basis (Wright et al., 2004). The greater efficiency by which high SLA species utilize leaf N for photosynthesis contributes to their superior intrinsic growth rate (Poorter et al., 1990), and the mechanisms that contribute to this efficiency are now well-understood (Onoda et al., 2017). The leaves of high SLA species generally exhibit lower stomatal and mesophyll resistance (higher conductance) to CO_2 movement and therefore achieve efficient CO_2 transfer from the atmosphere to carboxylation sites (Onoda et al., 2017). Further, high SLA species allocate less leaf N to structural components such as cell walls, and more N to photosynthesis (Hikosaka, 2004; Onoda et al., 2017; Poorter & Evans, 1998).

Metabolic engineering to enhance lipid content in vegetative biomass could enhance future oil yields (Durrett et al., 2008; Xu & Shanklin, 2016). While the effect of introducing a new

energy-dense C sink on plant growth is typically negative (Vanhercke et al., 2019), this may depend on the crop species or cultivar (2.4.2; 4.4.4), levels and expression patterns of different transgene combinations, or the strategy by which lipids are protected from catabolism [3.4.4 c.f. (Vanhercke et al., 2017)]. For example, co-expression of the gene pair DGAT1 + cysteine-oleosin (1.2.5) in the leaves of *Lolium perenne* (referred to as HME PR) enhanced leaf FA content by 15–96%, and also induced a high SLA and photosynthesis per unit leaf mass (A_{mass}), leading to increased plant growth (2.3.2; 3.3.2; 4.3.2). A higher SLA was also recently reported in high lipid/low sugar transgenic tobacco during vegetative growth (Mitchell et al., 2020).

Enhancing photosynthetic efficiency is an important target for the sustainable intensification of agriculture (Evans & Lawson, 2020) and a wide variety of potential targets for manipulation have been put forward (Zhu et al., 2020). Many proposed manipulations have a theoretical associated 'N-cost' (Evans & Clarke, 2019) which can range from effectively zero e.g. (Slattery et al., 2017), to 'high' e.g. (Sharwood et al., 2016). Changes in the rate of C gain per unit of associated variation in leaf N (ΔPNUE) may become an important criterion for evaluating strategies of photosynthetic improvement (Evans & Clarke, 2019). Researchers have yet to investigate the effect of altering the leaf FA content or the SLA of transgenic crop lines on ΔPNUE.

An important question regarding HME PR leaf physiology is whether the high SLA trait leads to a dilution of leaf N on an area basis. If so, one or more HME leaf traits would need to be modified in order to enhance HME PNUE and prevent A_{area} from being penalized. To investigate this, photosynthesis - leaf nitrogen (A-N) relationships were examined for HME PR with a range of elevated leaf fatty acids (FA) levels, within different genetic backgrounds and plant developmental stages, and with different sources of mineral N. Then, for a selected high lipid HME PR line, several major determinants of PNUE were assessed, including leaf internal CO_2 diffusion rate and within-leaf N partitioning to different photosynthetic and non-photosynthetic pools.

5.2 Materials and Methods

5.2.1 Plant material and summary of experimental design

Data from four indoor spaced pot experiments are presented in this chapter. A full description of the plant material, growth chamber conditions, and experimental design of experiments 1-3 is provided in chapters 2-4 and a brief summary is given in Table 5.1. Experiments 1, 2 and 4 were conducted in controlled temperature rooms with red/blue LED lights (LEDgrowlights, Hamilton, NZ), while experiment 3 was conducted in a Conviron BDW 120 plant growth room (Thermo-Fisher, Auckland, NZ) with white light from metal halide bulbs (400 W Venture Ltd., Mount Maunganui, NZ) and soft tone, white incandescent bulbs (100 W, Philips, Auckland, NZ). The light intensity was similar in all experiments (500 ± 100 μmol photons m^{-2} s^{-1}), the day/night temperature was 20/15 °C, and the photoperiod was 12 h. Washed sand was used as the growth media and a basal nutrient solution described in Andrews et al. (1989) was used to flush the pots every 1 or 2 days. The N source differed between each of the experiments (Table 5.1).

In experiment 1 (see Chapter 2), five independently-transformed T_0 green tissue-expressing DGAT1 + cysteine-oleosin PR genotypes (HME1-5) and three corresponding non-transformed control genotypes (WT1-3) (*n*=10) were regrown under 4 mM NH_4NO_3 (2.2.3). The transgenic genotypes exhibited 15–75% higher leaf fatty acid (FA) content relative to the untransformed controls (Figure 2.1). Leaf total N% (leaf N_{mass}), net photosynthetic rate per unit leaf area (A_{area}) near ambient irradiance (600 μmol photons m^{-2} s^{-1}), and specific leaf area (SLA) were determined 3–4 weeks after defoliation. In experiment 2 (see Chapter 3), the HME line from experiment 1 with the highest lipids (HME5) relative to the corresponding non-transformed control (WT3) was regrown under 5 concentrations of KNO_3^- (1–7.5 mM) under ambient atmospheric [CO_2] as part of the larger experiment described in 3.2. HME5 had 67–96% higher leaf fatty acid (FA) content than WT3. Leaf N_{mass}, A_{area} near saturating irradiance (1500 μmol photons m^{-2} s^{-1}), and SLA were determined 3–4 weeks after defoliation. In experiment 3 (see Chapter 4), the HME-segregating T_2 population derived from the transformation event 'ODR4501' (T_0 event HME2 described in 4.2.1) was grown from seed under 4 mM NH_4NO_3 as described in 4.2.3. The HME+ progeny exhibited 32% higher leaf FA than the null progeny. Leaf N_{mass}, A_{area} near saturating irradiance (1500 μmol photons m^{-2} s^{-1}) and SLA were determined 38–40 days after germination. In experiment 4, HME5 and WT3 were regrown under 5 mM

NO_3^- supply under conditions otherwise similar to experiment 1. Leaf N_{mass}, soluble protein, rubisco, chlorophyll, and a range of leaf gas exchange and chlorophyll fluorescence parameters (see below) were determined 3–4 weeks after defoliation.

Table 5.1. Summary of growth chamber conditions, plant material and experimental designs used for investigating photosynthesis-nitrogen relationships in HME *Lolium perenne*.

Experiment	Generation	HME lines	Control lines	Growth room light source	N source	A_{area} light level	Relative increase in HME leaf FA	*n*
1	T_0	5	3	red/blue (LED)	4 mM NH_4NO_3	600	15–75%	10
2	T_0	1	1	white light (metal halide + incandescent)	1–7.5 mM KNO_3^-	1500	67–96%	3–5
3	T_2	NA*		red/blue (LED)	4 mM NH_4NO_3	1500	32%	20
4	T_0	1	1	red/blue (LED)	5mM KNO_3^-	600	-	6–10

*Segregating population of seed (4.2.3)

5.2.2 Gas exchange and fluorescence measurements

Gas exchange and chlorophyll fluorescence measurements were made for 3 tillers per replicate plant, on a 3 cm section of the youngest fully expanded leaves, starting approximately 5 cm from the leaf tip. Either a Li-COR 6800 (Li-COR Biosciences Ltd, Nebraska, USA; experiments 1 and 4) or Li-COR 6400 (experiments 2 and 3) infrared gas exchange system was used, and leaves were adjusted under the following chamber conditions; 400–415 ppm CO_2, 70% RH, 20–23 °C. PAR was provided by red/blue light, at an intensity which varied between experiments as shown in Table 5.1. After 15–20 mins A_{area}, stomatal conductance (g_s) and transpiration were measured.

For experiment 4, mesophyll conductance (g_m) was calculated via the 'variable J' method (Harley et al., 1992), using:

$$g_m = \frac{A}{C_i - \frac{\Gamma^*[J + 8\,(A + R_d)]}{J - 4\,(A + R_d)}}$$

Where J represents the electron transport rate derived via chlorophyll fluorescence (0.5 x Φ PSII x PAR x α) (Pons et al., 2009). Absorptance (α), was estimated as [Chl]/([Chl] + 76) as in (Evans & Poorter, 2001), where [Chl] is the total chlorophyll per unit leaf area expressed in µmol m^{-2}. J was adjusted according to Pons et al. (2009), using the relationship between J derived via chlorophyll fluorescence and J derived via gas exchange [4 x (A + R_d)] at low C_i under non-photorespiratory conditions, and these data are presented in Supplementary figure D4.1. A-C_i curves were performed as follows; ambient O_2 A-C_i curves were performed first using the following external CO_2 concentrations (ppm); 400, 300, 200, 100, 50, 0, 400, 400, 400, 600, 700, 800, 900, 1000, 1200. At each step, leaves were given 3 mins to acclimate before data logging. The air supply was then switched to 2% O_2 provided by supplementary gas (2% O_2 in N; BOC Limited, NSW, Australia). Leaves were given an additional 30 mins to adjust before the A-C_i procedure was repeated. Rapid light response curves were used for determination of R_d via the Kok method (Kok, 1948), modified after Yin et al. (2011). The same ambient O_2 chamber and acclimation conditions described above were used, except leaves were first acclimated under 1500 µmol photons m^{-2} s^{-1} before dropping PAR to 0 across 10 steps, with 5 mins acclimation at each. R_d was then substituted into the regression equation of the initial A-C_i curve to solve for C_i* (Brooks & Farquhar, 1985). Γ* was solved simultaneously with g_m by substituting Γ* with C_i* + R_d/g_m into the g_m equation above (Warren, 2006). This delivered a single converging value for each g_m and Γ*. V_{cmax} was then derived using the A-C_i analysis function of the Sharkey Excel tool (Sharkey, 2016) with values of g_m, Γ* and R_d fixed as above. Slow light-response curves were completed for determination of J_{max}, and the raw data are presented in Supplementary figure D4.2B. The same chamber conditions were used, however PAR was increased from 0 to 1500 µmol photons m^{-2} s^{-1} across 10 steps with 30 mins acclimation at each. J_{max} was then derived using the light response curve analysis function of the Sharkey Excel tool (Sharkey, 2016), with g_m and R_d fixed.

5.2.3 Leaf nitrogen biochemistry

Sampling for leaf biochemical measurements occurred for tillers harvested 5–6 cm from the shoot base. This material was largely composed of leaf lamina, although a small proportion of leaf sheath was also present. The material was cut to ~2 cm lengths and thoroughly mixed before subsampling. Fresh subsamples were then taken and weighed, then oven-dried and weighed again so that measurements could be converted from a FW to DW basis. Total N

concentration (N_{mass}) was determined on 200 mg of dried and powdered samples using a CN elemental analyser (Elementar VarioMax CN analyser, Hanau, Germany).

In experiment 4, total soluble protein was quantified according to Bradford (1976). Approximately 500 mg leaf FW was ground to a powder under liquid N, then soluble protein was twice extracted in 15 ml of 50 mM sodium phosphate buffer (pH 7) containing 5 mM DTT. The extract was centrifuged (4000 *g*, 15 min, 4 °C) and 5 µl of the supernatant was combined with 200 µl Bio-Rad protein assay dye (Bio-Rad, CA, USA), then the sample absorbance was measured at 595 nm using bovine serum albumin (MP biomedical, Auckland, NZ) as the protein standard. Rubisco was determined according to Makino et al. (1986) with minor modifications. The total soluble protein extract (20 µl) was combined (1:1) with 2X Laemmli Buffer (Sigma S3401-10VL) and the mixture was heated at 95 °C for 5 min. The protein samples were then separated by SDS–PAGE (Bio-Rad, 4–15% Mini-PROTEAN TGX Stain-free) for 30 min at 180 V. Afterwards, the gels were stained with 0.25% CBB-R dye in 40% methanol and 10% acetic acid solution overnight, then rinsed repeatedly with 40% methanol and 10% acetic acid solution until the background was colourless. Large (52 kDa) and small (15 kDa) rubisco subunits were excised from the gel and transferred into tubes with 0.75 ml of formamide and shaken at 50 °C for 6 h. The absorbance of the formamide extracts was measured at 595 nm using the background gel as a blank and bovine serum albumin as the protein standard. N associated with soluble protein (N_s) rubisco (N_r) was calculated assuming protein contains 16% N.

Chlorophyll (Chl) was twice extracted with 10ml 95% EtOH from approximately 200 mg leaf FW ground to a powder under liquid N. The extracts were stored in the dark for 6–8 h with regular vortexing, then centrifuged (4000 *g*, 15 min, 4 °C). The supernatant was removed, diluted 2 fold, then the extract absorbance was measured at 648 and 664 nm. Chl *a* and *b* were estimated according to the equations in Lichtenthaler (1987) using the pathlength correction formula described in Warren (2008). N associated with pigment-protein complexes (N_p) was calculated assuming 37.3 mol N mol^{-1} total Chl (Evans & Clarke, 2019). N associated with electron transport and ATP synthesis (collectively 'bioenergetics') per unit leaf area (N_e) was calculated indirectly from electron transport capacity (J_{max}) at 25 °C, which was derived from light-response curves (as described above), utilising the temperature adjustment calculations in June et al. (2004). A linear correlation between cytochrome *f* (cyt *f*) content per unit leaf area and J_{max} at 25 °C, of 155 mol electron mol^{-1} cyt *f* s^{-1} was assumed (Evans, 1987).

Recently revised ratios of cyt *f* to the other components of electron transport and ATP synthesis were used to calculate an N_e cost of 10.86 mol N $mmol^{-1}$ cyt *f* (Evans & Clarke, 2019). The 'remaining' leaf N (N_o) was calculated as N_{mass} - N_s - N_p - N_e. N_{mass}, N_s, N_r and N_p were first calculated on a DW basis and were then converted onto a leaf area basis by dividing by SLA.

5.2.4 Statistical analysis

Data from experiment 1 was first analysed by two-way ANOVA, treating PR genetic background and the presence of the HME transgenes as independent variables. Treatment means were compared, with *p*-values adjusted using the Benjamini-Hochberg (BH) method. Regression analysis was then used to investigate relationships between mean percentage increase in leaf FA among each of the five transgenic lines compared to their corresponding controls, and corresponding percentage differences in the parameters leaf N_{mass}, leaf N_{area} and $PNUE_{amb}$. Polynomial terms were tested in each of the models to account for non-linear responses. Data from experiment 2 were modelled to investigate the relationships between genotype (WT3 and HME5) and NO_3^- supply on A_{sat}, SLA, leaf N_{mass}, leaf N_{area}, g_s and $PNUE_{sat}$. NO_3^- concentration was treated as a continuous variable. A forward stepwise procedure was used for selecting variables. Variables and interaction terms with a *p*-value <0.05 were retained in the final models. The same procedure was used for investigating the relationships between genotype and leaf N content on photosynthesis. Quadratic terms were tested in each of the models to account for non-linear responses to NO_3^- supply or leaf N. Data from experiments 3 and 4 were compared by Student's t test or Wilcoxon rank sum test.

5.3 Results

5.3.1 Experiment 1 – HME PNUE across a range of elevated fatty acid levels

The three control lines exhibited differences in leaf N_{mass} (WT1 = WT2 > WT3) (Figure 5.1). Out of five independently transformed T_0 HME PR lines, the three with the highest leaf FA relative to the corresponding controls (HME3-5) also exhibited significantly higher leaf N_{mass} than the corresponding controls (Figure 5.1), and the relative increase in leaf FA correlated positively with the relative increase in leaf N_{mass} (r^2=0.97; *p*=0.003; Figure 5.2). HME5 exhibited a significantly lower N_{area} than the corresponding control WT3 and all the other genotypes (Figure 5.1). The relative increase in leaf FA correlated negatively with the relative change in leaf N_{area} (r^2=0.99; *p*=0.025; Figure 5.2). Measured at ambient irradiance, HME3-5 had a higher photosynthetic rate per unit leaf nitrogen ($PNUE_{amb}$) than the corresponding controls (Figure 5.1). None of the five HME PR lines, however, exhibited a higher $PNUE_{amb}$ than the WT1 genotype, and WT2 and WT3 both had a lower $PNUE_{amb}$ than WT1 (Figure 5.1). The relative increase in leaf FA did not correlate with the relative increase in $PNUE_{amb}$.

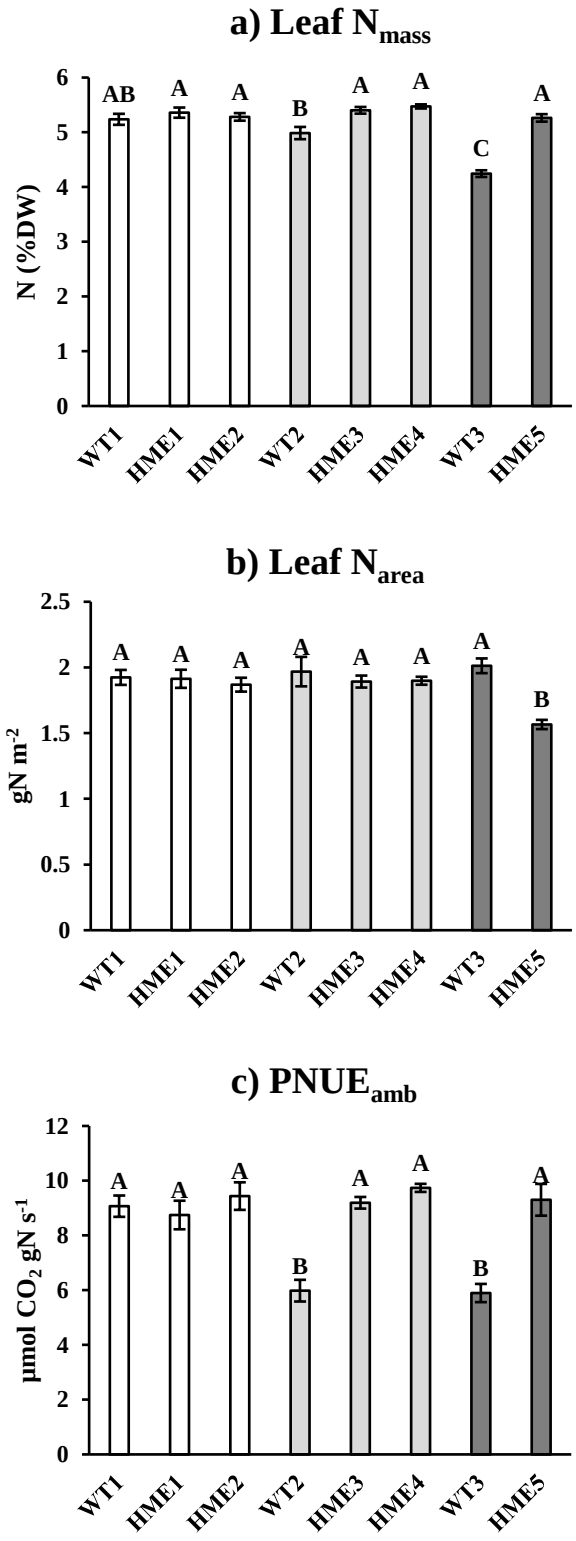

Figure 5.1. Leaf N concentration (N_{mass}), N per unit area (N_{area}) and photosynthetic nitrogen use efficiency measured at 600 µmol photons m^{-2} s^{-1} ($PNUE_{amb}$) for five independently transformed clonal HME *Lolium perenne* genotypes (HME1-5) and three non-transformed control genotypes (WT1-3) regrown under 4 mM NH_4NO_3. Matching genetic backgrounds are shaded together. Data represent means ± S.E. (*n*=10). Different letters indicate statistically significant differences in predicted means at $p<0.05$ obtained from two-way ANOVA, with *p*-values adjusted according to the BH method.

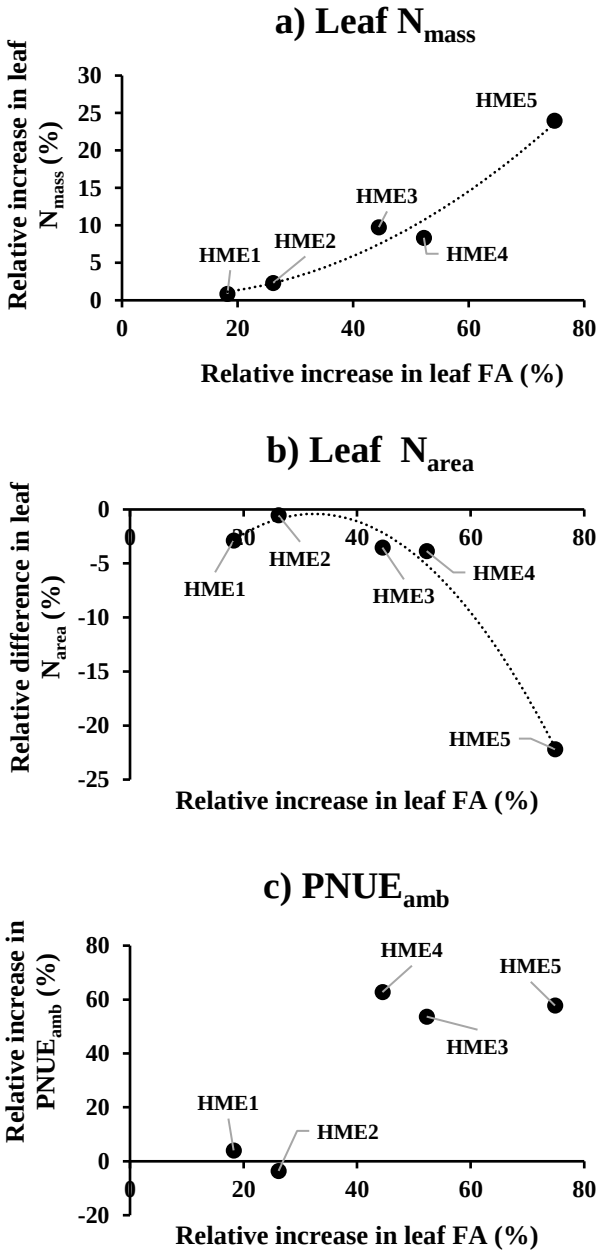

Figure 5.2. Relationship between relative increase in leaf FA concentration versus relative changes in leaf N concentration (N_{mass}), N per unit area (N_{area}), and photosynthetic nitrogen use efficiency measured at 600 μmol photons $m^{-2} s^{-1}$ ($PNUE_{amb}$), for five independently transformed clonal HME *Lolium perenne* genotypes (HME1-5) compared to corresponding non-transformed controls. Plants were regrown under 4 mM NH_4NO_3. The curved dotted lines indicate a significant non-linear relationship at $p<0.05$.

5.3.2 Experiment 2 – HME5 A-N relationships across a NO_3^- supply range

HME5 had a higher SLA than WT3 at 1–7.5 mM NO_3^- supply (Genotype effect, $p<0.001$), but the difference was smaller at high NO_3^- supply (Genotype x Concentration interaction $p<0.05$) (Figure 5.3). Measured at saturating irradiance, photosynthetic rate (A_{sat}) increased with NO_3^- supply for both genotypes (Concentration effect, $p<0.001$) up until 2–5 mM NO_3^- supply (Quadratic concentration effect, $p<0.001$) (Figure 5.3). HME5 had a similar A_{sat} to WT3 at 1–3 mM NO_3^- supply and a higher A_{sat} than WT3 at 5–7.5 mM NO_3^- supply (Genotype x Concentration interaction, $p<0.01$) (Figure 5.3). Stomatal conductance (g_s) was not significantly influenced by NO_3^- supply and was consistently higher for HME5 than for WT (Genotype effect, $p<0.001$).

Leaf N_{mass} increased linearly across the entire NO_3^- supply range used (Concentration effect, $p<0.001$). HME5 had a higher leaf N_{mass} than WT3 at all levels of NO_3^- supply (Genotype effect, $p<0.001$), especially high NO_3^- supply (Genotype x Concentration interaction $p<0.001$). However, N_{area} was lower for HME5 than WT3 up to 5 mM NO_3^- supply (Genotype effect, $p<0.001$) (Figure 5.3) and was similar for the two genotypes at the 7.5 mM NO_3^- supply (Genotype x Concentration interaction, $p<0.05$) (Figure 5.3). For both genotypes, $PNUE_{sat}$ was highest at 2 mM N supply and declined slightly between 2–7.5 mM N supply. HME5 exhibited a higher $PNUE_{sat}$ than WT3 across the entire NO_3^- supply range (Genotype effect, $p<0.001$) (Figure 5.3).

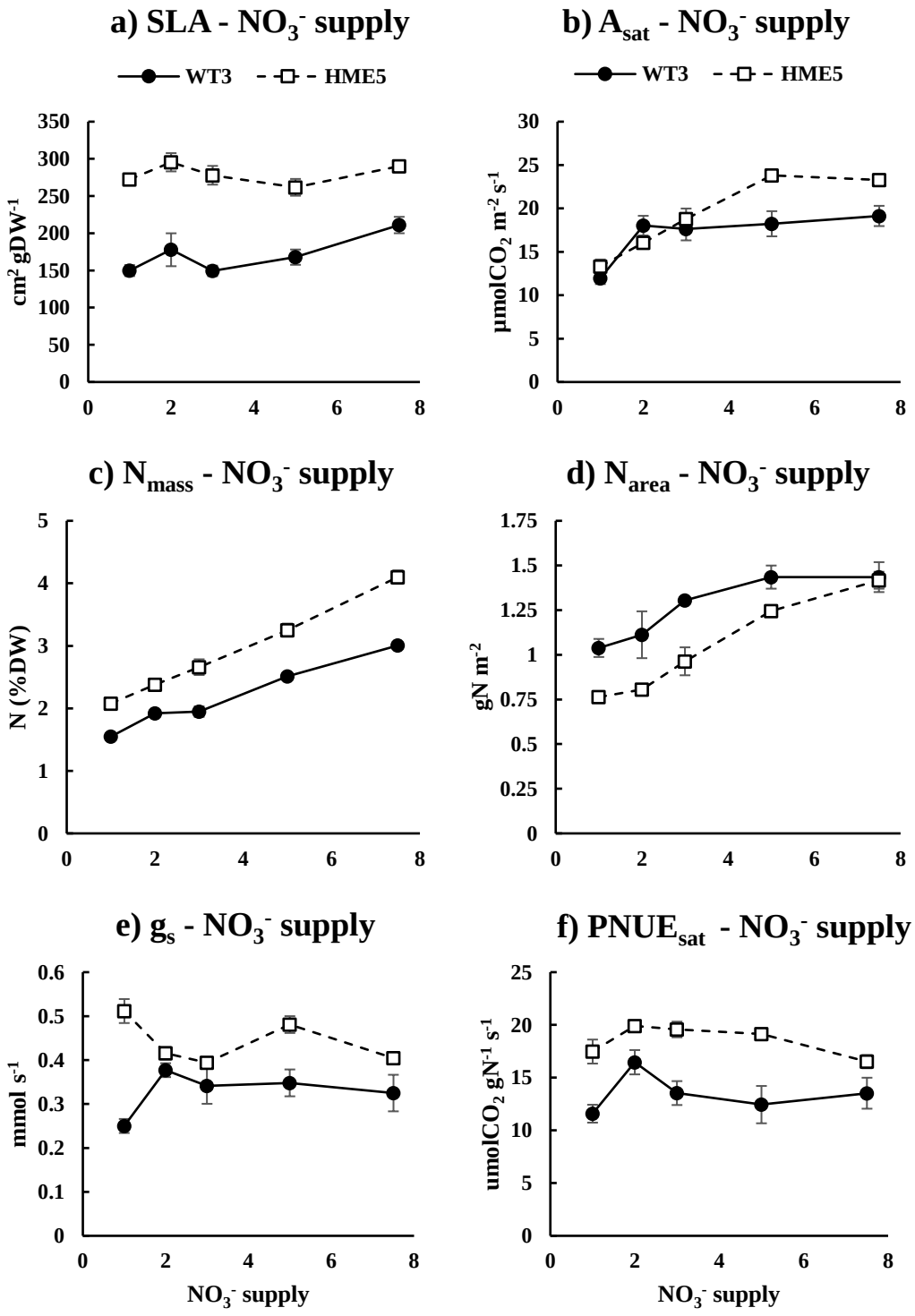

Figure 5.3. Specific leaf area (SLA) (a), photosynthesis measured at 1500 µmol photons m^{-2} s^{-1} (A_{sat}) (b), leaf N concentration (N_{mass}) (c), N per unit area (N_{area}) (d), stomatal conductance (g_s) (e), and photosynthetic nitrogen use efficiency ($PNUE_{sat}$) (f) of a clonal HME *Lolium perenne* genotype (HME5) and a non-transformed control genotype (WT3) regrown under 1–7.5 mM NO_3^- supply. Values represent means ± S.E. (*n*=3 for 1, 2 and 3 mM treated plants, *n*=5 for 5 and 7.5 mM treated plants).

Photosynthesis and leaf N correlated positively for WT3 and HME5, regardless of whether measurements were expressed on a mass or area basis (Leaf N effect, $p<0.001$) (Figure 5.4). The slope of the A_{mass} – leaf N_{mass} relationship was, however, steeper for HME5 than for WT3 across much of the leaf N_{mass} range observed (Genotype x Leaf N_{mass} interaction, $p<0.05$) (Figure 5.4). A_{mass} exhibited a saturating response to high leaf N_{mass} (Quadratic leaf N_{mass} effect, $p<0.01$). A_{area} exhibited an even stronger saturating response to N_{area} beyond approximately 1.25 $gN.m^{-2}$ (Quadratic N_{area} effect, $p<0.001$) (Figure 5.4).

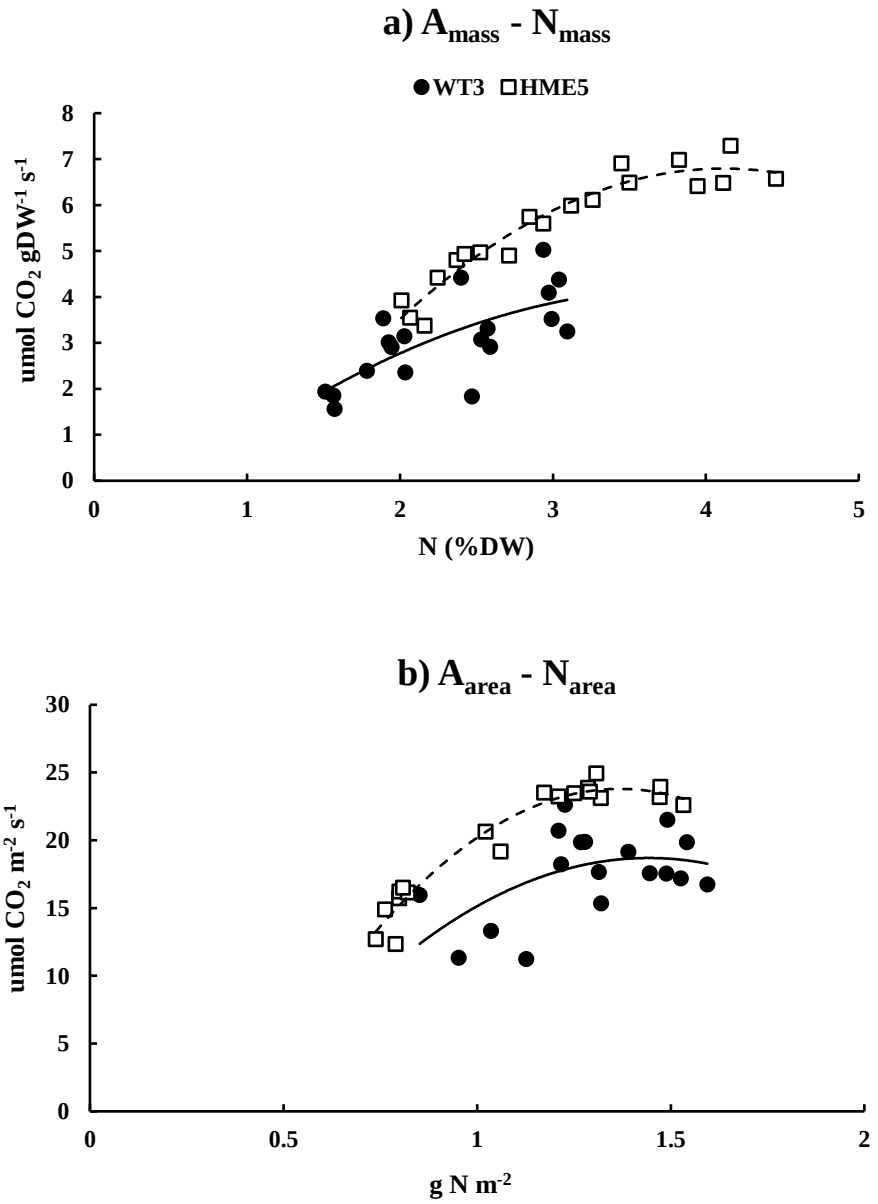

Figure 5.4. Photosynthesis versus leaf N, expressed on a mass (a) and area (b) basis, for a clonal HME *Lolium perenne* genotype (HME5) and a non-transformed control genotype (WT3) regrown under 1–7.5 mM NO_3^- supply. Photosynthesis measurements were made at 1500 μmol photons m^{-2} s^{-1}.

5.3.3 Experiment 3 – HME PNUE in a T_2 segregating population

Null and HME+ T_2 PR seedlings exhibited no difference in leaf N_{mass} after 40 days growth from seed (Figure 5.5). However, a significantly higher SLA in the HME+ seedlings (and a similar A_{area} at saturating irradiance; Table 4.2) resulted in a lower N_{area} and greater $PNUE_{sat}$ for the HME+ compared to null control seedlings (Figure 5.5).

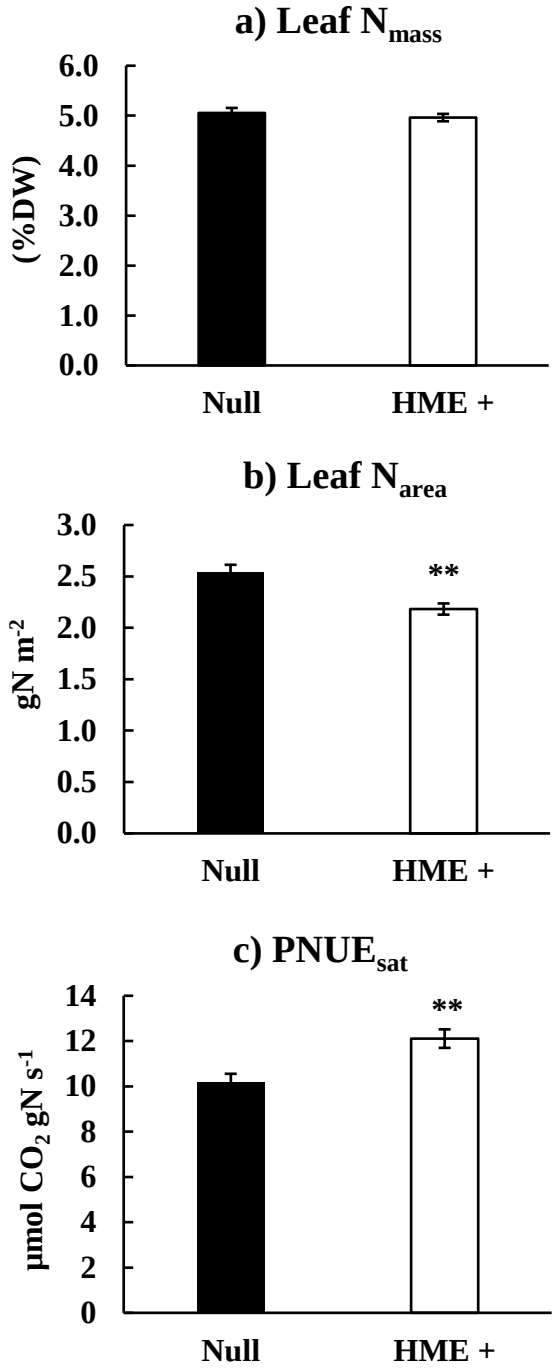

Figure 5.5. Leaf nitrogen concentration (N_{mass}), N per unit area (N_{area}) and photosynthetic N use efficiency measured at 1500 μmol photons m^{-2} s^{-1} ($PNUE_{sat}$) for an HME segregating T_2 *Lolium perenne* population grown from seed under 4 mM NH_4NO_3. Data represent means ± S.E. (*n*=20). ** denotes a significant difference at $p<0.01$ according to student's t test.

5.3.4 Experiment 4 – HME5 within-leaf CO_2 diffusion and N partitioning

Under 5 mM NO_3^- supply there was no significant difference in intercellular CO_2 concentration (C_i) between HME5 and WT3. However, HME5 exhibited a 39% increase in mesophyll conductance (g_m) compared to WT3 (Table 5.2). Therefore, chloroplast CO_2 concentration (C_c) was 5% greater and the CO_2 drawdown from substomatal cavities to chloroplasts (C_i-C_c) was 24% lower for HME5 than for WT3 leaves (Table 5.2). The carboxylation efficiency (CE; initial slope of A-C_i response) and J_{max} were significantly greater for HME5, whereas C_i*, Γ* and V_{cmax} did not significantly differ between HME5 and WT3 (Table 5.2).

Table 5.2. Gas exchange and chlorophyll fluorescence parameters for a clonal HME *Lolium perenne* transformant (HME5) and a non-transformed control (WT3) regrown under 5 mM NO_3^- supply.

Parameter		WT3	HME5
CE	Dimensionless	0.08 ± 0.005	0.10 ± 0.005 **
V_{cmax}	µmol m^{-2} s^{-1}	54 ± 1.4	57.5 ± 1.1
J_{max}	µmol m^{-2} s^{-1}	123.5 ± 9.6	171.9 ± 2.9 **
R_d	µmol m^{-2} s^{-1}	0.71 ± 0.05	0.81 ± 0.01
C_i*	µmol mol^{-1}	28.5 ± 1.3	26.8 ± 1.4
Γ*	µmol mol^{-1}	31.3 ± 1.5	28.9± 1.5
g_m	mol m^{-2} s^{-1}	0.29 ± 0.04	0.40 ± 0.02 *
C_c	µmol mol^{-1}	226 ± 4	237 ± 3 *
C_i-C_c	µmol mol^{-1}	59.9 ± 5.8	45.3 ± 2.6 *

Plants were regrown for 20–31 days after defoliation before making measurements. CE = carboxylation efficiency as determined by the initial slope of A-C_i regression, V_{cmax} = maximum rubisco carboxylation rate, J_{max} = maximum electron transport rate, R_d = day respiration, C_i* = intercellular CO_2 compensation point; Γ* = chloroplast CO_2 compensation point, g_m = mesophyll conductance, C_c = chloroplast CO_2 concentration, C_i-C_c = CO_2 drawdown. Values represent means ± S.E. (*n*=6-10). * = *p*<0.05, ** = *p*<0.01, indicating a significant difference between WT3 and HME5 obtained from Student's t test or Wilcoxon rank sum test.

Under 5 mM NO_3^- supply, HME5 leaves had higher N_{mass} than WT3, but due to a much greater SLA, also had lower N_{area} than WT3. Rubisco per unit leaf mass was higher for HME5, but rubisco per unit leaf area did not significantly differ for HME5 and WT3. HME5 had lower total soluble protein and lower chlorophyll per unit leaf area than WT3, and higher estimated cytochrome *f* content (cyt *f*) per unit leaf area than WT3 (Figure 5.6). HME5 and WT3 invested similar proportions of leaf N into rubisco (N_r/N) and pigment-protein complexes (N_p/N), while HME5 invested a significantly greater proportion of leaf N to bioenergetics (N_e/N) than WT3 (Figure 5.6). Due primarily to this increase in HME5 N_e/N, investment in total 'photosynthetic-N' = ($[N_{r + p + e}]/N$) was significantly greater for HME5 than for WT3, while investment in all remaining pools N_o/N = ($[N – N_s – N_p – N_e]/N$) was significantly lower for HME5 than for WT3 (Figure 5.6). N investment in non-rubisco soluble protein (N_{s-r})/N did not significantly differ for HME5 and WT3.

Parameter		WT3	HME5
N_{mass}	%DW	3.18 ± 0.09	4.06 ± 0.17 ***
N_{area}	gN m^{-2}	1.90 ± 0.05	1.50 ± 0.05 ***
$PNUE_{500}$	µmol CO_2 gN s^{-1}	7.73 ± 0.29	12.91 ± 0.36 ***
$PNUE_{1500}$	µmol CO_2 gN s^{-1}	8.34 ± 0.41	15.49 ± 0.37 ***
Soluble protein	g m^{-2}	4.79 ± 0.13	3.96 ± 0.15 **
Rubisco	g m^{-2}	2.33 ± 0.11	2.02 ± 0.15
Chl	µmol m^{-2}	453 ± 13	386 ± 9 ***
Chl *a: b*	mol mol^{-1}	3.44 ± 0.01	3.79 ± 0.02 ***
Cyt *f*	µmol m^{-2}	0.86 ± 0.06	1.20 ± 0.02 **

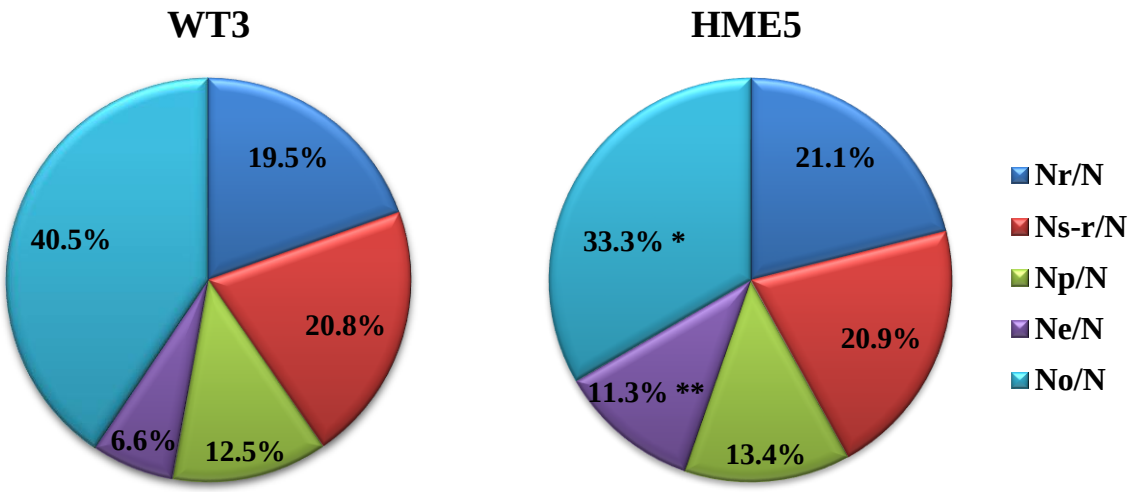

Figure 5.6. Leaf N biochemistry and partitioning for a clonal HME *Lolium perenne* transformant (HME5) and a non-transformed control (WT3) regrown under 5 mM NO_3^- supply. Plants were regrown for 20–26 days after defoliation before making measurements. N = Total leaf N concentration, N_r = N invested in rubisco, $N_{s\text{-}r}$ = N invested in non-rubisco soluble protein, N_p = N invested in pigment-protein complexes, N_e = N invested in 'bioenergetics', N_o = 'other' N. Values represent means ± S.E. (n=6–8). * = p<0.05, ** = p<0.01, *** = p<0.001 indicating a significant difference between WT3 and HME5 obtained from Student's t test or Wilcoxon rank sum test.

5.4 Discussion

In experiments 1 and 3, higher leaf FA content associated with DGAT1 + cysteine-oleosin (HME) expression in PR leaves enhanced net CO_2 assimilation per unit leaf nitrogen (PNUE) in three different genetic backgrounds and two distinct plant developmental stages. In the four out of the six HME lines/populations which displayed an increase in leaf FA of at least 32% there was an increase in PNUE of 19–63% compared to the non-transformed controls (Figure 5.1; Figure 5.5). However, the basic traits contributing to the high HME PNUE (N_{mass}, A_{area} and SLA) differed for each HME and control line comparison. Since PNUE = A_{area}/N_{area}, changes in either A_{area} or N_{area} can modulate PNUE. In experiment 1, the T_0 lines HME3 and HME4 had similar N_{area} and substantially higher A_{area} than WT2 at ambient irradiance. By contrast, HME5 had substantially lower N_{area} than WT3 and moderately higher A_{area}. The overall effect was that HME3-5 all exhibited a similar relative increase in $PNUE_{amb}$ compared to non-transformed controls (54–63%) (Figure 5.2). In experiment 3, the 19% higher $PNUE_{sat}$ in T_2 HME+ compared to null seedlings could be almost fully accounted for by lower N_{area} (Figure 5.5) associated with a higher SLA (Table 4.2).

5.4.1 Enhanced carbon assimilation due to HME expression does not occur in some *Lolium perenne* cultivars

In the two out of the six HME transformation events which displayed an increase in leaf FA of less than 32% (HME1 and HME2) there was no increase in PNUE compared to the control line (Figure 5.1). HME1-2 were derived from WT1; a transformation genotype from the cultivar 'Alto' (2.2.3). Unlike HME3-5, HME1-2 did not exhibit reduced leaf WSC and displayed no difference in SLA, A_{mass} or RGR compared to the respective non-transformed controls (2.3). In Chapter 2, we were unable to conclude whether carbon allocation into lipids was too low in HME1 and HME2 or whether the response to HME expression was different in the WT1 background (2.4.2). To resolve this, we measured leaf FA, leaf WSC, RGR, SLA and A_{mass} for a high expressing WT1-transformed HME line (Supplementary table D4.1). Despite 59% higher leaf FA than WT1 (c.f. 18–26% in HME1 and HME2), and a 22% reduction in leaf WSC (c.f. no significant change in HME1 and HME2), this HME line exhibited no significant difference in RGR, SLA or A_{mass} compared to WT1 (Supplementary table D4.1). A similar (relative) increase in leaf FA content induced greater SLA, A_{mass} and RGR for HME3-5 compared to controls (Figure 2.2). This supports speculation that there may be little or no capacity to increase photosynthesis or growth in WT1 through the addition of a leaf lipid carbon sink (2.4.2). For

all the other HME PR lines/populations examined, leaf FA accumulation was associated with increased A_{mass} and also increased PNUE. Interestingly, however, factors such as the concentration of applied N, transgene expression levels, and the leaf physiological plasticity within each transformation background all appeared important for how these efficiencies were achieved.

5.4.2 Variation in leaf N delivers greater incremental changes in HME5 photosynthesis

HME5 was selected for examination of the effect of HME expression on A-N relationships under 1–7.5 mM external NO_3^- supply (5.3.2), and for detailed biochemical and physiological analysis of photosynthesis and PNUE at 5 mM NO_3^- supply (5.3.4). Leaf physiological plasticity was found to be greatest in the 'Impact' transformation genotypes (2.4.2; 5.4.1) and of the three T_0 'Impact' HME lines examined, HME5 exhibited the greatest relative increase in leaf FA compared to the corresponding control line WT3 (Figure 2.2). HME5 exhibited a substantially higher SLA than WT3, which was associated with a reduction in N_{area} (Figure 5.1). WT3 and HME5 were considered appropriate for detailed study because i) relative changes in N_{area} correlated negatively with the relative increase in leaf FA across five HME lines from three genetic backgrounds (Figure 5.2), and ii) the high SLA and associated low N_{area} trait was recorded in HME+ progeny from a segregating population of T_2 seedlings (Figure 5.5).

HME5 had higher leaf N_{mass} than WT3 at 1–7.5 mM external NO_3^- supply, and the difference became greater as NO_3^- supply increased. However, below 7.5 mM NO_3^- supply HME5 also had lower N_{area} than WT3. HME5 displayed similar A_{area} to WT3 at 1–3 mM NO_3^- supply, and higher A_{area} than WT3 at 5–7.5 mM NO_3^- supply (Figure 5.3). When A_{mass} was plotted against leaf N_{mass} for HME5 and WT3, variation in leaf N (achieved by varying the NO_3^- supplied in nutrient media) delivered greater incremental changes in A_{mass} for HME5 than for WT3 (Figure 5.4). The difference between the slope of the WT3 and HME5 A_{mass}-N_{mass} relationship mirrors interspecific comparisons showing that species with an intrinsically high SLA exhibit a steeper A-N slope than species with an intrinsically low SLA (Reich et al., 1998). Evidently, HME expression can increase both the concentration of N in leaves (Figure 5.3) and can make photosynthesis more responsive to variation in leaf N (Figure 5.4). Both traits may contribute to a higher HME5 growth rate under high external N supply (Figure 3.2) (Poorter et al., 1990).

5.4.3 Factors influencing PNUE

Under a given set of conditions PNUE is determined by a range of factors including the amount of light absorbed, the proportion of N invested in photosynthesis, the proportion of photosynthetic-N devoted to rate-limiting photosynthetic processes, the kinetic properties and activation state of rubisco, the rate of CO_2 diffusion from the atmosphere to carboxylation sites, and differences in day respiration (Poorter & Evans, 1998). HME5 leaves exhibited lower N_{area} than WT3 at 5 mM NO_3^- supply (Figure 5.6) and given the large N requirements of the photosynthetic machinery, this may have been expected to penalize A_{area}. However, HME5 had higher A_{area} than WT3, implying chemical and/or physical modifications to HME5 leaves in order to enhance PNUE. To investigate the underlying mechanisms, we assessed several major determinants of PNUE including CO_2 diffusion rates from the atmosphere to the sites of carboxylation, and within-leaf N partitioning to different photosynthetic and non-photosynthetic pools. N partitioning was measured by dividing leaf N into two soluble components: rubisco (N_r) and non-rubisco soluble protein (N_{s-r}), and two thylakoid membrane-associated components: light harvesting (N_p) and electron transport plus ATP synthesis (collectively 'bioenergetics') (N_e). For both WT3 and HME5, the estimated proportions of total leaf N invested in N_r, N_p, and N_e fell into the range observed for ten C3 plant species grown under 1000 μmol photons m^{-2} s^{-1} by Evans & Poorter (2001), who used broadly similar methods and calculations, except that calculations were made on a nitrate-free basis. The proportion of N invested in total soluble protein and therefore N_{s-r}/N measured here (~21% for both WT3 and HME5) was lower than in Evans & Poorter (2001) (28–45%), while the estimated proportion of N associated with neither soluble protein or thylakoids ($N_o/N = [N – N_s – N_p – N_e]/N$) was higher here than in Evans & Poorter (2001). N_o in our study included nitrate as well as N associated with cell walls, amino acids, nucleic acids, hormones, and secondary defence compounds. For HME5, the amount of N in cysteine oleosin was estimated at 0.04-0.28% of total leaf N. This estimate assumed that HME5 had 2 %DW of additional FA present as lipid droplets, which, depending on diameter, consist of 0.5-3.5% protein (Tzen & Huang 1992).

5.4.4 Reasons for high HME5 PNUE: greater rubisco carboxylation efficiency associated with increased mesophyll conductance

Under the growth conditions (600 μmol photons m^{-2} s^{-1} and 415 ppm CO_2), the photosynthetic rate of WT3 and HME5 occurred at the intersection of the 'rubisco-limited' and the 'RuBP-

limited' region of the A-C_i curve in *L. perenne* (Supplementary figure D4.2A). Rubisco content was measured directly using the methodology of Makino et al. (1986), and neither rubisco content per unit leaf area or N_r/N significantly differed between HME5 and WT3 (Figure 5.6). Given the identical genetic backgrounds of these lines, rubisco likely had identical kinetic properties. Although HME5 exhibited higher stomatal conductance (g_s) than WT3 in some experiments, this finding was not consistently associated with enhanced PNUE, and never enhanced C_i for HME5. On the other hand, HME5 displayed 39% higher mesophyll conductance (g_m) to CO_2, delivering a 5% increase in chloroplast [CO_2] (C_c) at ambient atmospheric [CO_2] (Table 5.2). Further, when the estimated g_m value for each separate WT3 and HME5 replicate (the averages g_m values are presented in table 5.2) were fixed in the Sharkey et al. (2016) A-C_i model, WT3 and HME5 exhibited no significant difference in average V_{cmax} (Table 5.2) suggesting that enhanced g_m could account for the high carboxylation efficiency (CE) in HME5 leaves (Table 5.2; see also Figure 3.4). A separate estimate of g_m using the data presented in Table 3.2 and Supplementary table B2.2 also suggested that HME5 had a significantly higher g_m and C_c than WT3 at ambient atmospheric [CO_2] (Supplementary table D4.2; see also Figure 3.4). The g_m describes the CO_2 diffusion rate from substomatal air spaces to carboxylation sites in the chloroplast. Finite g_m reduces CE directly by reducing substrate availability, and indirectly by lowering the chloroplast CO_2 : O_2 ratio and therefore increasing competitive inhibition of carboxylation by rubisco oxygenase activity (photorespiration) (Flexas et al., 2012). Changes in g_m due to sink capacity manipulation have been reported previously for several crops (Detmann et al., 2012; Sugiura et al., 2019; Sugiura et al., 2020), and may explain the reduction in HME5 photorespiration previously recorded (Table 3.2). Enhancing g_m would be expected to lower the N cost of CO_2 fixation which would have a positive effect on ΔPNUE. Day respiration (R_d) can have a negative effect on apparent PNUE under high irradiance (Poorter & Evans, 1998), but did not differ for HME5 and WT3 (Table 5.2).

5.4.5 Reasons for high HME5 PNUE: greater N investment in bioenergetics

HME5 invested 19% more total leaf N into rubisco plus the thylakoids ([N_{r+p+e}]/N) and correspondingly 17% less into N_o/N than WT3, while $N_{s\text{-}r}$/N was similar for the two genotypes. Similar overall results were obtained in a preliminary N partitioning experiment (Supplementary figure D4.3). The sum of rubisco plus thylakoid N is a conservative estimate of total 'photosynthetic-N' because it ignores all Calvin cycle enzymes other than rubisco

(Poorter & Evans, 1998). RuBP-regeneration-limited photosynthetic rate is typically attributed to insufficient electron transport (Sharkey et al., 2007). The requirement for electrons could be lessened by reducing photorespiration and its associated ATP and NADPH costs, which could be achieved via increased g_m. Alternatively, RuBP-regeneration-limited photosynthesis could be enhanced by investing more N into the enzyme complexes responsible for photosynthetic electron transport capacity and ATP synthesis (collectively 'bioenergetics') (N_e). We estimated cyt *f* and N_e indirectly here, assuming that WT3 and HME5 shared the same fixed relationship between J_{max}, cyt *f* and N_e (Evans, 1987; Evans & Seemann, 1989). Under this assumption, HME5 exhibited 73% higher N_e/N than WT (Figure 5.6), which could account for most (64%) of the difference in 'photosynthetic-N' between the genotypes. However, estimates of the N cost of bioenergetics vary, and are sensitive to the amount of ATP synthase assumed (Evans & Clarke, 2019). Such estimates have not been validated for plants with modifications to central metabolism, which could alter the requirements for reducing power (Kramer & Evans, 2011). In general, CE and J_{max} are closely coordinated when factors like irradiance and external N are varied (Evans, 1996; Von Caemmerer & Farquhar, 1981).

5.4.6 Reasons for high HME5 PNUE: N-efficient light capture

HME5 exhibited 15% lower total chlorophyll per unit leaf area [Chl] than WT3 (Figure 5.6). Lower [Chl] can penalize light absorption, which can reduce A_{area} at low irradiance but has less effect near saturating irradiance, which might partially explain why the difference between WT3 and HME5 A_{area} (and PNUE) was smaller at sub-saturating irradiance (500 µmol photons m^{-2} s^{-1}; Figure 5.6). Increases in light absorption (α) per unit of additional [Chl] are small as [Chl] approaches 400 µmol m^{-2} (Evans & Poorter, 2001). For this reason, estimated α was 2% lower, but absorptance per chlorophyll molecule (α/[Chl]) was 14% higher for HME5 than for WT3 leaves. Assuming the same pigment-protein stoichiometry in WT3 and HME5 leaves [37.3 mol N mol^{-1} total Chl, as in Evans & Clarke (2019)], spreading Chl over a greater leaf area would be expected to reduce the N cost of light harvesting which would have a positive effect on ΔPNUE. However, pigment-protein stoichiometry and therefore the N cost of light harvesting varies naturally. For example, acclimation to high irradiance involves increasing the Chl *a : b* ratio, and since chlorophyll *b* is only present in the light-harvesting complexes, this reflects an increase in PSI and PSII relative to light harvesting complexes, which increases the protein cost of complexing the pigments under high irradiance (Evans, 1996; Leong & Anderson, 1984). HME5 exhibited a 10% higher Chl *a : b* ratio than WT3 (Figure 5.6), suggesting that the

protein/N cost of complexing Chl was higher in HME5 leaves. This may have partially offset the positive ΔPNUE effect due to higher α/[Chl].

5.4.7 Future direction for HME photosynthetic physiology research

The availability of N is often limiting for growth (Andrews et al., 2013) so it is important for plants to use N efficiently (Hikosaka & Terashima, 1995). PNUE is an important component of whole plant N use efficiency, but little is known about the mechanisms underlying intraspecific differences in PNUE (Mu et al., 2016). This is the first study to investigate changes in PNUE, within-leaf CO_2 diffusion and within-leaf N partitioning in relation to synthetically enhanced leaf FA content and SLA in a transgenic crop line. The higher PNUE observed in HME5 could be explained by greater mesophyll conductance to CO_2, greater N investment in bioenergetics, and higher estimated α/[Chl]. Thus, the changes in photosynthetic physiology induced by HME5 expression mirrored those typically associated with an intrinsically high SLA (see 5.1). Further work is required to confirm whether these traits contributed to the high PNUE recorded in other HME PR lines, and it would also be informative to assess the relative importance of each using sensitivity analysis [as in Poorter & Evans (1998)]. Whether these traits can deliver increased A_{area} *per se* in genetic backgrounds other than WT2 and WT3 may depend upon the available plasticity within basic leaf traits such as SLA and N_{mass}. Assessment of HME photosynthesis in a broader range of plant backgrounds is needed. Linking these detailed PNUE measurements with analysis of N partitioning between shoots and roots under variable N supply could yield valuable information about the relationships between leaf lipid sinks and whole-plant growth and N use efficiency.

Chapter 6

Final Discussion: crops with higher energy density and yield?

The primary research objective of this thesis was to test the hypothesis that leaf DGAT1 + cysteine-oleosin (HME) expression in leaves would increase growth in *Lolium perenne* L. (PR). We sought to comprehensively evaluate this counterintuitive hypothesis by measuring growth for multiple independently-transformed HME PR lines/populations with a range of elevated leaf fatty acids (FA) levels, in different genetic backgrounds and plant developmental stages. Growth was measured using both destructive methods, including RGR and total plant DW (2.3.2; 3.3.2; 4.3.2), and non-destructive methods including leaf extension and tillering (4.3.1) and herbage DW under regular mechanical defoliation (4.3.3; 4.3.4). Most lines of evidence supported the hypothesis that HME expression in leaves can enhance PR growth under favourable growing conditions, including adequate light (4.4.3) and nitrogen (N) (3.4.2).

The second research objective was to investigate whole-plant, and especially leaf-level physiological, morphological, and biochemical traits related to photosynthesis that could account for enhanced growth in HME PR. Several robust lines of evidence indicated that the HME growth advantage was caused primarily by an increase in specific leaf area (SLA; Figure 2.1; Figure 2.2; Table 4.2); a trait which can provide more leaf area for light interception and gas exchange and therefore enhance net C assimilation per plant, providing that net photosynthetic rate per unit leaf area (A_{area}) and DW allocation to leaves (LMF) are approximately maintained (Poorter et al., 1990). In all genetic backgrounds where HME expression enhanced SLA, projected total leaf area and growth were also greater under high N supply (Table 2.2; Table 4.2). Further, HME A_{area} was enhanced in some genetic backgrounds (Table 2.3) and maintained in others (Table 4.2), resulting in higher photosynthetic rate per unit leaf mass (A_{mass}).

Increased leaf N% and rubisco per unit leaf DW could partly account for high HME A_{mass} in some genetic backgrounds (5.3.1; 5.3.4), but HME photosynthesis was also consistently enhanced on a per unit N basis (PNUE; 5.3). Enhanced mesophyll conductance to CO_2, greater N allocation to electron transport and ATP synthesis, and higher estimated light absorptance per chlorophyll molecule (α/[Chl]) were identified as mechanisms contributing to the high

HME PNUE (5.3.4). The correspondence between high leaf FA and increased A_{mass}/PNUE/growth among independent HME lines was found to depend upon a reduction in leaf WSC occurring (2.4.1). HME expression also made light-saturated A_{mass} more responsive to elevated atmospheric [CO_2] (3.4.3). Both lines of evidence suggested that the diversion of carbohydrate into a lipid C sink can remove feedback inhibition of photosynthesis, inducing the leaf physiological changes which increased net C assimilation.

The final research objective of this thesis was to study the translation from spaced pots indoors to field canopies, of the FA, GE, and growth enhancing traits associated with HME expression in PR. Herbage FA was consistently higher for HME+ miniswards (4.3.3; 4.3.4), and in all instances where the difference in FA content between HME+ and null swards exceeded 0.8 %DW, HME+ swards exhibited +0.2–0.5 kJ gDW^{-1} higher herbage GE (4.3.3; 4.3.4). HME+ swards exhibited a herbage yield advantage in miniswards arranged in spaced rows indoors, but this did not reliably translate into greater herbage production in dense indoor swards (high LAI; 4.3.3) or field swards (4.3.4), highlighting the complex transition from the laboratory to the field when testing novel secondary traits. Overall, this work supports the potential for using leaf lipids as alternative sinks for photosynthate to increase plant growth potential and for leaf lipid accumulation to enhance pasture energy density.

6.1 Fundamental science required to understand HME growth advantage mechanism

In all cases where HME expression led to an increase in growth, an increase in leaf FA at the expense of WSC was also recorded, except for the experiments in Chapter 4 where WSC was not satisfactorily quantified (4.4.2). This led to speculation that conferring a lipid C sink to leaves can remove feedback inhibition of photosynthesis (2.4.1; 3.4.3; 4.4.5). It has been speculated previously that introducing a new C sink in the form of TAG in leaves might influence photosynthesis (Fan et al., 2019; Vanhercke et al., 2017; Xu & Shanklin, 2016), however most other manipulations of lipid metabolism have led to plant growth penalties. Further, with the exception of Singh et al. (2016), there have been no reports of increased leaf-level photosynthesis, regardless of the basis of expression. There are many possible reasons for this (3.4.4), which are currently not possible to resolve because of the numerous and varied transgene combinations employed to enhance vegetative lipid content, the range of plant species used for transformation, and the variable growth regimes reported in the

literature. Many early technologies likely imposed too small of a lipid C sink to affect photosynthesis (Vanhercke, 2014), especially if the lipids were not protected and were rapidly catabolised (3.4.4; 6.1.2). Conversely, it is well-established that too great a lipid sink can hinder overall plant development (Kelly et al., 2013; Mitchell et al., 2020; Zhai et al., 2017) and that the use of global transcription factors to enhance oil accumulation can impede normal cellular function through negative pleiotropic effects (Grimberg et al., 2015; Vanhercke et al., 2017). It might simply be that few other researchers have examined growth or photosynthesis in sufficient detail, especially under conditions of high C availability [e.g. light as in Fan et al., (2019)] and/or N availability.

We focused primarily on measuring changes in leaf-level photosynthetic physiology that could account for enhanced growth in HME PR at high external N supply. However, plant growth is better associated with total daily C assimilation from shoot photosynthesis minus C losses from respiration throughout shoots and roots (Poorter, 2002). The HME growth advantage was primarily caused by an increase in SLA (Table 2.3; Table 4.2). However, for the high-expressing T_0 HME line selected for detailed investigation of photosynthesis-related traits (HL/HME5) in chapter 3 and chapter 5, the proportion of total plant DW allocated to leaves (LMF) was decreased compared to the non-transformed control (WT/WT3). There was a corresponding increase in the proportion of total plant DW allocated to HL roots (RMF), and this effect was quite substantial at low N supply (up to 26%; Supplementary figure B2.2). Similarly, RMF was 20% higher for HME+ progeny from a segregating population of T_2 seedlings grown at high N supply (Table 4.2). SLA multiplied by LMF determines the total leaf area per unit of plant DW (LAR), which strongly dictates photosynthesis per plant (Poorter, 1989a). Although the increase in HL SLA outweighed the reduction in LMF (i.e. LAR was still increased compared to WT at high N supply) (3.3.3), the reduction in HL LMF was unexpected because SLA and LMF often co-vary. For example, both increase under conditions of low C availability/carbohydrate accumulation such as low light (Poorter et al., 2009, Poorter et al., 2012b).

Increased partitioning of DW to roots usually occurs when below ground-acquired resources (nutrients and water) limit growth relative to above ground-acquired resources (Poorter et al., 2012b). It is not clear why leaf HME expression would increase RMF, especially since root structure and metabolism require significant C investment. Indeed, the estimated amount of

additional C present in the HL plants due to increased root biomass was greater than that due to leaf lipid accumulation (Supplementary figure B2.2). Andrews et al. (2005) argued that when there is an increase in shoot N substrate available for growth (e.g. leaf protein content), this in conjunction with the proximity of the shoot to the supply of C stimulates shoot growth relative to root growth, leading to an increased S:R (and reduced RMF). However, HL had higher leaf protein and a higher RMF than WT, indicating that another process was controlling partitioning. One possible mechanism is a reduction in N% and an increase in the C:N ratio in HL at the whole-plant level, which may signal to increase allocation to roots. Using the plants grown under 1-10 mM NO_3^- (ambient CO_2) as an example; although N% was consistently higher in HL leaves, LMF was lower, and at 10 mM NO_3^- supply, N% in the sheath and root system were lower for HL (Supplementary figure B2.2). Although we did not obtain the data at low N supply, these trends suggest that whole-plant C:N may have been higher for HL (see also Supplementary figure C3.4). Another possible factor is the greater HL water requirement per unit leaf mass, associated with greater SLA and transpiration per unit leaf area (Figure 5.3; Supplementary figure B2.2). It is also possible that under some circumstances, the addition of an energy/C consuming sink in leaves could disrupt the the specific metabolic requirements required for efficient leaf growth [e.g. by reducing levels of key metabolic precursors (Mitchell et al., 2020) or some component of 'structural N' included in 'N_o/N'; Figure 5.6], without penalizing translocation of carbohydrate from the leaves to the root system.

While uncertainty remains as to why HME biomass partitioning was altered, the growth response to external N was well characterised. A medium to high N supply (4–10 mM) maximised the RGR difference between the HL and WT (Figure 3.2), and several traits were identified which contributed to this altered growth response to N. Firstly, although HL allocated less biomass to leaves at low N supply, HL LMF increased more steeply as N supply increased (Figure 3.2). Secondly, HME expression increased the concentration of N in leaves (Figure 5.2; Figure 5.3). Thirdly, HME expression enhanced PNUE (Figure 5.3; Figure 5.5) and made photosynthesis more responsive to variation in leaf N (Figure 5.4) due to enhanced mesophyll conductance to CO_2, greater N investment in electron transport and ATP synthesis, and higher estimated α/[Chl] (5.4.4; 5.4.5; 5.4.6). Linking these detailed photosynthesis and PNUE measurements with analysis of C and N partitioning between leaves, sheaths and roots under variable N supply would yield valuable information about the relationships between leaf lipid sinks, other major C sinks in the plant, and whole-plant growth and N use efficiency.

6.1.1 Alternative leaf sinks for photosynthate: opportunities and challenges

Plants evolved to achieve a dynamic balance between C assimilation (photosynthesis), C storage (mainly in the form of carbohydrate), and C utilisation (growth and metabolism) in a fluctuating environment. Regulating the accumulation, remobilization, and transport of (non-structural) carbohydrates is central to maintaining C and energy homeostasis (Smith & Stitt, 2007). Further, excessive leaf carbohydrate accumulation can cause cellular damage and photoinhibition (Sugiura et al., 2015). Plants must therefore sense their carbohydrate status and adjust their physiological state appropriately. Perturbations that cause leaf carbohydrates to accumulate generally have a negative feedback effect on photosynthetic (source) capacity (Paul & Foyer, 2001), but given adequate capacity to utilize C (sink capacity), leaf carbohydrate accumulation can be avoided, and photosynthetic capacity can be maintained even under elevated CO_2 (Ainsworth et al., 2004; Ruiz-Vera et al., 2017). It is well established that major C sinks in the form of reproductive structures, storage organs, and new growth can influence carbohydrate levels and photosynthetic traits in source leaves (Ainsworth et al., 2004; Ruiz-Vera et al., 2017; Sugiura et al., 2015), but mature leaves also consist of various metabolic and structural sinks which compete for C (Vanhercke et al., 2019). Thus, manipulating leaf sink capacity though metabolic engineering may enhance photosynthesis if C-rich compounds can accumulate in close proximity to photosynthesis without triggering evolved carbon-sensing mechanisms (Paul & Eastmond, 2020). This work shows that TAG in encapsulated form is capable of such an effect, so it must be asked if other valuable soluble and polymeric compounds (sugar derivatives, polysaccharides, proteins, or entirely novel bioproducts such as vitamins, drugs, or plastics) could be engineered to circumvent feedback inhibition? Creating an efficient C sink in metabolically active leaves is complex (Sweetlove et al., 2017). Introduced pathways must interfere minimally with desirable endogenous processes, and end-products should be metabolically inert or compartmentalised appropriately (Morandini, 2013). Futile cycles of synthesis and hydrolysis should be avoided (Winichayakul et al., 2013), and synthesis would ideally be turned on only once adequate source capacity has been established (Morandini, 2013). Despite this complexity, a growing range of options exists for fine-tuning the spatial and temporal synthesis of novel molecules in photosynthetic organisms (O'Neill & Kelly, 2017; Sweetlove et al., 2017). Many strategies remain to be explored by which leaf sink capacity could be enhanced, which is a relevant goal in the context of rising atmospheric CO_2 (3.1; 3.4.3; Dingkuhn et al., 2020) and may complement existing efforts to

increase C assimilation which focus primarily on improving photosynthetic energy conversion and photosynthate production (Long et al., 2006; Wu et al., 2019; Zhu et al., 2020).

6.1.2 Is greater lipid droplet stability key to the HME growth advantage?

Balanced upregulation of several components of TAG metabolism, including increased TAG assembly (pull), and reduced TAG turnover (protect) are likely necessary to create an efficient lipid sink (Sweetlove et al., 2017; Winichayakul et al., 2013). In chapter 3, we speculated that cysteine-oleosin-encapsulated lipid droplets (LDs) may behave as 'uniquely stable' leaf C sinks, and that slowing the degradation/turnover of TAG may be important for achieving the HME growth advantage (3.4.4; Winichayakul et al., 2013). Evidence of slower degradation of cysteine-oleosin-encapsulated LDs came from *in vitro* experiments quantifying TAG release from LDs exposed to common proteases; cysteine-protease (papain) and PNK [see Figure 5 in Winichayakul et al., (2013)]. Enhanced LD stability referred to slower TAG release compared to a control LD – encapsulated by a native (unmodified) oleosin (Winichayakul et al., 2013). However, enhanced LD stability due to HME expression has not yet been convincingly demonstrated *in planta* and should now be assessed by comparing TAG turnover in plants expressing cysteine-oleosin and native oleosin, using [^{14}C] acetate pulse-chase labelling experiments (Allen, 2016; Koo et al., 2004).

FA/TAG accumulation reflects relative rates of biosynthesis and turnover (Allen, 2016). The importance of LD stability is highlighted here because cycles of TAG biosynthesis and hydrolysis followed by FA recycling or beta-oxidation probably cause losses of energy and C. Conversely, excessive LD stability may create metabolic complications (Winichayakul et al., 2013), possibly associated with temporal shortages of readily-mobilizable energy and C. It seems likely that the degree to which a given quantity of TAG behaves as a stable end-product as opposed to a storage product (i.e. available for remobilization) will influence plant energy homeostasis (Fan et al., 2019; Yu et al., 2018), which in turn could alter the practical feasibility of crop energy densification through metabolic engineering. Further studies could examine rates of lipid turnover alongside whole-plant C budgets [e.g. as in Poorter et al. (1990)] for various lipid-enhancing transgene combinations, expressed within a single model species under a common growth regime. Directly comparing a native oleosin, various cysteine-oleosin configurations, and other strategies designed to package and protect accumulated TAG [e.g. SDP1 silencing and LEC2 overexpression as in Vanhercke et al. (2017)] might yield valuable information about the energetic consequences of different TAG protection strategies.

6.2 Further work needed to quantify the economic benefits of HME technology

HME expression enhanced PR herbage gross energy (GE) by 0.3–0.5 kJ gDW^{-1} under realistic growing conditions (Figure 4.3), supporting the potential for this technology to deliver the benefits of higher dietary metabolizable energy (ME) intake whilst maintaining low input pastoral farming methods (Chapter 4). Pastoral farming occupies 70% of total agricultural land, and despite an increasing proportion of ruminant agriculture based on grain feeding, pasture grasses remain the predominant ruminant feed type (by DM) worldwide (Lee, 2018). When meat and milk prices increase, pasture-based farming systems become less profitable than systems with high grain input, due in large part to limitations in per-animal production associated with the lower energy density of pasture (Wilkinson & Lee, 2018). Feeding ruminants grain, however, creates competition for scarce arable land currently used to feed monogastric livestock or humans directly, which has led some to suggest that grain inputs should be restricted to rectifying nutritional imbalances associated with all-pasture diets (Wilkinson & Lee, 2018). Such trade-offs could be delayed or avoided if pasture ME was enhanced. The next discussion section addresses the prospect of HME technology enhancing pasture ME and contrasts HME with conventional breeding as a strategy to enhance PR lipids.

6.2.1 Possible benefits of energy-dense pasture

When the energy requirements for body maintenance are met, increases in dietary ME intake have a linear positive impact on ruminant production because of the 'maintenance dilution' effect (Capper & Bauman, 2013). However, progress in breeding for higher ME in PR has been slow and has mainly been achieved indirectly via selection for the delayed appearance of reproductive tillers, which is associated with greater DM digestibility (Wims et al., 2017). For example, rates of gain in PR ME content have been estimated at 0.05 kJ gDW^{-1} per decade for European cultivars (Sampoux et al., 2011). Gene technologies offer prospects for large one-off gains in ME, but also face unique challenges for deployment (Badenhorst et al., 2016; Barrett et al., 2015; Ludemann et al., 2015; Parsons et al., 2011). For example, on-farm experimentation is costly and is limited by the availability of plant material at early stages of the transgenics breeding programme (Badenhorst et al., 2016; Parsons et al., 2011). Modelling can be useful for making early predictions about potential economic benefits (Wims et al., 2017). Ludemann et al. (2015) modelled the effect of an arbitrary 1 kJ gDW^{-1} increase in PR

ME for a PR grazing-based Australian dairy system and concluded that substantial increases in farm operating profit would occur regardless of how the additional ME was 'utilized' (i.e. whether stocking rate was kept constant or increased, or the amount of purchased concentrate was reduced).

Assuming it is readily metabolized (see discussion in 4.4.2), an additional 0.3–0.5 kJ gDW^{-1} of GE could also deliver step-change in farm operating profit. This change corresponded with an increase in herbage FA of 0.9–1.0 %DW in the field, while increases in FA of 2.2–2.5 %DW corresponded with 1.0–1.2 kJ gDW^{-1} of additional GE under controlled conditions (Winichayakul et al., 2020). Unfortunately, the prospect of realizing higher PR ME remains uncertain due to the preliminary nature of the field data obtained here (4.4.5; 6.2.2). Animal modelling relies heavily on assumptions about the partitioning of dietary energy to animal weight gain and milk solids production, but there are little data to quantify how these parameters respond to additional pasture ME (Ludemann et al., 2015). Further, the economic value of new PR cultivars also depends on annual and seasonal DM yields, and trait 'persistence' over time within mixed swards often containing white clover and fungal endophyte (Parsons et al., 2011; Wims et al., 2017). These factors will eventually need to be accounted for in order to accurately quantify the economic benefits of HME PR.

6.2.2 Strategies for delivering higher lipids to pastoral agriculture

Feeding high lipid plant biomass to animals is a straightforward commercial prospect because there are no processing costs associated with oil extraction (Durrett et al., 2008; Vanhercke et al., 2019). The optimal amount of fat in ruminant diets is known (6–8%), and supplementation trials demonstrate a positive feed utilisation efficiency response (Cosgrove et al., 2004; Hess et al., 2008; Schroeder et al., 2004). As well as increasing ME, increasing total lipids and certain FAs in the ruminant diet can have other benefits, which are discussed elsewhere (Grainger & Beauchemin, 2011; Hess et al., 2008; Schroeder et al., 2004; Weiss, 1998; Winichayakul et al., 2020). Interest in breeding PR for higher levels of certain FAs and total FA has emerged recently (Hegarty et al., 2013; Morgan et al., 2020; Wilkinson et al., 2020), mainly in response to the perceived human health benefits of consuming meat and milk products from pasture-fed animals (Morgan et al., 2020). Could modern breeding methods deliver the same magnitude of benefits as HME technology while avoiding some of the technical and regulatory challenges for deployment?

A review of the literature revealed that some variation in PR herbage total FA content exists, with several early studies reporting a range (i.e. between the highest and lowest mean FA level among cultivars at a single cut) of 0.1–0.6 %DW (Dewhurst et al., 2002; Elgersma et al., 2003a, 2003b). A greater range was observed in later studies where a wider selection of cultivars were tested; 1.2–1.4 %DW (Hegarty et al., 2013; Morgan et al., 2020; Palladino et al., 2009). Also, in this thesis, herbage FA content varied among non-transgenic control genotypes by up to 1.1–1.4 %DW within a single experiment (Table 2.1; 4.3.1; 4.3.4). Hegarty et al. (2013) identified genomic regions significantly associated with natural variation in total FA content. However, a recent publication indicated that the transfer of this information to PR breeding programmes has been limited, and that considerably more time and effort are required for breeders to exploit existing variation in PR FA (Morgan et al., 2020).

HME expression enhanced PR herbage FA content by a maximum of 0.9–1.0 %DW in the field. This change was achieved in plants with multiple copies of the HME transgenes expressed in the hemizygous condition, whereas an HME cultivar would consist of 'single-copy' T_0 events bred into the homozygous condition. It is therefore unclear if HME lines in commercial development will further enhance field FA content. Encouragingly, FA was increased by 1.6 %DW for the single copy (hemizygous) T_0 HME line 'HME3' grown indoors (Table 2.1) (c.f. several multi-copy T_0 lines for which FA was increased by 2.0–2.5 %DW; Table 2.1; Figure 3.1; Supplementary table D4.1; Winichayakul et al., 2020). The maximum treatment mean herbage FA content in the field was 4.3 %DW (Figure 4.3). Given the substantial capacity for leaves to accumulate TAG in the presence of 'push factor modulation' (i.e. genetic upregulation of FA synthesis) (Vanhercke et al., 2017), higher FA levels could probably be attained in the field with iterative metabolic engineering. However, for a variety of reasons, this might also reduce the feasibility of commercial deployment (discussed in 4.1; 6.1).

In addition to maximum attainable herbage FA levels, there may be other advantages associated with the transgenic versus breeding approach for generating a high lipid PR cultivar, although it should be noted that the two approaches need not remain exclusive, especially since neither has yet elevated FA near to the target of 6–8 %DW in the field [see further discussion in Badenhorst et al. (2016)]. A theoretical advantage of simple transgenic interventions is that new traits can be 'locked in', and so loss of trait expression due to G x E interactions can be avoided (Parsons et al., 2011). In contrast, polygenic traits may be under the control of complex environmental cues – as has been observed for the conventionally-

bred ‘high sugar grasses’ (Parsons et al., 2004; Rivero et al., 2019). In the present work, the high HME FA trait was reliably expressed, however, it was diminished in some contexts such that the high GE trait was only significant for the final harvest of the field season (Figure 4.3), for unknown reasons (4.4.2). A second consideration is the inadvertent effects on other traits when enhancing herbage FA. Since plant FAs naturally concentrate in protein-rich thylakoid membranes within leaves, herbage FA and CP (and N) tend to correlate. Conversely, WSC are higher in the sheath than in the leaf. Therefore, selecting for high FA may inadvertently reduce the WSC:CP ratio (Morgan et al., 2020; Palladino et al., 2009). In principle, accumulating FA in TAG rather than in membranes could decouple this relationship. This was proven possible in one experiment here (Supplementary figure C3.4) but see also (Figure 2.2; Figure 5.2). Interestingly, the form of additional lipid may also alter rumen microbial processes such as fibre digestion (Wilkinson et al., 2020; Winichayakul et al., 2020).

6.3 Could HME expression enhance PR yield?

Although the primary benefit of HME technology is expected to come from increasing the energy density of pasture, successful translation of the growth advantage to the field would add further value. This will require that the physiological mechanism(s) are compatible with growth in a field sward, which preliminary data in chapter 4 provide suggest may be possible in some contexts (4.4.3; 4.4.4; 4.4.5). This final discussion section considers the range of contexts under which a HME growth advantage was recorded and further speculates about scenarios where a PR yield benefit could be expected.

Firstly, since the HME SLA effect was indirect, and because SLA is a trait which is highly responsive to changes in the external environment [especially those that modify C availability (Poorter et al., 2009)], outside influences could mask the comparatively small pleiotropic effect due to HME expression (Table 4.5; 4.4.4; 4.4.5). Secondly, realizing a higher SLA can enhance plant growth rate before canopy closure, but not afterwards (Poorter et al., 2009). Therefore, HME PR herbage accumulation may be greater under frequent defoliation (low canopy LAI), but the establishment of a supra-optimal canopy LAI could penalize herbage yield under longer defoliation intervals. Thirdly, over a range of crop growing conditions, cell expansion and growth are more sensitive to temperature than photosynthesis (Poorter et al., 2016). The photothermal ratio (PTR; daily PAR integral divided by average temperature), the factor that has been proposed to dictate the overall balance of activity between source leaves

and various sinks throughout the plant, is greater outdoors than in most growth chambers (Table 4.1), and increases with latitude (Poorter et al., 2016). It seems logical to speculate that the assimilation benefits associated with HME technology are more likely to be realized in environments where the PTR is high (i.e. when C utilization by growing sinks is low, and leaf carbohydrate accumulation occurs). Fourthly, under any given set of growing conditions and FA level, the HME growth advantage may be diminished by the introduction of modern germplasm (2.4.2; 4.4.4; 5.4.1). The magnitude of the A_{mass}/PNUE/growth advantage was smaller when HME was expressed in T_2 HME segregating populations compared to 'Impact' T_0 transformation genotypes (4.4.4). Also, HME expression in an 'Alto' T_0 transformation genotype (2.4.2) had no effect on growth (Table 2.2; Supplementary table D4.1). It is worth noting that both 'Impact' controls displayed lower growth and higher leaf WSC than the 'Alto' control (Table 2.2; Table 2.1), which suggests that C utilisation (e.g. translocation) was already high in 'Alto' (2.4.2). Crop varieties differ in the capacity to produce new sinks (Dingkuhn et al., 2020), the capacity to accumulate carbohydrates in different leaf cellular compartments (Chu et al., 2020), and in the sensitivity of photosynthesis to feedback regulation by different carbohydrates (Paul & Foyer, 2001; Sugiura et al., 2019). Thus, assessment of HME photosynthesis in a range of plant backgrounds is needed to test the broader relevance of the hypothesis that leaf lipid accumulation can remove feedback inhibition of photosynthesis.

To summarize, the growth advantage conferred by HME transformation was greatest in PR genetic backgrounds with the lowest existing sink activity (2.4.1; 2.4.2), was enhanced under elevated CO_2 (3.4.3), and was neutralized under high LAI (4.4.3). A general picture emerges, where the HME growth advantage is most likely realized when the potential for C assimilation is high relative to C utilization by other growing sinks. This highlights an important general consideration regarding the utility of engineered C sinks to enhance photosynthesis and growth. Benefits may depend upon the overall balance of activity between source leaves and various sinks throughout the plant, and therefore may vary with environmental conditions, crop variety, and the stage of plant growth and development.

Appendix A - supplementary tables from Chapter 2

Supplementary table A1. 1. DW of ramets at the time of propagation and 'post-establishment' (i.e. three weeks after propagation) for five independently transformed clonal HME *Lolium perenne* genotypes (HME1-5) and three non-transformed control genotypes (WT1-3).

	Propagation DW (g)	**Post-Establishment DW (g)**
WT1	0.009 ± 0.0005	0.82 ± 0.04
HME1	0.010 ± 0.0005	0.70 ± 0.02 *
HME2	0.010 ± 0.0005	0.82 ± 0.04
WT2	0.011 ± 0.0008	0.57 ± 0.03
HME3	0.011 ± 0.0006	0.73 ± 0.03 **
HME4	0.011 ± 0.0005	0.72 ± 0.05 *
WT3	0.011 ± 0.0011	0.55 ± 0.02
HME5	0.009 ± 0.0005	0.65 ± 0.05

Matching genetic backgrounds are grouped together. Data represent means ± S.E. (n=10). Asterisks indicate statistically significant differences within different genetic backgrounds, obtained from two-way ANOVA, with p-values adjusted according to the BH method. * = p<0.05, ** = p<0.01.

Supplementary table A1. 2. Specific leaf area (SLA) of a clonal HME genotype (HME4) and a non-transformed control genotype (WT2) regrown under 5 mM NO_3^- or NH_4^+.

N form	Genotype	SLA
NO_3^-	WT2	157.8 ± 4.6 A
	HME4	217.8 ± 3.1 C
NH_4^+	WT2	154.6 ± 10.2 A
	HME4	189.9 ± 5.9 B
ANOVA		
G		***
N		*
G x N		-

Values represent means (*n*=6) ± S.E. G = genotype effect, N = N form effect significant in a two-way ANOVA. * = $p<0.05$, *** = $p<0.001$. Different letters indicate statistically significant differences in predicted means obtained from a two-way ANOVA, with *p*-values adjusted according to BH method.

Appendix B - supplementary figures and tables from Chapter 3

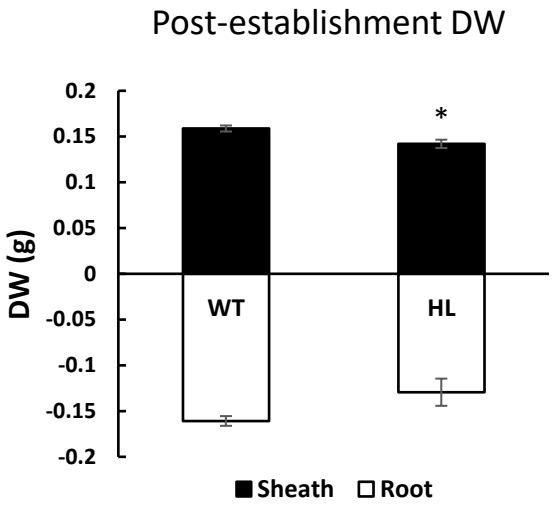

Supplementary figure B2. 1. Sheath and root DW of a defoliated clonal HME PR transformant (HL) and a wild type control (WT) genotype. Plants were established from 3–4 tillers for 23 days at 2 mM NO_3^- supply at ambient CO_2. Bars represent means ± S.E. (*n*=5). * = denotes a significant difference at the $p<0.05$ level in DW, according to student's t test.

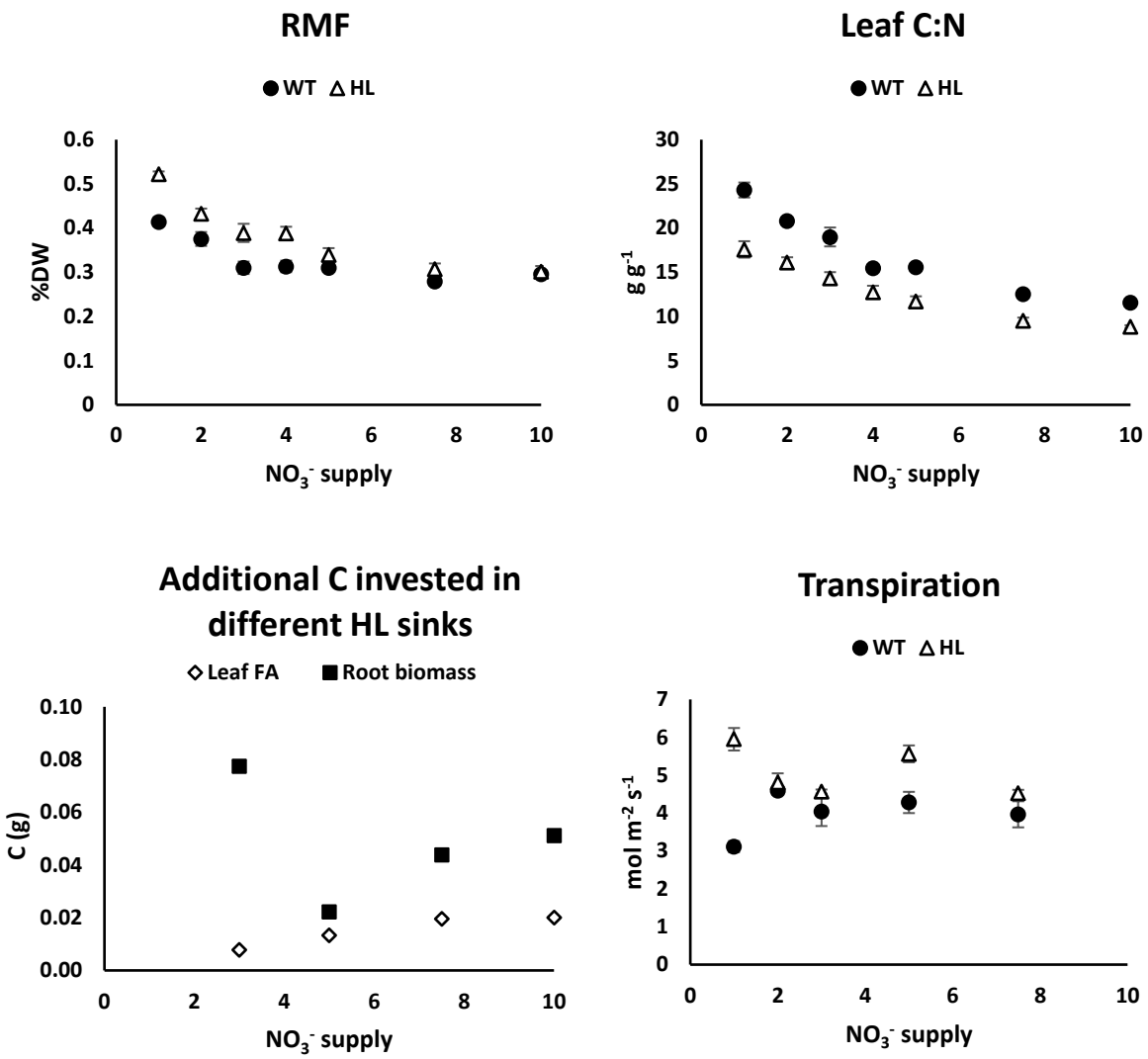

Sheath and root composition at 10 mM NO_3^-

Organ	Genotype	N%	C%	C:N
Sheath	WT	3.8 ± 0.1	37.4 ± 0.2	9.9 ± 0.3
	HL	3.0 ± 0.1	36.7 ± 0.4	12.2 ± 0.3
Root	WT	2.6 ± 0.1	28.8 ± 1.1	11.3 ± 0.6
	HL	2.2 ± 0.2	32.1 ± 0.6	15.1 ± 1.6

Supplementary figure B2.2. Additional morphological, biochemical and gas exchange parameters of a clonal HME *Lolium perenne* transformant (HL; open triangles) and a wild type control (WT; closed circles) genotype. Plants were regrown for 28–29 days after defoliation at 1–10 mM NO_3^- supply at ambient CO_2 only (400 ppm). Data points represent means (*n*=5) ± S.E. Additional C in different HL sinks was estimated assuming that FA contain 78% C and Root biomass contains 30% C. RMF = the proportion of total plant DW allocated to roots.

Supplementary table B2.1. Sharkey (2016) A/ci model outputs after re-analysis of the raw data presented in Figure 3.4. The same rate limiting processes used in Figure 3.4 were assigned to the data before modelling. Instead of fixing Ci*, the temperature-adjusted Arabidopsis value of 4.24 was assumed for Γ* for both WT and HL. The improved estimates of the parameters g_m and R_d presented in i) Table 5.2 and ii) Supplementary table D4.2 were also fixed.

CO_2	Genotype	V_{cmax} (µmol m^{-2} s^{-1})	J_{1500} (µmol m^{-2} s^{-1})	TPU (µmol m^{-2} s^{-1})	V_{cmax}/J_{1500}	Model fit
i)						
Ambient	**WT**	66.6 ± 8.1	153.6 ± 8.9	9.6 ± 0.7	0.43 ± 0.03	3.6 ± 0.3
	HL	95.4 ± 2.2	165.2 ± 5.3	11.5 ± 0.3	0.58 ± 0.01	2.7 ± 0.2
ii)						
Ambient	**WT**	91.9 ± 12.5	158.9 ± 9.2	10.4 ± 0.8	0.57 ± 0.05	1.2 ± 0.4
	HL	98.5 ± 2.0	167.9 ± 5.6	11.7 ± 0.3	0.59 ± 0.01	0.7 ± 0.2

Plants were regrown at 5 mM NO_3^- supply under ambient CO_2 (400 ppm). Measurements were made at 1500 µmol photons m^{-2} s^{-1} at a leaf temperature of 23 °C.

Supplementary table B2. 2. Intercellular CO_2 compensation point in the absence of dark respiration in the light (C_i*) and F_v/F_m measured alongside the quantum efficiency of photosystem II (Φ PSII) and photosynthesis (A_{area}) of a clonal HME *Lolium perenne* transformant (HL) and a wild type control (WT) genotype.

A)	C_i* experiment		B)	F_v/F_m experiment		
Genotype	**C_i* (ppm)**	**R_d (µmol CO_2 m^{-2} s^{-1})**		**F_v/F_m**	**Φ PSII**	**A_{area} (µmol CO_2 m^{-2} s^{-1})**
WT	27.87 ± 1.48	0.71 ± 0.07		0.79 ± 0.003	0.48 ± 0.01	17.83 ± 0.40
HL	35.50 ± 1.11	0.41 ± 0.05		0.80 ± 0.002	0.51 ± 0.01	20.63 ± 0.89
***p*-value**	**	**		*	**	*

Measurements were taken in two separate regrowth experiments, approximately 3 weeks after the defoliation of vegetative clones regrown in potting mix. C_i* was determined according to Brooks & Farquhar (1985). Values represent means ± S.E. (n=6 for C_i* experiment, n=10 for F_v/F_m experiment). p-values are from Welch two sample t-tests or Wilcoxon rank sum test. * = p<0.05, ** = p<0.01.

Supplementary table B2. 3. Preliminary experiment specific leaf area (SLA), light saturated photosynthetic rate per unit leaf area (A_{sat}), leaf fatty acid (FA) and leaf water-soluble carbohydrates (WSC) of two clonal HME PR lines; 3501 and 6205 (HL) and a wild type control (WT) genotype.

CO_2	Genotype	SLA (cm^2 gDW^{-1})	A_{sat} (µmol CO_2 m^{-2} s^{-1})	Leaf FA (mg gDW^{-1})	Leaf WSC (mg gDW^{-1})
	WT	249 ± 15 BC	19.8 ± 1.5 C	24.8 ± 0.76 C	156.2 ± 18.2 B
Ambient	**3501**	310 ± 24 AB	26.0 ± 0.6 B	41.1 ± 2.02 AB	ND
	6205 (HL)	369 ± 12 A	27.1 ± 2.3 B	46.2 ± 0.56 A	86.9 ± 13.8 C
	WT	196 ± 9 C	22.3 ± 1.9 BC	22.7 ± 0.07 C	236.1 ± 10.3 A
Elevated	**3501**	266 ± 22 B	36.4 ± 1.5 A	38.8 ± 2.41 B	ND
	6205 (HL)	300 ± 8 B	37.0 ± 1.6 A	43.6 ± 1.34 AB	97.2 ± 5.6 C
	G	***	***	***	***
ANOVA	**CO_2**	**	***	-	**
	G x CO_2	-	*	-	*

Plants were regrown for 33–34 days after defoliation at 5 mM NO_3^- supply at either ambient (400 ppm) or elevated CO_2 (760 ppm). Data points represent means (n=4–6) ± S.E. G = genotype effect, CO_2 = CO_2 effect significant in a two-way ANOVA. * = p<0.05, ** = p<0.01, *** = p<0.001. ND = not detected. Different letters indicate statistically significant differences in predicted means obtained from two-way ANOVA, with p-values adjusted according to BH method. ND = not determined.

Appendix C – supplementary figures and tables from Chapter 4

A) INDOOR 'SPACED ROW' **B) INDOOR 'DENSE SWARD'**

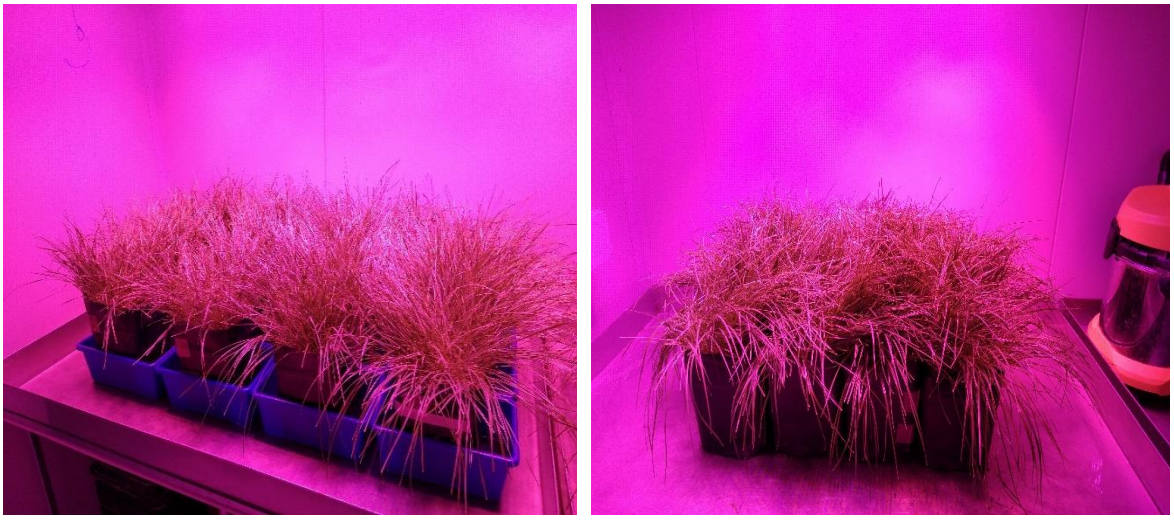

C) FIELD SWARD

Supplementary figure C3. 1. 'Spaced row' (A) and 'dense sward' (B) pot arrangements from the indoor minisward experiment. A replicate sward from the field experiment (C). The central nine plants were harvested from the field swards.

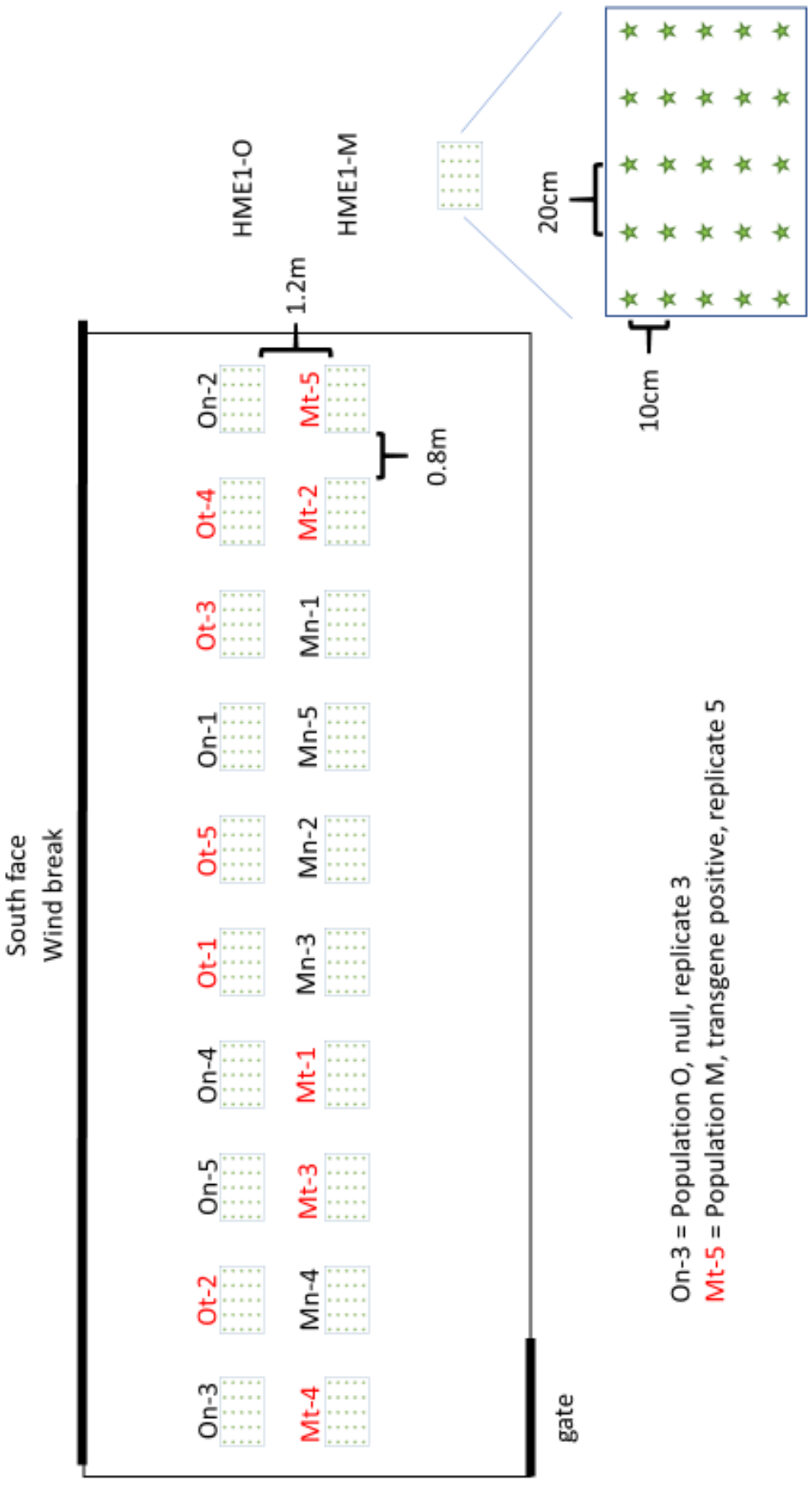

Supplementary figure C3. 2. Field trial layout, and the dimensions of a replicate sward.

A) Example leaf immunoblots for the recombinant oleosin protein in leaves

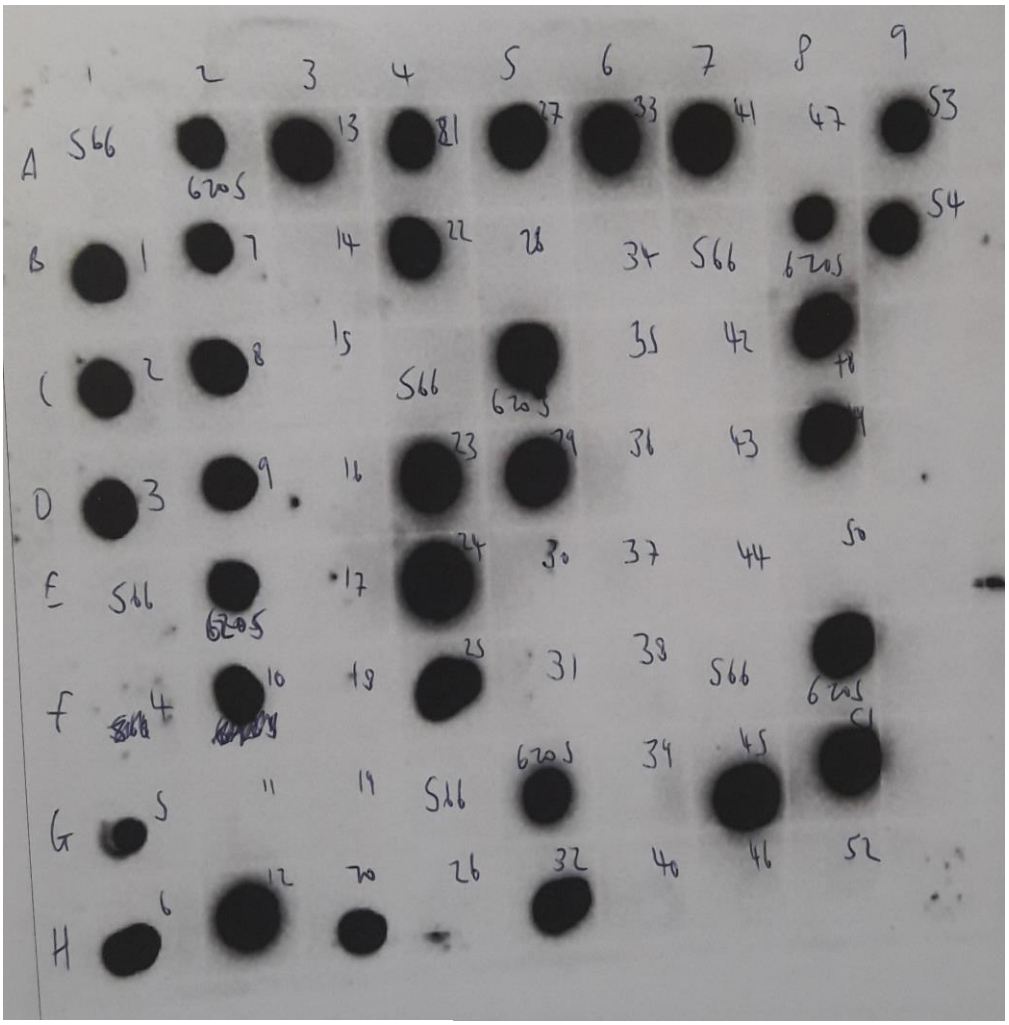

B) Total leaf FA

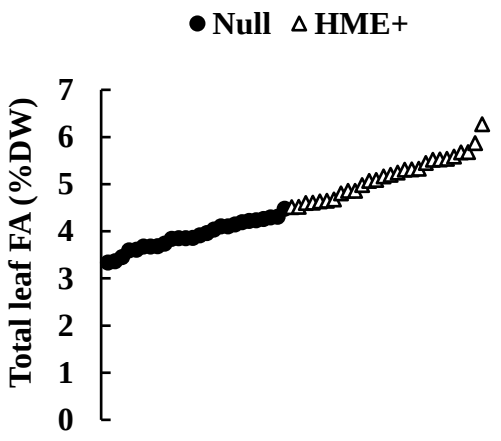

C) Leaf C18:1/C18:3

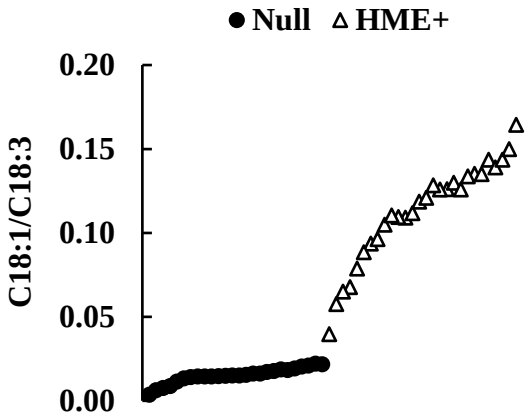

Supplementary figure C3. 3. A) example leaf immunoblots for the oleosin protein in ryegrass leaves, and corresponding B) total leaf fatty acid content and C) leaf C18:1 to C18:3 fatty acid ratio. Open triangle symbols indicate plants that tested positive for the oleosin protein in leaves (HME+), closed circles indicate plants that tested negative for the oleosin protein in leaves (Null).

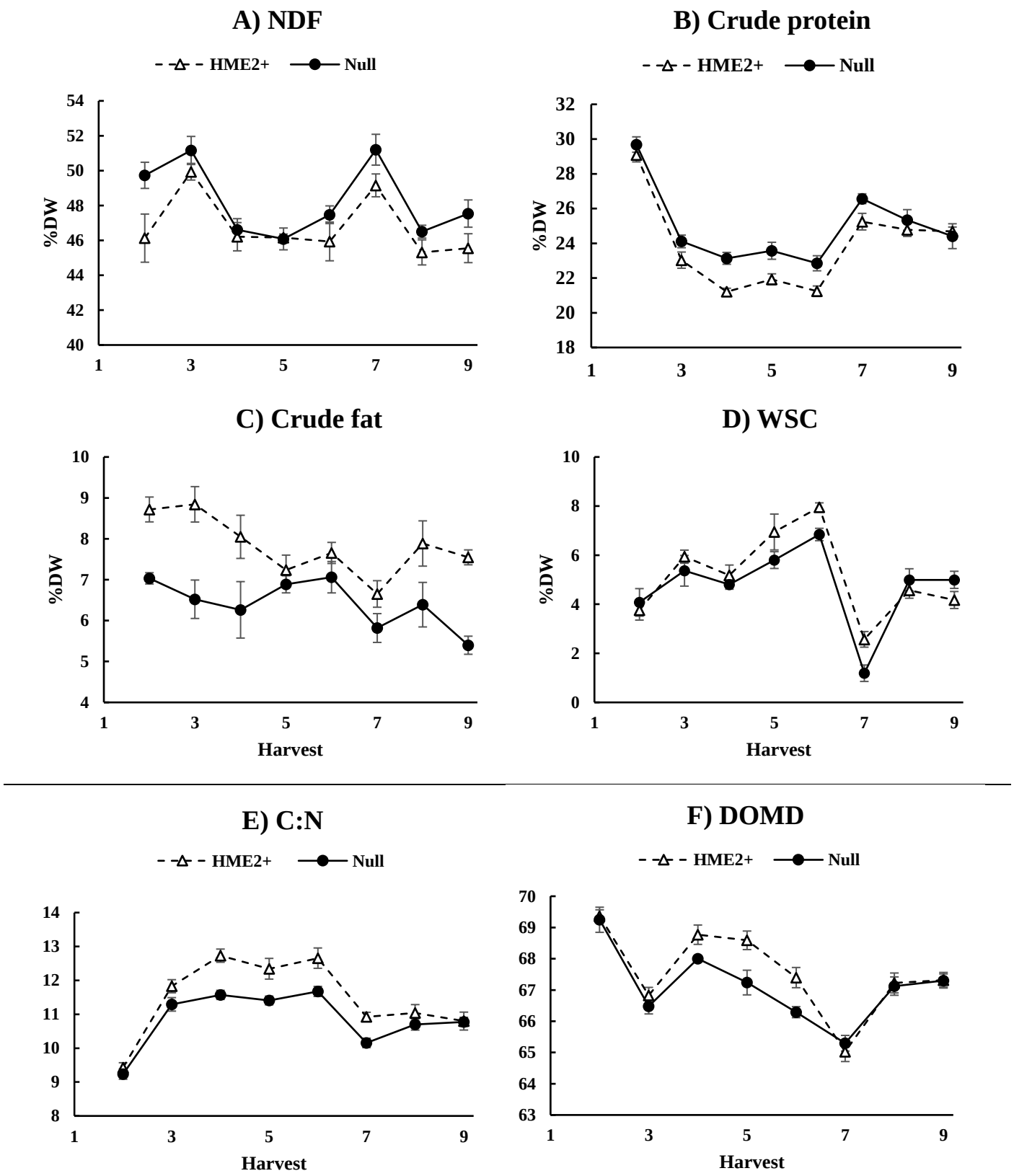

Supplementary figure C3. 4. Herbage biochemical composition in an HME+ and null segregating T_2 *Lolium perenne* population (HME2), grown in indoor miniswards under regular defoliation. Pots were spaced apart from one another for harvests 2–6 and packed tightly together for harvests 7–9. NDF = neutral detergent fibre, WSC = water-soluble carbohydrate, DOMD = dry organic matter digestibility. Data represent means ± S.E. (*n*=6).

Supplementary table C3. 1. Mean (±S.E.) net photosynthesis, transpiration, and stomatal conductance of attached and detached *Lolium perenne* leaves. *n*=12.

	Attached	**Detached**	***p*-value**
Net photosynthesis (µmol m^{-2} s^{-1})	15.3 ± 0.2	15.6 ± 0.2	0.7
Transpiration (mmol m^{-2} s^{-1})	3.2 ± 0.1	3.2 ± 0.1	0.9
Stomatal conductance (mol m^{-2} s^{-1})	0.38 ± 0.01	0.39 ± 0.01	0.9

Non-transformed *Lolium perenne* was regrown in spaced pots. A single tiller was removed from each pre-dawn. For each tiller, the youngest fully expanded leaf was identified, the base of the leaf was submerged under water, re-cut and while submerged, placed in a 15 ml Falcon tube. Each plant and respective detached leaf were then kept in the dark for 4 h. For each plant, net photosynthesis, stomatal conductance, and transpiration were measured on an attached and detached leaf using a Li-COR 6800 portable photosynthesis system. 30 mins prior to measurement, whole spaced pot plants and respective detached leaves were pre-acclimated to 550 µmol photons m^{-2} s^{-1} red/blue light provided by a Cree Cob Series 2000W LED bank (Philizon, Shenzhen, China). Five mins before each measurement, leaves were acclimated in the 6800 chamber under 550 µmol photons m^{-2} s^{-1} red/blue light, 20 °C, 65% RH, 415 ppm CO_2 and flow rate of 400 µmol s^{-1}. Paired t-tests were used to compare attached and detached leaves.

Supplementary table C3. 2 Fatty acid profiles for an HME+ and null segregating T_2 *Lolium perenne* population (HME2) grown in indoor miniswards.

Spacing	Transgene status	C16:0 (%FA)	C16:1 (%FA)	C18:0 (%FA)	C18:1 (%FA)	C18:2 (%FA)	C18:3 (%FA)	Total FA (%DW)
Spaced row (harvest 10)	**Null**	15.0 ± 0.1 A	2.3 ± 0.1 A	1.7 ± 0.2 A	3.0 ± 0.1 A	13.2 ± 0.1 A	64.7 ± 0.3 A	3.1 ± 0.1 A
	HME2+	14.2 ± 0.1 C	2.0 ± 0.0 B	1.3 ± 0.0 A	8.1 ± 0.2 B	22.0 ± 0.3 B	52.5 ± 0.4 B	4.3 ± 0.1 B
Dense sward (harvest 10)	**Null**	15.9 ± 0.4 B	2.4 ± 0.0 A	1.6 ± 0.1 A	3.1 ± 0.1 A	13.1 ± 0.4 A	63.9 ± 0.4 A	3.2 ± 0.1 A
	HME2+	14.1 ± 0.3 C	2.0 ± 0.0 B	1.4 ± 0.1 A	8.1 ± 0.3 B	21.7 ± 0.2 B	52.7 ± 0.6 B	4.7 ± 0.1 C

For the 10th regrowth cycle, the higher-yielding miniswards were reassigned to a spaced row, while the lower-yielding miniswards were kept in the tightly packed pot arrangement. Values for each FA class represent a mean percentage of total FA ± S.E. (n=6). Different letters indicate statistically significant differences at p<0.05 obtained using the BH method, after performing a two-way ANOVA.

Appendix D – supplementary figures and tables from Chapter 5

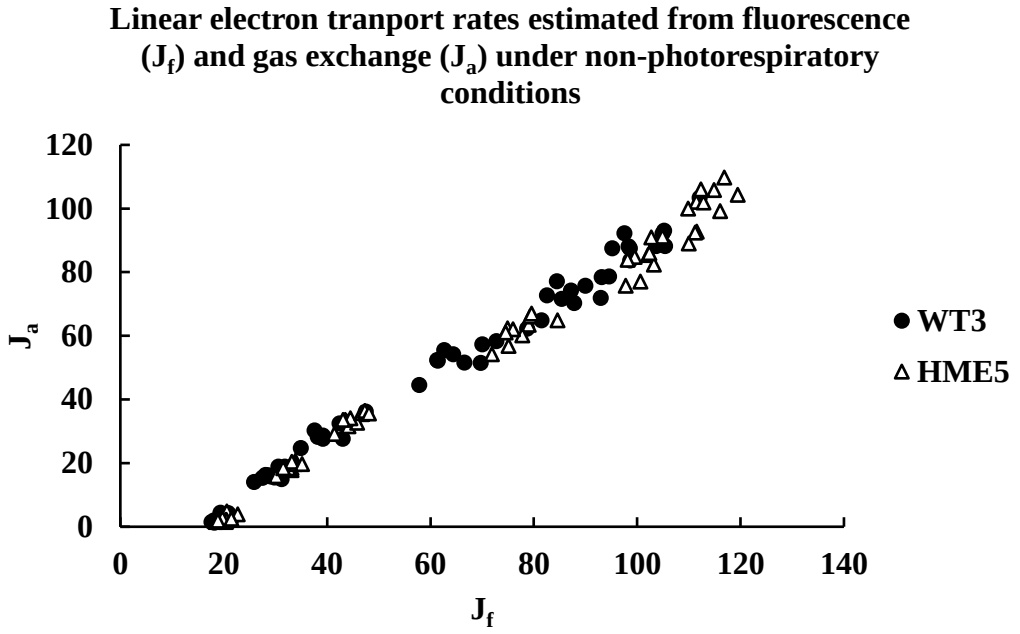

Supplementary figure D4.1. Calibration of apparent linear electron transport rates estimated from Chlorophyll fluorescence (J_f) and gas exchange (J_a) under non-photorespiratory conditions across the range of 50-400 ppm external CO_2 used to estimate mesophyll conductance in table 5.2. The relationship for WT3 was: $J_a = 1.019 \times J_f - 14.3$ and for HME5 was $J_a = 1.007 \times J_f - 15.2$.

A) Response of net photosynthesis per unit leaf area (A) and quantum efficiency of PSII (Φ PSII) to intercellular CO_2 concentration (C_i).

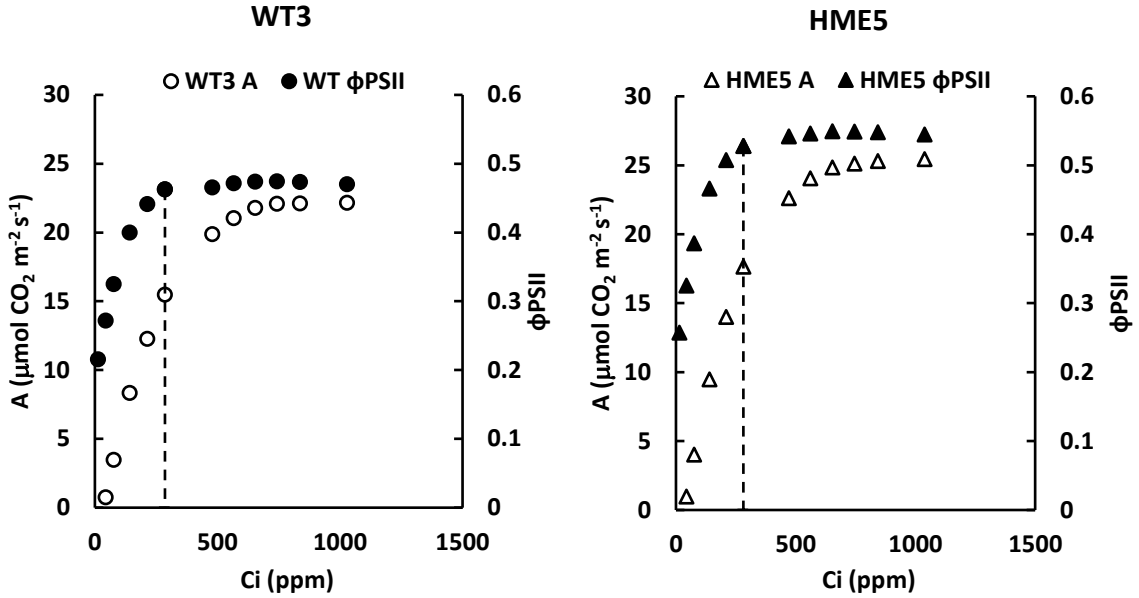

B) Response of net photosynthesis per unit leaf area (A) to irradiance.

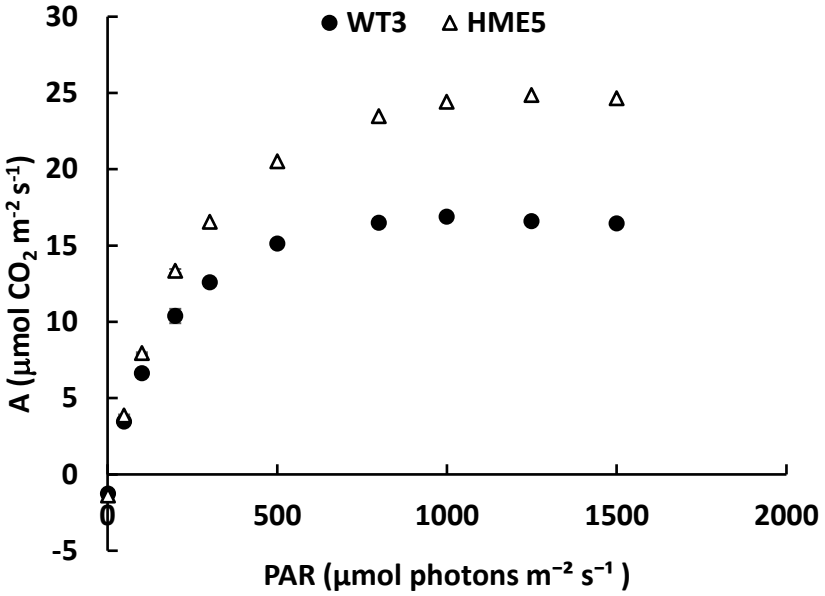

Supplementary figure D4. 2. A) Response of net photosynthesis per unit leaf area (A) and quantum efficiency of PSII (Φ PSII) to intercellular CO_2 concentration (C_i) of a clonal HME *Lolium perenne* transformant (HME5; triangles) and a wild type control genotype (WT3; circles) made at 600 µmol photons m^{-2} s^{-1} at ambient oxygen (*n*=10). The dotted lines indicate the C_i operating point at which plants were grown (corresponding to 415 ppm atmospheric [CO_2]). B) Response of net photosynthesis per unit leaf area (A) to irradiance at 415 ppm atmospheric [CO_2] for WT3 and HME5 (*n*=6). Plants were regrown under 5 mM NO_3^- supply.

Preliminary N partitioning experiment

Parameter		WT3	HME5
N_{mass}	%DW	3.27 ± 0.06	3.97 ± 0.08 ***
N_{area}	gN m^{-2}	1.79 ± 0.06	1.48 ± 0.05 **
$PNUE_{1500}$	µmol CO_2 gN s^{-1}	16.68 ± 0.40	10.35 ± 0.41 ***
Soluble protein	g m^{-2}	5.10 ± 0.22	4.37 ± 0.27
Rubisco	g m^{-2}	2.80 ± 0.14	2.77 ± 0.11
Chl	µmol m^{-2}	449 ± 29	340 ± 16 *
Chl *a*: *b*	mol mol^{-1}	3.34 ± 0.03	3.72 ± 0.11*
Cyt *f*	µmol m^{-2}	0.96 ± 0.01	1.15 ± 0.01 ***

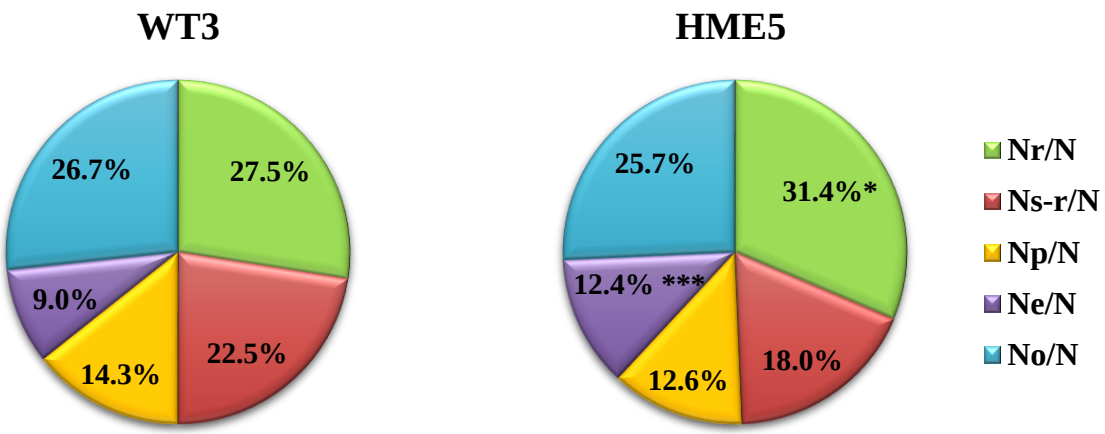

Supplementary figure D4. 3. Preliminary experiment within-leaf N biochemistry and partitioning for a clonal HME *Lolium perenne* transformant (HME5) and a non-transformed control (WT3) regrown under 5 mM NO_3^- supply. Plants were regrown for 25–33 days after defoliation, before making measurements. N = Total leaf N concentration, N_r = N invested in rubisco, $N_{s\text{-}r}$ = N invested in non-rubisco soluble protein, N_p = N invested in pigment-protein complexes, N_e = N invested in 'bioenergetics', N_o = 'other' N. Values represent means ± S.E. (*n*=3–5). * = *p*<0.05, ** = *p*<0.01, *** = *p*<0.001, with *p*-values obtained from Student's t test or Wilcoxon rank sum test.

Supplementary table D4. 1. Total leaf fatty acid (FA) and total leaf water-soluble carbohydrates (WSC), relative growth rate (RGR), specific leaf area (SLA), and light-saturated photosynthetic rate per unit leaf mass (A_{mass}) of a clonal HME PR line 'RCR 6703' and a wild type control (WT1) genotype derived from the cultivar 'Alto'.

Genotype	**Total leaf FA** ($mg\ gDW^{-1}$)	**Total leaf WSC** ($mg\ gDW^{-1}$)	**RGR** ($g\ g^{-1}\ day^{-1}$)	**SLA** ($cm^{-2}\ g$)	**A_{mass}** ($\mu mol\ CO_2\ m^{-2}\ s^{-1}$)
WT1	36.9 ± 0.4	57.3 ± 2.3	0.086 ± 0.003	206 ± 6	0.64 ± 0.02
RCR 6703	58.6 ± 1.0	44.7 ± 3.8	0.085 ± 0.002	197 ± 7	0.62 ± 0.02
***p*-value**	0.007	0.027	0.817	0.363	0.527

Plants were regrown for 20–21 days after defoliation under 5 mM NO_3^- supply. Values represent means ± S.E. (*n*=5 for FA and WSC, *n*=10 for RGR, SLA and A_{mass}). *p*-values are from Students t-tests or Wilcoxon rank sum test.

Supplementary table D4. 2. Independent estimates of mesophyll conductance to CO_2 (g_m), chloroplast CO_2 compensation point (Γ*), and CO_2 drawdown (C_i-C_c) for a clonal HME *Lolium perenne* transformant (HME5) and a non-transformed control (WT3) regrown under 5 mM NO_3^- or NH_4^+ supply.

N form	Genotype	g_m (µmol m^{-2} s^{-1})	Γ* (µmol mol^{-1})	C_i-C_c (µmol mol^{-1})
NO_3^-	**WT3**	0.20 ± 0.03 ^{A}	36.8 ± 0.8 ^{A}	72 ± 7 ^{A}
	HME5	0.49 ± 0.08 ^{B}	38.8 ± 0.7 ^{A}	36 ± 3 ^{B}
NH_4^+	**WT3**	0.18 ± 0.03 ^{A}	40.0 ± 1.4 ^{A}	65 ± 7 ^{A}
	HME5	0.53 ± 0.14 ^{B}	39.4 ± 1.1 ^{A}	37 ± 7 ^{B}
	G	***	-	***
	N	-	-	-
	G x N	-	-	-

Data points represent means ± S.E. Plants were regrown for 21–23 days after defoliation before making measurements. The values of g_m were log-transformed before analysis. G = genotype effect, N = N form effect, in a two-way ANOVA. ** = p<0.01, *** = p<0.001. These parameters were retrospectively calculated from the data presented in Table 3.2. (ambient [CO_2] only) utilizing the values of C_i* and R_d presented in Supplementary table B2.2. J was calibrated using the relationship between J derived via chlorophyll fluorescence and J derived via gas exchange under non-photorespiratory conditions, assuming J derived from gas exchange was equal to 4.2 x (A + R_d) i.e. assuming some engagement of non-photochemical electron sinks (Earl & Ennahli, 2004). Note that in both Table 3.2. and Supplementary table B2.2. WT3 and HME5 are referred to as WT and HL, respectively.

Reference list

Ainsworth E. A., Davey, P., Hymus, G., Osborne, C., Rogers, A., Blum, H., . . . Long, S. (2003). Is stimulation of leaf photosynthesis by elevated carbon dioxide concentration maintained in the long term? A test with *Lolium perenne* grown for 10 years at two nitrogen fertilization levels under Free Air CO_2 Enrichment (FACE). *Plant, Cell & Environment, 26*(5), 705-714.

Ainsworth E. A., & Rogers, A. (2007). The response of photosynthesis and stomatal conductance to rising [CO_2]: mechanisms and environmental interactions. *Plant, Cell & Environment, 30*(3), 258-270.

Ainsworth E.A., Rogers, A., Nelson, R., & Long, S. P. (2004). Testing the "source–sink" hypothesis of down-regulation of photosynthesis in elevated [CO_2] in the field with single gene substitutions in *Glycine max*. *Agricultural and forest meteorology, 122*(1-2), 85-94.

Allen, D. K. (2016). Assessing compartmentalized flux in lipid metabolism with isotopes. *Biochimica et Biophysica Acta (BBA) - Molecular and Cell Biology of Lipids, 1861*(9), 1226-1242.

Altpeter, F., Xu, J., & Ahmed, S. (2000). Generation of large numbers of independently transformed fertile perennial ryegrass (Lolium perenne L.) plants of forage-and turf-type cultivars. *Molecular Breeding, 6*(5), 519-528.

Andrews M., Condron, L. M., Kemp, P. D., Topping, J. F., Lindsey, K., Hodge, S., & Raven, J. A. (2019). Elevated CO_2 effects on nitrogen assimilation and growth of C_3 vascular plants are similar regardless of N-form assimilated. *Journal of Experimental Botany, 70*(2), 683-690.

Andrews M., Love, B. G., & Sprent, J. I. (1989). The effects of different external nitrate concentrations on growth of *Phaseolus vulgaris* cv. Seafarer at chilling temperatures. *Annals of Applied Biology, 114*(1), 195-204.

Andrews M., Raven, J. A., & Lea, P. J. (2013). Do plants need nitrate? The mechanisms by which nitrogen form affects plants. *Annals of Applied Biology, 163*(2), 174-199.

Andrews M., Raven, J. A., Lea, P. J., & Sprent, J. I. (2006). A role for shoot protein in shoot–root dry matter allocation in higher plants. *Annals of Botany, 97*(1), 3-10.

Arojju, S. K., Cao, M., Jahufer, M. Z., Barrett, B. A., & Faville, M. J. (2020). Genomic predictive ability for foliar nutritive traits in perennial ryegrass. *G3: Genes, Genomes, Genetics, 10*(2), 695-708.

Badenhorst, P. E., Panter, S., Palanisamy, R., Georges, S., Smith, K., Mouradov, A., . . . Spangenberg, G. (2018). Molecular breeding of transgenic perennial ryegrass (*Lolium perenne* L.) with altered fructan biosynthesis through the expression of fructosyltransferases. *Molecular Breeding, 38*(2), 21.

Badenhorst, P. E., Smith, K. F., & Spangenberg, G. (2016). Development of a molecular breeding strategy for the integration of transgenic traits in outcrossing perennial grasses. *Agronomy, 6*(4), 56.

Bajaj, S., Ran, Y., Phillips, J., Kularajathevan, G., Pal, S., Cohen, D., . . . Puthigae, S. (2006). A high throughput *Agrobacterium tumefaciens*-mediated transformation method for functional genomics of perennial ryegrass (*Lolium perenne* L.). *Plant Cell Reports, 25*(7), 651-659.

Balmford, A., Amano, T., Bartlett, H., Chadwick, D., Collins, A., Edwards, D., . . . Smith, P. (2018). The environmental costs and benefits of high-yield farming. *Nature Sustainability, 1*(9), 477-485.

Barre, P., Turner, L. B., & Escobar-Gutiérrez, A. J. (2015). Leaf length variation in perennial forage grasses. *Agriculture, 5*(3), 682-696.

Barrett, B., Faville, M., Nichols, S., Simpson, W., Bryan, G., & Conner, A. (2015). Breaking through the feed barrier: options for improving forage genetics. *Animal Production Science, 55*(7), 883-892.

Bellasio, C., Burgess, S. J., Griffiths, H., & Hibberd, J. M. (2014). A high throughput gas exchange screen for determining rates of photorespiration or regulation of C4 activity. *Journal of Experimental Botany, 65*(13), 3769-3779.

Bloom, A. J. (2015). The increasing importance of distinguishing among plant nitrogen sources. *Current Opinion in Plant Biology, 25*, 10-16.

Bradford, M. M. (1976). A rapid and sensitive method for the quantitation of microgram quantities of protein utilizing the principle of protein-dye binding. *Analytical Biochemistry, 72*(1-2), 248-254.

Brooks, A., & Farquhar, G. D. (1985). Effect of temperature on the CO_2/O_2 specificity of ribulose-1, 5-bisphosphate carboxylase/oxygenase and the rate of respiration in the light. *Planta, 165*(3), 397-406.

Browse, J., McCourt, P. J., & Somerville, C. R. (1986). Fatty acid composition of leaf lipids determined after combined digestion and fatty acid methyl ester formation from fresh tissue. *Analytical Biochemistry, 152*(1), 141-145.

Capper, J. L., & Bauman, D. E. (2013). The role of productivity in improving the environmental sustainability of ruminant production systems. *Annual Review of Animal Biosciences, 1*(1), 469-489.

Capstaff, N. M., & Miller, A. J. (2018). Improving the yield and nutritional quality of forage crops. *Frontiers in Plant Science, 9*, 535.

Causton, D. R., & Venus, J. C. (1981). *The Biometry of Plant Growth*. London: Edward Arnold.

Chapman, D., Dyer, J. M., & Mullen, R. T. (2013). Commentary: why don't plant leaves get fat? *Plant Science, 207*, 128-134.

Chapman, D., Bryant, J., McMillan, W., & Khaembah, E. (2012). Economic values for evaluating pasture plant traits. *Journal of New Zealand Grasslands, 74*, 209-216.

Chapman, D., Bryant, J., Olayemi, M., Edwards, G., Thorrold, B., McMillan, W., . . . Moorhead, A. (2017). An economically based evaluation index for perennial and short-term ryegrasses in New Zealand dairy farm systems. *Grass and Forage Science, 72*(1), 1-21.

Chaves, M. M., Maroco, J. P., & Pereira, J. S. (2003). Understanding plant responses to drought—from genes to the whole plant. *Functional Plant Biology, 30*(3), 239-264.

Chen, Y., Xiao, C., Chen, X., Li, Q., Zhang, J., Chen, F., . . . Mi, G. (2014). Characterization of the plant traits contributed to high grain yield and high grain nitrogen concentration in maize. *Field Crops Research, 159*, 1-9.

Chu, K., Jenkins, L. M., Bailey, S. R., Kambhampati, S., Koley, S., Foley, K., . . . Allen, D. K. (2020). Shifting carbon flux from non-transient starch to lipid allows oil accumulation in transgenic tobacco leaves. *BioRxiv*.

Cosgrove, G., Anderson, C., Knight, T., Roberts, N., & Waghorn, G. (2004). Forage lipid concentration, fatty acid profile and lamb productivity. *Journal of New Zealand Grasslands, 66,* 251-256.

Cosgrove, G., Koolaard, J., Luo, D., Burke, J., & Pacheco, D. (2009). The composition of high sugar ryegrasses. *Journal of New Zealand Grasslands,* 71, 187-193.

Detmann, K. C., Araújo, W. L., Martins, S. C., Sanglard, L. M., Reis, J. V., Detmann, E., . . . DaMatta, F. M. (2012). Silicon nutrition increases grain yield, which, in turn, exerts a feed-forward stimulation of photosynthetic rates via enhanced mesophyll conductance and alters primary metabolism in rice. *New Phytologist, 196*(3), 752-762.

Dewhurst, R. J., Moorby, J. M., Scollan, N. D., Tweed, J. K., & Humphreys, M. O. (2002). Effects of a stay-green trait on the concentrations and stability of fatty acids in perennial ryegrass. *Grass and Forage Science, 57*(4), 360-366.

Dewhurst, R. J., Scollan, N., Lee, M., Ougham, H., & Humphreys, M. (2003). Forage breeding and management to increase the beneficial fatty acid content of ruminant products. *Proceedings of the Nutrition Society, 62*(2), 329-336.

Dingkuhn, M., Luquet, D., Fabre, D., Muller, B., Yin, X., & Paul, M. J. (2020). The case for improving crop carbon sink strength or plasticity for a CO_2-rich future. *Current Opinion in Plant Biology*.

Durrett, T. P., Benning, C., & Ohlrogge, J. (2008). Plant triacylglycerols as feedstocks for the production of biofuels. *The Plant Journal, 54*(4), 593-607.

Earl, H. J., & Ennahli, S. (2004). Estimating photosynthetic electron transport via chlorophyll fluorometry without Photosystem II light saturation. *Photosynthesis Research, 82*(2), 177-186.

Edwards, G. R., Parsons, A., Rasmussen, S., & Bryant, R. H. (2007). High sugar ryegrasses for livestock systems in New Zealand. *Journal of New Zealand Grasslands, 69,* 161-171.

Elgersma, A., Ellen, G., Van der Horst, H., Muuse, B., Boer, H., & Tamminga, S. (2003a). Comparison of the fatty acid composition of fresh and ensiled perennial ryegrass (*Lolium perenne* L.), affected by cultivar and regrowth interval. *Animal Feed Science and Technology, 108*(1-4), 191-205.

Elgersma, A., Ellen, G., Van Der Horst, H., Muuse, B., Boer, H., & Tamminga, S. (2003b). Influence of cultivar and cutting date on the fatty acid composition of perennial ryegrass (*Lolium perenne* L.). *Grass and Forage Science, 58*(3), 323-331.

Ellis, J., Dijkstra, J., Bannink, A., Parsons, A., Rasmussen, S., Edwards, G., . . . France, J. (2011). The effect of high-sugar grass on predicted nitrogen excretion and milk yield simulated using a dynamic model. *Journal of Dairy Science, 94*(6), 3105-3118.

Ellis, J., Dijkstra, J., France, J., Parsons, A., Edwards, G., Rasmussen, S., . . . Bannink, A. (2012). Effect of high-sugar grasses on methane emissions simulated using a dynamic model. *Journal of Dairy Science, 95*(1), 272-285.

Evans, J. R. (1987). The relationship between electron transport components and photosynthetic capacity in pea leaves grown at different irradiances. *Functional Plant Biology, 14*(2), 157-170.

Evans, J. R. (1989). Photosynthesis and nitrogen relationships in leaves of C_3 plants. *Oecologia, 78*(1), 9-19.

Evans, J. R. & Clarke, V. C. (2019). The nitrogen cost of photosynthesis. *Journal of Experimental Botany, 70*(1), 7-15.

Evans, J. R., & Lawson, T. (2020). From green to gold: agricultural revolution for food security. *Journal of Experimental Botany, 71*(7), 2211-2215.

Evans, J. R., & Poorter, H. (2001). Photosynthetic acclimation of plants to growth irradiance: the relative importance of specific leaf area and nitrogen partitioning in maximizing carbon gain. *Plant, Cell & Environment, 24*(8), 755-767.

Evans, J. R., & Seemann, J. R. (1989). The allocation of protein nitrogen in the photosynthetic apparatus: costs, consequences, and control. *Photosynthesis, 8*, 183-205.

Evans, J. R. (1996). Developmental constraints on photosynthesis: effects of light and nutrition. In *Photosynthesis and the Environment* (pp. 281-304). New York: Springer.

Fan, J., Zhou, C., Yu, L., Li, P., Shanklin, J., & Xu, C. (2019). Diversion of carbon flux from sugars to lipids improves the growth of an Arabidopsis starchless mutant. *Plants, 8*(7), 229.

FAO. (2019). *The state of food security and nutrition in the world 2019: safeguarding against economic slowdowns and downturns.* Rome.

Faville, M., Richardson, K., Gagic, M., Mace, W., Sun, X., Harrison, S., . . . Pirlo, S. (2010). Genetic improvement of fibre traits in perennial ryegrass. *Journal of New Zealand Grasslands 72,* 71-78.

Faville, M., Cao, M., Schmidt, J., Ryan, D. L., Ganesh, S., Jahufer, Z., . . . Barrett, B. A. (2020). Divergent Genomic Selection for Herbage Accumulation and Days-To-Heading in Perennial Ryegrass. *Agronomy 10*(3), 340.

Fischer, B., Frehner, M., Hebeisen, T., Zanetti, S., Stadelmann, F., Lüscher, A., . . . Nösberger, J. (1997). Source-sink relations in *Lolium perenne* L. as reflected by carbohydrate concentrations in leaves and pseudo-stems during regrowth in a free air carbon dioxide enrichment (FACE) experiment. *Plant, Cell & Environment, 20*(7), 945-952.

Flexas, J., Barbour, M. M., Brendel, O., Cabrera, H. M., Carriquí, M., Diaz-Espejo, A., . . . Gago, J. (2012). Mesophyll diffusion conductance to CO_2: an unappreciated central player in photosynthesis. *Plant Science, 193*, 70-84.

Fulkerson, W., & Donaghy, D. (2001). Plant-soluble carbohydrate reserves and senescence-key criteria for developing an effective grazing management system for ryegrass-based pastures: a review. *Australian Journal of Experimental Agriculture, 41*(2), 261-275.

Gebremedhin, A., Badenhorst, P. E., Wang, J., Spangenberg, G. C., Smith, K. F. (2029). Prospects for Measurement of Dry Matter Yield in Forgae Breeding Programs Using Sensor Technologies. *Agronomy 9*(2), 65.

Glasser, F., Doreau, M., Maxin, G., & Baumont, R. (2013). Fat and fatty acid content and composition of forages: A meta-analysis. *Animal Feed Science and Technology, 185*(1-2), 19-34.

Grainger, C., & Beauchemin, K. (2011). Can enteric methane emissions from ruminants be lowered without lowering their production? *Animal Feed Science and Technology, 166*, 308-320.
Grimberg, Å., Carlsson, A. S., Marttila, S., Bhalerao, R., & Hofvander, P. (2015). Transcriptional transitions in Nicotiana benthamiana leaves upon induction of oil synthesis by WRINKLED1 homologs from diverse species and tissues. *BMC Plant Biology, 15*(1), 192.
Guo, J., Trotter, C. M., & Newton, P. C. (2006). Initial observations of increased requirements for light-energy dissipation in ryegrass (*Lolium perenne*) when source/sink ratios become high at a naturally grazed free air CO_2 enrichment (FACE) site. *Functional Plant Biology, 33*(11), 1045-1053.
Guo, S., Zhou, Y., Shen, Q., & Zhang, F. (2007). Effect of ammonium and nitrate nutrition on some physiological processes in higher plants-growth, photosynthesis, photorespiration, and water relations. *Plant Biology, 9*(1), 21-29.
Hagemann, M., Hemme, T., Ndambi, A., Alqaisi, O., & Sultana, M. N. (2011). Benchmarking of greenhouse gas emissions of bovine milk production systems for 38 countries. *Animal Feed Science and Technology, 166*, 46-58.
Harley, P. C., Loreto, F., Di Marco, G., & Sharkey, T. D. (1992). Theoretical considerations when estimating the mesophyll conductance to CO_2 flux by analysis of the response of photosynthesis to CO_2. *Plant Physiology, 98*(4), 1429-1436.
Hegarty, M., Yadav, R., Lee, M., Armstead, I., Sanderson, R., Scollan, N., . . . Skøt, L. (2013). Genotyping by RAD sequencing enables mapping of fatty acid composition traits in perennial ryegrass (*Lolium perenne* L.). *Plant Biotechnology Journal, 11*(5), 572-581.
Hess, B., Moss, G., & Rule, D. (2008). A decade of developments in the area of fat supplementation research with beef cattle and sheep. *Journal of Animal Science, 86*(suppl_14), E188-E204.
Hikosaka, K. (2004). Interspecific difference in the photosynthesis–nitrogen relationship: patterns, physiological causes, and ecological importance. *Journal of Plant Research, 117*(6), 481-494.
Hikosaka, K., & Terashima, I. (1995). A model of the acclimation of photosynthesis in the leaves of C_3 plants to sun and shade with respect to nitrogen use. *Plant, Cell & Environment, 18*(6), 605-618.
Hoffmann, W. A., & Poorter, H. (2002). Avoiding bias in calculations of relative growth rate. *Annals of Botany, 90*(1), 37-42.
Hofvander, P., Ischebeck, T., Turesson, H., Kushwaha, S. K., Feussner, I., Carlsson, A. S., & Andersson, M. (2016). Potato tuber expression of Arabidopsis WRINKLED1 increase triacylglycerol and membrane lipids while affecting central carbohydrate metabolism. *Plant Biotechnology Journal, 14*(9), 1883-1898.
Humphreys, M. (1989). Water-soluble carbohydrates in perennial ryegrass breeding: I. Genetic differences among cultivars and hybrid progeny grown as spaced plants. *Grass and Forage Science, 44*(2), 231-236.
Ju, C., Buresh, R. J., Wang, Z., Zhang, H., Liu, L., Yang, J., & Zhang, J. (2015). Root and shoot traits for rice varieties with higher grain yield and higher nitrogen use efficiency at lower nitrogen rates application. *Field Crops Research, 175*, 47-55.
June, T., Evans, J. R., & Farquhar, G. D. (2004). A simple new equation for the reversible temperature dependence of photosynthetic electron transport: a study on soybean leaf. *Functional Plant Biology, 31*(3), 275-283.
Kebeish, R., Niessen, M., Thiruveedhi, K., Bari, R., Hirsch, H.-J., Rosenkranz, R., . . . Peterhänsel, C. (2007). Chloroplastic photorespiratory bypass increases photosynthesis and biomass production in *Arabidopsis thaliana*. *Nature Biotechnology, 25*(5), 593.
Kelly, A. A., van Erp, H., Quettier, A.-L., Shaw, E., Menard, G., Kurup, S., & Eastmond, P. J. (2013). The sugar-dependent1 lipase limits triacylglycerol accumulation in vegetative tissues of Arabidopsis. *Plant Physiology, 162*(3), 1282-1289.
King, C., McEniry, J., Richardson, M., & O'Kiely, P. (2012). Yield and chemical composition of five common grassland species in response to nitrogen fertiliser application and phenological growth stage. *Acta Agriculturae Scandinavica, Section B–Soil & Plant Science, 62*(7), 644-658.
Kingston-Smith, A., & Theodorou, M. (2000). Tansley Review No. 118 Post-ingestion metabolism of fresh forage. *The New Phytologist, 148*(1), 37-55.

Kok, B. (1948). A critical consideration of the quantum yield of Chlorella photosynthesis. *Enzymologia, 13*, 625-631.
Koo, A. J., Ohlrogge, J. B., & Pollard, M. (2004). On the export of fatty acids from the chloroplast. *Journal of Biological Chemistry, 279*(16), 16101-16110.
Kramer, D. M., & Evans, J. R. (2011). The importance of energy balance in improving photosynthetic productivity. *Plant Physiology, 155*(1), 70-78.
Lee, J. M., Sathish, P., Donaghy, D. J., & Roche, J. R. (2010). Plants modify biological processes to ensure survival following carbon depletion: a *Lolium perenne* model. *PLoS One, 5*(8), e12306.
Lee, M. A. (2018). A global comparison of the nutritive values of forage plants grown in contrasting environments. *Journal of Plant Research, 131*(4), 641-654.
Leong, T.-Y., & Anderson, J. M. (1984). Adaptation of the thylakoid membranes of pea chloroplasts to light intensities. I. Study on the distribution of chlorophyll-protein complexes. *Photosynthesis research, 5*(2), 105-115.
Lichtenthaler, H. K. (1987). [34]. Chlorophylls and carotenoids: pigments of photosynthetic biomembranes. In *Methods in enzymology* (Vol. 148, pp. 350-382). Amsterdam: Elsevier.
Long, S. P., Zhu, X. G., Naidu, S. L., & Ort, D. R. (2006). Can improvement in photosynthesis increase crop yields? *Plant, Cell & Environment, 29*(3), 315-330.
Ludemann, C., Eckard, R., Cullen, B., Jacobs, J., Malcolm, B., & Smith, K. (2015). Higher energy concentration traits in perennial ryegrass (*Lolium perenne* L.) may increase profitability and improve energy conversion on dairy farms. *Agricultural Systems, 137*, 89-100.
Makino, A., Mae, T., & Ohira, K. (1986). Colorimetric measurement of protein stained with Coomassie Brilliant Blue R on sodium dodecyl sulfate-polyacrylamide gel electrophoresis by eluting with formamide. *Agricultural and Biological Chemistry, 50*(7), 1911-1912.
Matthew, C., Lemaire, G., Hamilton, N. S., & Hernandez-Garay, A. (1995). A modified self-thinning equation to describe size/density relationships for defoliated swards. *Annals of Botany, 76*(6), 579-587.
McEvoy, M., O'Donovan, M., & Shalloo, L. (2011). Development and application of an economic ranking index for perennial ryegrass cultivars. *Journal of Dairy Science, 94*(3), 1627-1639.
Mitchell, M. C., Pritchard, J., Okada, S., Zhang, J., Venables, I., Vanhercke, T., & Ral, J.-P. (2020). Increasing growth and yield by altering carbon metabolism in a transgenic leaf oil crop. *Plant Biotechnology Journal, 18*(10), 2042-2052.
Monteith, J. (1972). Solar radiation and productivity in tropical ecosystems. *Journal of Applied Ecology, 9*(3), 747-766.
Morandini, P. (2013). Control limits for accumulation of plant metabolites: brute force is no substitute for understanding. *Plant Biotechnology Journal, 11*(2), 253-267.
Morgan, S. A., Huws, S. A., Lister, S. J., Sanderson, R., & Scollan, N. D. (2020). Phenotypic Variation and Relationships Between Fatty Acid Concentrations and Feed Value of Perennial Ryegrass Genotypes from a Breeding Population. *Agronomy, 10*(3), 343.
Mu, X., Chen, Q., Chen, F., Yuan, L., & Mi, G. (2016). Within-leaf nitrogen allocation in adaptation to low nitrogen supply in maize during grain-filling stage. *Frontiers in Plant Science, 7*, 699.
Napier, J. A., Haslam, R. P., Beaudoin, F., & Cahoon, E. B. (2014). Understanding and manipulating plant lipid composition: metabolic engineering leads the way. *Current Opinion in Plant biology, 19*, 68-75.
Neuhaus, H., & Emes, M. (2000). Nonphotosynthetic metabolism in plastids. *Annual Review of Plant biology, 51*(1), 111-140.
O'Neill, E. C., & Kelly, S. (2017). Engineering biosynthesis of high-value compounds in photosynthetic organisms. *Critical Reviews in Biotechnology, 37*(6), 779-802.
OECD. (2019). *OECD-FAO Agricultural Outlook 2019-2028*. Rome.
Ohlrogge, J. B., & Jaworski, J. G. (1997). Regulation of fatty acid synthesis. *Annual Review of Plant Biology, 48*(1), 109-136.
Onoda, Y., Wright, I. J., Evans, J. R., Hikosaka, K., Kitajima, K., Niinemets, Ü., . . . Westoby, M. (2017). Physiological and structural tradeoffs underlying the leaf economics spectrum. *New Phytologist, 214*(4), 1447-1463.

Palladino, R., O'donovan, M., Kennedy, E., Murphy, J., Boland, T., & Kenny, D. (2009). Fatty acid composition and nutritive value of twelve cultivars of perennial ryegrass. *Grass and Forage Science, 64*(2), 219-226.

Pang, J., Milroy, S. P., Rebetzke, G. J., & Palta, J. A. (2015). The influence of shoot and root size on nitrogen uptake in wheat is affected by nitrate affinity in the roots during early growth. *Functional Plant Biology, 42*(12), 1179-1189.

Parsons, A., & Chapman, D. (2000). The principles of pasture growth and utilization. In *Grass, its production and utilization* (pp 31-89). London: Blackwell Science.

Parsons, A., Edwards, G., Newton, P., Chapman, D., Caradus, J., Rasmussen, S., & Rowarth, J. (2011). Past lessons and future prospects: plant breeding for yield and persistence in cool-temperate pastures. *Grass and Forage Science, 66*(2), 153-172.

Parsons, A., Rasmussen, S., Liu, Q., Xue, H., Ball, C., & Shaw, C. (2013). Plant growth–resource or strategy limited: insights from responses to gibberellin. *Grass and Forage Science, 68*(4), 577-588.

Parsons, A., Rasmussen, S., Xue, H., Newman, J., Anderson, C., & Cosgrove, G. (2004). Some 'high sugar grasses' don't like it hot. *Journal of New Zealand Grasslands 66,* 265-271.

Paul, M. J., & Eastmond, P. J. (2020). Turning sugar into oil: making photosynthesis blind to feedback inhibition. *Journal of Experimental Botany, 71*(7), 2216-2218.

Paul, M. J., & Foyer, C. H. (2001). Sink regulation of photosynthesis. *Journal of Experimental Botany, 52*(360), 1383-1400.

Pons, T. L., Flexas, J., Von Caemmerer, S., Evans, J. R., Genty, B., Ribas-Carbo, M., & Brugnoli, E. (2009). Estimating mesophyll conductance to CO_2: methodology, potential errors, and recommendations. *Journal of Experimental Botany, 60*(8), 2217-2234.

Poorter, H. (1989a). Interspecific variation in relative growth rate: on ecological causes and physiological consequences. In *Causes and consequences of variation in growth rate and productivity of higher plants* (pp. 45-68). Hague: SPB Academic Publishing.

Poorter, H. (1989b). Plant growth analysis: towards a synthesis of the classical and the functional approach. *Physiologia Plantarum, 75*(2), 237-244.

Poorter, H. (2002). Plant growth and carbon economy. In *Encyclopedia of Life Sciences* (pp 1-6). Berlin: Nature Publishing Group.

Poorter, H., Bühler, J., van Dusschoten, D., Climent, J., & Postma, J. A. (2012a). Pot size matters: a meta-analysis of the effects of rooting volume on plant growth. *Functional Plant Biology, 39*(11), 839-850.

Poorter, H., & Evans, J. R. (1998). Photosynthetic nitrogen-use efficiency of species that differ inherently in specific leaf area. *Oecologia, 116*(1-2), 26-37.

Poorter, H., Fiorani, F., Pieruschka, R., Wojciechowski, T., Putten, W. H., Kleyer, M., . . . Postma, J. (2016). Pampered inside, pestered outside? Differences and similarities between plants growing in controlled conditions and in the field. *New Phytologist, 212*(4), 838-855.

Poorter, H., Niinemets, Ü., Poorter, L., Wright, I. J., & Villar, R. (2009). Causes and consequences of variation in leaf mass per area (LMA): a meta-analysis. *New Phytologist, 182*(3), 565-588.

Poorter, H., Niklas, K. J., Reich, P. B., Oleksyn, J., Poot, P., & Mommer, L. (2012b). Biomass allocation to leaves, stems and roots: meta-analyses of interspecific variation and environmental control. *New Phytologist, 193*(1), 30-50.

Poorter, H., Remkes, C., & Lambers, H. (1990). Carbon and nitrogen economy of 24 wild species differing in relative growth rate. *Plant Physiology, 94*(2), 621-627.

Reich, P. B., Ellsworth, D., & Walters, M. (1998). Leaf structure (specific leaf area) modulates photosynthesis–nitrogen relations: evidence from within and across species and functional groups. *Functional Ecology, 12*(6), 948-958.

Rivero, M. J., Balocchi, O. A., Moscoso, C. J., Siebald, J. A., Neumann, F. L., Meyer, D., & Lee, M. R. (2019). Does the "high sugar" trait of perennial ryegrass cultivars express under temperate climate conditions? *Grass and Forage Science, 74*(3), 496-508.

Rosenzweig, C., Elliott, J., Deryng, D., Ruane, A. C., Müller, C., Arneth, A., . . . Khabarov, N. (2014). Assessing agricultural risks of climate change in the 21st century in a global gridded crop

model intercomparison. *Proceedings of the National Academy of Sciences, 111*(9), 3268-3273.

Ruiz-Vera, U. M., De Souza, A. P., Long, S. P., & Ort, D. R. (2017). The role of sink strength and nitrogen availability in the down-regulation of photosynthetic capacity in field-grown *Nicotiana tabacum* L. at elevated CO_2 concentration. *Frontiers in Plant Science, 8*, 998.

Sampoux, J.-P., Baudouin, P., Bayle, B., Béguier, V., Bourdon, P., Chosson, J.-F., . . . Noël, D. (2011). Breeding perennial grasses for forage usage: an experimental assessment of trait changes in diploid perennial ryegrass (*Lolium perenne* L.) cultivars released in the last four decades. *Field Crops Research, 123*(2), 117-129.

Sartie, A., Easton, H., & Matthew, C. (2009). Plant morphology differences in two perennial ryegrass cultivars. *New Zealand Journal of Agricultural Research, 52*(4), 391-398.

Schroeder, G., Gagliostro, G. A., Bargo, F., Delahoy, J., & Muller, L. (2004). Effects of fat supplementation on milk production and composition by dairy cows on pasture: a review. *Livestock Production Science, 86*(1-3), 1-18.

Schwender, J., Goffman, F., Ohlrogge, J. B., & Shachar-Hill, Y. (2004). Rubisco without the Calvin cycle improves the carbon efficiency of developing green seeds. *Nature, 432*(7018), 779.

Sharkey, T. D. (2016). What gas exchange data can tell us about photosynthesis. *Plant, Cell & Environment, 39*(6), 1161-1163.

Sharkey, T. D., Bernacchi, C. J., Farquhar, G. D., & Singsaas, E. L. (2007). Fitting photosynthetic carbon dioxide response curves for C_3 leaves. *Plant, Cell & Environment, 30*(9), 1035-1040.

Sharwood, R. E., Ghannoum, O., Kapralov, M. V., Gunn, L. H., & Whitney, S. M. (2016). Temperature responses of Rubisco from Paniceae grasses provide opportunities for improving C_3 photosynthesis. *Nature Plants, 2*(12), 1-9.

Singh, V., Singh, P. K., Siddiqui, A., Singh, S., Banday, Z. Z., & Nandi, A. K. (2016). Over-expression of *Arabidopsis thaliana* SFD1/GLY1, the gene encoding plastid localized glycerol-3-phosphate dehydrogenase, increases plastidic lipid content in transgenic rice plants. *Journal of Plant Research, 129*(2), 285-293.

Slattery, R. A., VanLoocke, A., Bernacchi, C. J., Zhu, X.-G., & Ort, D. R. (2017). Photosynthesis, light use efficiency, and yield of reduced-chlorophyll soybean mutants in field conditions. *Frontiers in Plant Science, 8*, 549.

Smith, A. M., & Stitt, M. (2007). Coordination of carbon supply and plant growth. *Plant, Cell & Environment, 30*(9), 1126-1149.

Smith, K., Reed, K., & Foot, J. (1997). An assessment of the relative importance of specific traits for the genetic improvement of nutritive value in dairy pasture. *Grass and Forage Science, 52*(2), 167-175.

Sugiura, D., Betsuyaku, E., & Terashima, I. (2015). Manipulation of the hypocotyl sink activity by reciprocal grafting of two *Raphanus sativus* varieties: its effects on morphological and physiological traits of source leaves and whole-plant growth. *Plant, Cell & Environment, 38*(12), 2629-2640.

Sugiura, D., Betsuyaku, E., & Terashima, I. (2019). Interspecific differences in how sink–source imbalance causes photosynthetic downregulation among three legume species. *Annals of Botany, 123*(4), 715-726.

Sugiura, D., Terashima, I., & Evans, J. R. (2020). A Decrease in Mesophyll Conductance by Cell-Wall Thickening Contributes to Photosynthetic Downregulation. *Plant Physiology, 183*(4), 1600-1611.

Sweetlove, L. J., Nielsen, J., & Fernie, A. R. (2017). Engineering central metabolism–a grand challenge for plant biologists. *The Plant Journal, 90*(4), 749-763.

Temme, A. A., Liu, J. C., van Hal, J., Cornwell, W. K., Cornelissen, J. H. H., & Aerts, R. (2017). Increases in CO_2 from past low to future high levels result in “slower” strategies on the leaf economic spectrum. *Perspectives in Plant Ecology, Evolution and Systematics, 29*, 41-50.

Turner, L. B., Humphreys, M. O., Cairns, A. J., & Pollock, C. J. (2001). Comparison of growth and carbohydrate accumulation in seedlings of two varieties of *Lolium perenne*. *Journal of Plant Physiology, 158*(7), 891-897.

Tzen, J., & Huang, A. (1992). Surface structure and properties of plant seed oil bodies. *The Journal of Cell Biology, 117*(2), 327-335.
Van Loo, E.N. (1993). *On the relation between tillering, leaf area dynamics and growth of perennial ryegrass (Lolium perennne L.).* (Doctoral thesis, Wageningen University, 1993).
Vanhercke, T., Divi, U. K., El Tahchy, A., Liu, Q., Mitchell, M., Taylor, M. C., . . . Blundell, C. (2017). Step changes in leaf oil accumulation via iterative metabolic engineering. *Metabolic Engineering, 39*, 237-246.
Vanhercke, T., Dyer, J. M., Mullen, R. T., Kilaru, A., Rahman, M. M., Petrie, J. R., . . . Singh, S. P. (2019). Metabolic engineering for enhanced oil in biomass. *Progress in Lipid Research, 74*, 103-129.
Vanhercke, T., Petrie, J. R., & Singh, S. P. (2014). Energy densification in vegetative biomass through metabolic engineering. *Biocatalysis and Agricultural Biotechnology, 3*(1), 75-80.
Venus, J. C., & Causton, D. (1979). Plant growth analysis: a re-examination of the methods of calculation of relative growth and net assimilation rates without using fitted functions. *Annals of Botany, 43*(5), 633-638.
Von Caemmerer, S., & Farquhar, G. D. (1981). Some relationships between the biochemistry of photosynthesis and the gas exchange of leaves. *Planta, 153*(4), 376-387.
Warren, C. (2006). Estimating the internal conductance to CO_2 movement. *Functional Plant Biology, 33*(5), 431-442.
Warren, C. (2008). Rapid measurement of chlorophylls with a microplate reader. *Journal of Plant Nutrition, 31*(7), 1321-1332.
Weiss, W. (1998). Estimating the Available Energy Content of Feeds for Dairy Cattle. *Journal of Dairy Science, 81*(3), 830-839.
White, A. C., Rogers, A., Rees, M., & Osborne, C. P. (2015). How can we make plants grow faster? A source–sink perspective on growth rate. *Journal of Experimental Botany, 67*(1), 31-45.
Wilkinson, J., & Lee, M. (2018). Use of human-edible animal feeds by ruminant livestock. *Animal, 12*(8), 1735-1743.
Wilkinson, J., Lee, M., Rivero, M. J., & Chamberlain, A. T. (2020). Some challenges and opportunities for grazing dairy cows on temperate pastures. *Grass and Forage Science, 75*(1), 1-17.
Wims, C., Ludemann, C., Phillips, H., & Chapman, D. (2017). The economic value to dairy systems of genetic gains in the nutritive value of perennial ryegrass in grass–clover pastures. *Animal Production Science, 57*(7), 1357-1365.
Winichayakul, S., Beechey-Gradwell, Z., Muetzel, S., Molano, G., Crowther, T., Lewis, S., . . . Roberts, N. (2020). In vitro gas production and rumen fermentation profile of fresh and ensiled genetically modified high–metabolizable energy ryegrass. *Journal of Dairy Science, 103*(3), 2405-2418.
Winichayakul, S., Cookson, R., Scott, R., Zhou, J., Zou, X., Roldan, M., . . . Roberts, N. (2008). Delivery of grasses with high levels of unsaturated, protected fatty acids*. Journal of New Zealand Grasslands 70,* 211-216.
Winichayakul, S., Scott, R. W., Roldan, M., Hatier, J.-H. B., Livingston, S., Cookson, R., . . . Roberts, N. J. (2013). In vivo packaging of triacylglycerols enhances Arabidopsis leaf biomass and energy density. *Plant Physiology, 162*(2), 626-639.
Wong, S., Cowan, I., & Farquhar, G. D. (1979). Stomatal conductance correlates with photosynthetic capacity. *Nature, 282*(5737), 424.
Wright, I. J., Reich, P. B., Westoby, M., Ackerly, D. D., Baruch, Z., Bongers, F., . . . Diemer, M. (2004). The worldwide leaf economics spectrum. *Nature, 428*(6985), 821.
Wu, A., Hammer, G. L., Doherty, A., von Caemmerer, S., & Farquhar, G. D. (2019). Quantifying impacts of enhancing photosynthesis on crop yield. *Nature Plants, 5*(4), 380.
Xu, C., & Shanklin, J. (2016). Triacylglycerol metabolism, function, and accumulation in plant vegetative tissues. *Annual Review of Plant Biology, 67*, 179-206.
Yin, X., Sun, Z., Struik, P. C., & Gu, J. (2011). Evaluating a new method to estimate the rate of leaf respiration in the light by analysis of combined gas exchange and chlorophyll fluorescence measurements. *Journal of Experimental Botany, 62*(10), 3489-3499.
Yu, L., Fan, J., Yan, C., & Xu, C. (2018). Starch Deficiency Enhances Lipid Biosynthesis and Turnover in Leaves. *Plant Physiology, 178*(1), 118-129.

Zale, J., Jung, J. H., Kim, J. Y., Pathak, B., Karan, R., Liu, H., . . . Zhai, Z. (2016). Metabolic engineering of sugarcane to accumulate energy-dense triacylglycerols in vegetative biomass. *Plant Biotechnology Journal, 14*(2), 661-669.

Zhai, Z., Liu, H., Xu, C., & Shanklin, J. (2017). Sugar potentiation of fatty acid and triacylglycerol accumulation. *Plant Physiology, 175*(2), 696-707.

Zhong, K. (2017). *Growth and feed quality of five perennial ryegrass (Lolium perenne L.) cultivars under three water treatments.* (Masters thesis, Lincoln University, 2017).

Zhu, X.-G., Ort, D. R., Parry, M. A., & von Caemmerer, S. (2020). A wish list for synthetic biology in photosynthesis research. *Journal of Experimental Botany, 71*(7), 2219-2225.